Dipl.-Ing., Martin KUPPER, BSc

Harsh Environment Particle Sensing

Doctoral Thesis

to achieve the university degree of

Doktor der technischen Wissenschaften

Doctoral School: Informaiton and Communications Engineering

submitted to

Graz University of Technology

Supervisor

Univ.-Prof. Mag.rer.nat. Dr.rer.nat. Alexander Bergmann

Institute of Electronic Sensor Systems

Graz, December 2019

Für meine Eltern

und ein kleines Bisschen auch für mich, Nadja und irgendwie auch für Alex

This document was created by adaptation of the TU Graz LaTeX template and was compiled with Overleaf and `Biber`.

The TU Graz LaTeX template is based on KOMA script and can be found online: https://github.com/novoid/LaTeX-KOMA-template

Affidavit

I declare that I have authored this thesis independently, that I have not used other than the declared sources/resources, and that I have explicitly indicated all material which has been quoted either literally or by content from the sources used. The text document uploaded to TUGRAZonline is identical to the present doctoral thesis.

Date	Signature

Acknowledgement

First of all I want to express my sincerest thanks to Alexander Bergmann, for making it even possible for me to start with a PhD and the guidance throughout the whole time. Especially for the support for every thematic excursion I tackled and the insistence to bring everything to an end.

I also want to thank Martin Kraft very very much for the guidance, the support and the possibility to follow every (sometimes rather stupid) intuition I had.

Many thanks also to my colleagues from the Institute of Electronic Sensor Systems for the collegiality, the pleasant environment and the helpful discussions. Especially I want to thank Partick, Lucas, Michael and Michael for the collaboration and the contribution to our research. Furthermore, many many thanks to Jožef Pulko for the collaboration and the support with LII and also many many thanks to Matija Tomšič for the collaboration and the support regarding SAXS. Sincerely, it was a pleasure to work with you all.

Of course I am very thankful to my parents, Samo and Katja, for facilitating my education and career, hence this work would not have been possible without you, thus I dedicate it to you. I also want to thank Nadja for the support throughout and the distraction when I needed it. And although they will never read it, I want to thank Arika and Nanga for the counterbalance to my job.

This work was done within the Competence Centre ASSIC - Austrian Smart Systems Research Center, co-funded by the Austrian Federal Ministries of Transport, Innovation and Technology (bmvit) and Science, Research and Economy (bmwfw) and the Federal Provinces of Carinthia and Styria within the COMET Programme. This work was also supported by AVL List GmbH.

Abstract

Performing particle measurements in harsh environments like automotive exhaust, requires appropriate preconditioning to adapt the sample to the operating conditions of the sensor. This procedure influences the sample in a very rough way, but since preconditioning is necessary the procedure was standardized and the influences were studied very detailed. Nevertheless, because direct measurements are not possible until now, experimental evidence for these considerations is missing.

European emission legislation prescribes the monitoring of two measurands regarding particles: particle mass (PM) and particle number (PN). This work deals with the realization of measurement devices for direct application on raw automotive exhaust gas, focusing on the more fragile PN measurement. Thus, a High-Temperature Condensation Particle Counter (HTCPC) was realized, operating at temperatures above the dew point of volatile exhaust compounds. The concept is basing on a feasibility study published by Nick Collings from the University of Cambridge in 2013. With a systematic investigation on the scientific fundamentals, suitable working fluids and an optimized design a reliable and stable concept of a HTCPC can be presented.

Also, the feasibility of a direct PM measurement technique was investigated. A setup for Laser Induced Incandescence (LII) was realized using components for a compact in-situ probe and tested in the laboratory and on automotive exhaust at a combustion engine testbed. Further an approach for a calibration method is proposed.

Contents

The Author's Contributions to Publications

Peer Reviewed Conference Contributions

Kupper, Martin, Martin Kraft, Jaroslav Kaszynski and Alexander Bergmann (2016). "A simulational and experimental attempt for a high temperature condensed nuclei magnifier based on long chained alkanes." Poster at the *European Aeosol Conference 2016*
Author Contribution: Writing, data analysis and presentation

Kupper, Martin, Jožef Pulko, Alexander Bergmann and Martin Kraft (2017). "Experimental Evaluation of Components for a Super Compact In-Situ LII Probe Applicable on Automotive Exhaust Pipes." Oral presentation at the 36^{th} *American Association of Aerosol Research Annual Meeting 2017*. Abstract available online.
Author Contribution: Writing, experimental work, data analysis and presentation

Kupper, Martin, Martin Kraft, Tristan Reinisch and Alexander Bergmann (2017). "A Study of Alternative Working Fluids and Corresponding Effects for Condensation Nuclei Counters Applied on Automotive Exhaust." Oral presentation at the 36^{th} *American Association of Aerosol Research Annual Meeting 2017*. Abstract available online.
Author Contribution: Writing, analytical modeling, data analysis and presentation

Kupper, Martin, Michael Kügler, Martin Kraft and Alexander Bergmann (2018). "A Long-Term Stable High-Temperature Condensation Particle Counter for Application on Raw Automotive Exhausts." Oral presentation at the 10^{th} *International Aerosol Conference 2018*. Abstract available online.
Author Contribution: Writing, experimental work, data analysis and

presentation

Kupper, Martin, Martin Kraft and Alexander Bergmann (2018). "Investigation of Dependencies of the Condensation Behaviour on Soot in CPCs." Oral presentation at the *10th International Aerosol Conference 2018*. Abstract available online.
Author Contribution: Writing, experimental work, analytical modeling, data analysis and presentation

Kupper, Martin, Jožef Pulko, Martin Kraft and Alexander Bergmann (2018). "First Steps Towards a Super-Compact in-situ Laser-Induced-Incandescence Sensor System." Poster at the *32nd Eurosensors Conference 2018*
Author Contribution: Writing, experimental work, data analysis and presentation

Kupper, Martin, Michael Kügler Martin Kraft and Alexander Bergmann (2018). "Development and Testing of an Aerosol Sensor for direct Measurements in Engine Exhaust." Poster at the *32nd Eurosensors Conference 2018*
Author Contribution: Writing, experimental work, data analysis and presentation

Peer Reviewed Conference Proceedings Paper

Kupper, Martin, Jožef Pulko, Martin Kraft, and Alexander Bergmann (2019)."First Steps towards a Super-Compact In-Situ Laser-Induced-Incandescence Sensor System." In: *Proceedings* 2.13, p.1017. ISSN: 2504-3900. DOI: 10.3390/proceedings2131017. URL:`https://www.mdpi.com/2504-3900/2/13/1017`
Author Contribution: Writing, experimental work, data analysis and presentation

Peer Reviewed Journal Paper

Martin Kupper, Adam Boies, Martin Kraft, and Alexander Bergmann (2019), "High-Temperature Condensation Particle Counter Using a Systematically Selected Dedicated Working Fluid For Automotive Applications".

In *Aerosol Science and Technology*. DOI:*10.1080/02786826.2019.1702920*.
Author Contribution: Writing, experimental work and data analysis

Martin Kupper, Michael Kügler, Michael Gleichweit, Martin Kraft, Markus Koch and Alexander Bergmann, "A High-Temperature Condensation Particle Counter Optimized for Engine Exhaust". In the *MDPI Sensors Journal*. Manuscript in preparation for publication.
Author Contribution: Writing, experimental work and data analysis

Issued Patents

Kupper, Martin and Anton Buchberger. "Kondensationspartikelzähler mit Trennelement." AT 519912 A1. 2018-11-15

Kupper, Martin and Anton Buchberger. "Kondensationspartikelzähler mit Lichtleiter." AT 519913 A1. 2018-11-15

Kupper, Martin, Martin Kraft and Alexander Bergmann. "Kondensationspartikelzähler mit Düsenvorrichtung". AT 520843 A1. 2019-08-15

Kupper, Martin, Martin Kraft and Alexander Bergmann. "Kondensationspartikelzähler mit Sättiger". AT 520844 A1. 2019-08-15

Kupper, Martin, Martin Kraft and Alexander Bergmann. "Verfahren und Anordnung umfassend Kondensationspartikelzähler, Betriebsstoff und Trägergas". AT 520828 B1. 2019-08-15

List of Figures

List of Tables

List of Abbreviations

AC Alternating Current

APC AVL Particle Counter

APD Avalanche Photo Diode

APG AVL Particle Generator

BC Black Carbon

CAD Computer Aided Design

CAST Combustion Aerosol Standard

CFD Computational Fluid Dynamics

CNC Condensation Nuclei Counter

CNM Condensation Nuclei Magnifier

CNT Classical Nucleation Theory

CO Carbon Monoxide

CPC Condensation Particle Counter

CS Catalytic Stripper

CVS Constant Volume Sampler

DC Direct Current

DMA Differential Mobility Analizer

DPF Diesel Particle Filter

DPSS Diode Pumped Solid State

EC Elemental Carbon

EE Engine Exhaust

ELPI Electrical Low-Pressure Impactor

ERMES European Research on Mobile Emission Sources

FT Frauenthal

GDI Gasoline Direct Injection

GPF Gasolilne Particle Filter

GRPE Working Party on Pollution and Energy

GTR Global Technical Regulation

HC Hydrocarbon

HEPA High Efficiency Particle Air

HiPoLas High Power Laser

HTCPC High-Temperature Condensation Particle Counter

HV High Voltage

IUFC Inrets - Urbain Fluide Court (*French*

LII Laser Induced Incandescence

LIS Laser Ignition System

MFC Mass Flow Controller

MSS Micro Soot Sensor

$NaCl$ Sodium Chloride

$NMHC$ Not Methan Hydrocarbon

NO_x Nitrogen Oxides

OA Organic Aerosol

OBD On-Board Diagnosis

OC Organic Carbon

OD Optical Density

OPC Optical Particle Counter

OT Outlet Tube

PAH Polycyclic Aromatic Hydrocarbon

PAS Photoacoustic Spectroscopy

PCF Particulate Pre-Classifier

PD Photodiode

$PEMS$ Portable Emission Measurement System

PID Proportional-Integral-Derivative

PM Particulate Matter/Mass

PMP Particle Measurement Program

PMT Photo Multiplier Tube

PN Particulate Number

PNC Particle Number Counter

POA Primary Organic Aerosol

PSP Particulate Sampling Probe

PTT Particulate Transfer Tube

RDE Reald Driving Emissions

SAS Small Angle Scattering

SAXS Small Angel X-Ray Scattering

SCR Selective Catalytic Reactor

SEM Scanning Electron Microscope

SiC Silicon Carbide

SIDI Spark Ignited Direct Injection

SiPM Silicon Photo Multiplier

SLS Static Light Scattering

SMPS Scanning Mobility Particle Sizer

SNR Signal to Noise Ratio

SOA Secondary Organic Aerosol

TD Thermodenuder

TP Tailpipe

UNECE United Nations Economic Commission for Europe

VOC Volatile Organic Compound

VPR Volatile Particle Remover

WAXS Wide Angle X-Ray Scattering

WMTC World Motorcycle Test Cycle

WO_x Tungsten Oxide

XRF X-Ray Flourescence Spectroscopy

1. Introduction

1.1. Motivation

Today's society is developing more and more awareness for the negative side effects of an industrialized and urbanized humanity. One associated long term subject is air pollution. Beginning with the Great Smog of London in 1952, which caused thousands of deaths [Davis, Bell, and Bates, 2002], air pollution is being monitored and regulated more and more in most parts of the world. Although the scope and limits differ between countries, the conditions of the industrial age have been overcome and at least for cities in the western world, the air pollution was lowered to a widely nonhazardous level [European Environment Agency, 2008; Koolen and Rothenberg, 2019]. But even at low levels, air pollution is still present and is known to cause numerous diseases and increased mortality [Cohen et al., 2017; European Environment Agency, 2017]. Also impacts with a less direct consequences have to be considered, like e.g. the global warming [Bond et al., 2013]. Thus, all goals are not reached yet and further effort is necessary for protection of humanity and the environment.

Anyway, every progress also brings new challenges, like new sources of air pollution. The most popular example therefore is the spread of cars with internal combustion engines, since it required a differentiated view on the problematic. Heavy pollutant industry was removed from populated areas, but with a mobile combustion engine, pollutants are emitted by a lot of small emitters spread over a wide area. Measuring at selected spots is still necessary but not sufficient, since local pollution might be much higher, as e.g. close to highly frequented road [Declercq et al., 2012; Pérez et al., 2010]. Further some compounds react with the environment and might not even reach the measuring station in its original state [Shiraiwa, Selzle, and Pöschl, 2012], also an accurate assignment of the emission to its source is

very difficult and not very detailed [Kozáková et al., 2018; Pey et al., 2009]. Approaching this concern, additionally to ambient thresholds the emission at the source was regulated. The first law was enacted in 1960 in California and in 1970 the first uniform emission standard for European countries were passed. Since then more components of the exhaust were limited and the limits itself became lower and lower [Johnson, 2016]. In the last few years a lot research is done to enable reliable measurements of the limited pollutants at the required concentrations, since the limits converged close to the detection limits and also on-road measurements became necessary [Fontaras et al., 2015; Giechaskiel, Maricq, et al., 2014; Hooftman et al., 2018].

Measurements of exhaust gases are very complex and were only possible in specialized test beds until a few years ago. They were not performed for every single vehicle, but just for one exemplary piece, identical in construction to the series. Thus, the vehicles performance was optimized on the test procedure [Ntziachristos, Mellios, et al., 2014]. Further the standardized test was performed the same way by the car manufacturer and the testing laboratory, so limits could be tricked, as it was found in 2013 and spread by media [Boretti, 2017; Landesanstalt für Umwelt Messungen und Naturschutz, 2014]. Therefore technologies are necessary, which allow random inspections at real conditions to assure compliance of the emissions with the legislation limits.

One compound of automotive exhaust is particulate matter, the so called "particles". This term comprises all solid ingredients of the exhaust [Official Journal of the European Union EN, 2015], what is mostly soot but also ashes and scoring from the engine [Eastwood, 2008]. Since particle pollution is a very obvious kind of air pollution, because it can be seen with the bare eye at high concentrations, limitations for it came relatively early. First limitations aimed at the particle mass per unit volume and in order to reduce the emissions, the combustion was optimized. Later also a particle number limitation was introduced, first for diesel and recently also for gasoline engines. This brought the wished result, further reduction of particulate emissions, but caused for some cases emissions of particles too small for the currently specified measurement range in very high quantities [Leach et al., 2019; Raza et al., 2018]. Considering this, the exhaust emission regulation regarding particle number is very likely to be adapted to smaller particle sizes and therefore complementary EU funded research

projects are currently ongoing [Bainschab et al., 2017; Baltzopoulou et al., 2018; Giechaskiel, Vanhanen, et al., 2017]. Although the impact of the so called "ultrafine" particles on human health is not clarified yet [Ohlwein et al., 2019], the nature and behavior of them has to be studied to enable a classification and, if necessary, enable counteractions.

The measurement of the particle number emitted by a combustion engine is very complex. The exhaust gas is very hot, contains a lot of moisture, residual fuel and lubricating oil and also aggressive compounds like sulphuric acid. Hence extensive preconditioning is necessary to enable the measurement. This preconditioning comprises the removal of coarse particles, a hot dilution, the removal of volatile compounds and finally a cold dilution [Giechaskiel, Chirico, et al., 2010a]. By this process the sample is influenced in an unknown degree since a measurement directly in the exhaust gas in impossible. For compliance, in the European Union the sampling procedure is well defined [Official Journal of the European Union EN, 2015], but still it is a heavy influence on the sample.

Although particle measurement is very complex, there are possibilities to perform the measurements in the raw automotive exhaust. One of these methods was presented in 2013 by Nick Collings and Kanchit Rongchai from the University of Cambridge. They built a measurement device which operates at high temperatures and showed its feasibility [Collings, Rongchai, and Symonds, 2014]. This concept of a so called High-Temperature Condensation Particle Counter (HTCPC) would be a very promising method for particle number measurements, minimizing the influence of the specimen and still enable reliable particle number measurements.

Another possibility, heading particle mass measurement, would be Laser Induced Incandescence (LII) [Zizak, 2000]. This technique is known for decades and was continuously improved for scientific purposes. The challenging physics [Bladh, Johnsson, and Bengtsson, 2008] of the measurement process require very fast and accurate detectors and a reliable high-power laser [Vander Wal, 2009]. Also an extensive data analysis is necessary and therefore it was nearly impossible to realize a system capable of real-time measurements for commercial purposes until a few years ago. Nowadays the critical components for realizing such a system are available. An appropriate design would enable in-situ measurements in the exhaust pipe of a combustion engine [Zhang, Stadlbauer, et al., 2014] and therewith an

accurate particle mass measurement.

The discipline of aerosol science is comparatively young and combines fields originating from different "classical" scientific disciplines like e.g. physics, chemistry, computational science and mathematics. Although the already reached possibilities are overwhelming, the understanding for fundamental processes is sometimes still in an early stage. The investigation and discovery of fundamentals reveals on one hand a better understanding for scientific purposes, but on the other hand it enables the realization of a whole new generation of measurement instrumentation, which can help to keep the air we breath clean.

1.2. Background Information

1.2.1. Definitions

Particles, Fine Dust and Haze

Particle is a common term in everyday life, describing various things. Thus it is important to discuss it before the use in a thesis. A meaningful definition was given in the book "Aerosol Chemistry and Physics: "*An aerosol particle may consist of a single continuous unit of solid or liquid containing many molecules held together by intermolecular forces and primarily lager than molecular dimensions (*>0.001 µm*); a particle may also consist of two or more such unit structures held together by interparticle adhesive forces such that it behaves as a single unit in suspension or on deposit*" [Seinfeld and Pandis, 2006]. Simplified one could summarize a particle as a continuous object, different to the surrounding by a phase boarder which is bigger than a molecule and to small to be seen with the bare eye, what is about 100 µm.

		(Dispersed) Particle medium		
		Gas	Liquid	Solid
Dispersion medium	Gas	-	Aerosol	Aerosol
	Liquid	Foam	Emulsion	Sol
	Solid	Foam	Gel	Sol

Table 1.1.: Table for classification of colloids [Seinfeld and Pandis, 2006].

Particulate describes a material with particle-like properties [Baron and Willeke, 2001]. E.g. by "particulate mass" the cumulative mass of particles in a certain volume is meant. The legislative definition of the term comprises everything what is collected from exhaust on a filter, except condensed water [Eastwood, 2008].

Dust describes **Airborne Particles**, what are the manifold particles suspended in the air of all sizes and shapes, like pollen, spores, bacteria, viruses, water droplets, soot, ashes, scoring from various sources and so on. Mass and number concentration, species and size distribution differ spatially, depending on existing sources and present transport mechanisms.

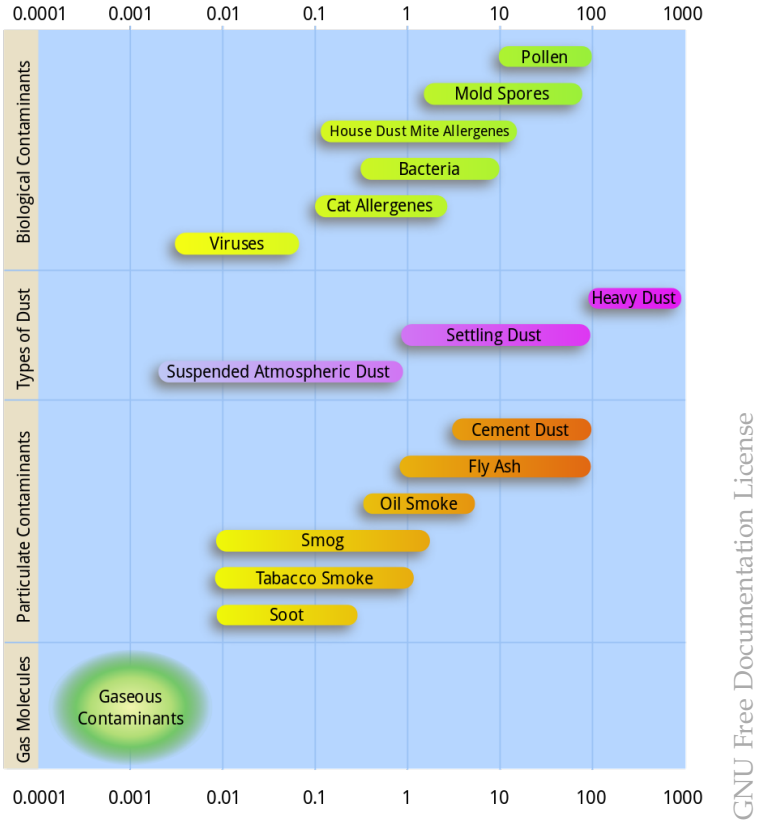

Figure 1.1.: Size chart for some airborne particles. Size scale is in µm

Fine dust is the popular scientific term for "particulate mass", also known as "particulate matter". More precisely there are two measures, PM_{10} comprises solid airborne particles with sizes between 10 µm and 2.5 µm and $PM_{2.5}$ solid airborne particles smaller than 2.5 µm and down to the detection limit of the device. These are the values which are regulated for

environmental protection and were correlated to various diseases and mortality in epidemiological studies [Cohen et al., 2017; Declercq et al., 2012; Raaschou-Nielsen et al., 2013].

Ultrafine Particles or simply **Ultrafines** are particles smaller 100 nm. They are considered as a special threat for human health since they can deposit very deep inside the lung and are small enough to enter the blood stream [Brook et al., 2010; Raaschou-Nielsen et al., 2013], although their impact is controversial since epidemiological studies are up to now still inconclusive [Ohlwein et al., 2019]. They were found to be emitted by some modern gasoline engines [Giechaskiel, Vanhanen, et al., 2017].

Particle Size is a versatile term. Depending on the measurement technique for the same particle different sizes can be determined. E.g. the mobility diameter describes the size basing on the behavior of a sphere in an electric field and the aerodynamic diameter describes the size basing on the behavior of a sphere in an aerodynamic flow.

Haze is the optical effect of the turbidity caused by aerosols.

Exhaust

Engine Exhaust is the product of the combustion inside an engine, typical compositions are listed in table 1.2.

Automotive Exhaust is the cleaned engine exhaust, which is let into the environment. Typical compositions are listed in table 1.2. Modern aftertreatment systems reduce the fraction of hazardous compounds to very low concentrations for single cars, the problematic arises from the high quantity of cars.

Exhaust Particles are particles found in an exhaust gas. These are mainly soot particles and traces of ashes and piston scoring, existing in three distinct types named ”nucleation mode”, ”accumulation mode” and ”coarse mode”. See section 1.2.4 for details.

Secondary Aerosol, **Secondary Particulate Matter** or **Secondary Particles** are the particles forming from the exhaust particles and oxidized volatile compounds, they are the particles existing in the environment. ”Big” particles have a higher deposition efficiency in the human respiratory tract

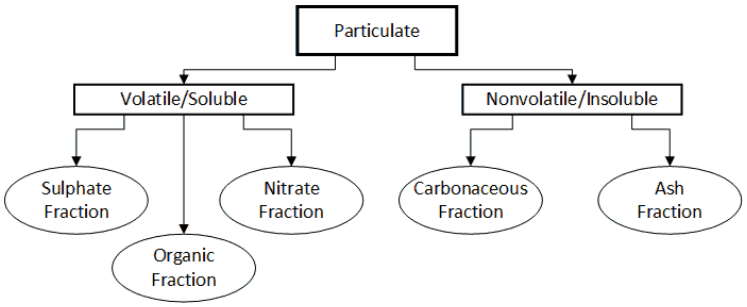

Figure 1.2.: Partition of particles in exhaust [Eastwood, 2008].

Species	Diesel			Gasoline		
	EE	TP	EURO 6d	EE	TP	EURO 6d
N_2	~67 %	~67 %		~71 %	~71 %	
CO_2	~12 %	~12 %		~14 %	~14 %	
H_2O	~11 %	~11 %		~13 %	~13 %	
O_2	~10 %	~10 %		-	-	
HC	<0.03 %	~0.005 %	180 mg km^{-1*}	<0.25 %	~0.02 %	100 mg km^{-1}
NO_X	<0.15 %	~0.06 %	80 mg km^{-1}	<0.25 %	~0.02 %	60 mg km^{-1}
CO	<0.045 %	~0.025 %	500 mg km^{-1}	1 % to 2 %	~0.25 %	1000 mg km^{-1}
PM	<0.045 %	~0.005 %	4.5 mg km^{-1}	-	-	4.5 mg km^{-1}
SO_2	<0.03 %	n.v.		-	-	
$PN^{\dagger}$	n.v.	n.v.	6×10^{11} km^{-1}	n.v.	n.v.	6×10^{11} km$^{-1\ddagger}$

Table 1.2.: Approximate composition of engine and tailpipe exhaust [Elliott, Nebel, and Rounds, 1955; Volkswagen Ag, 2012] and the limits for EURO 6d vehicles. EE... engine exhaust, TP... tailpipe exhaust, n.v.... no vlaues available,

than the gaseous volatile component has, thus arises their hazardousness [Gentner et al., 2012; Sauvain, Vu Duc, and Guillemin, 2003]. See section 1.9 for details.

Primary Particles are particles which can incorporate into larger particulate objects. This applies for basic compounds of fractal particles as well as for already stable agglomerates before changing into an unstable environment, like e.g. soot leaving the tailpipe into the environment.

Primary Organic Matter comprises the stable particulates which form after sampling, dilution and cooling of exhaust.

*Sum of HC and NO_X
†additionally to PM
‡For gasoline direct injection (GDI) engines

Soot is the result of incomplete combustion of organic matter, consisting of a solid carbon core and soluble organic compounds [Penner and Novakov, 1996]. It comprises the carbonaceous fraction of exhaust particles [Eastwood, 2008]. The term is not clearly defined.

Black Carbon (BC) describes the solid part of soot particles, it is an aggregate of smaller spherical carbon particles, the **Primary Soot Particles** [Bond et al., 2013].

Elemental Carbon (EC) is the analytical mass fraction of solid carbon in an aerosol, namely considering the primary particles [Bond et al., 2013].

Organic Carbon (OC) comprises the volatile and soluble compounds of soot [Bond et al., 2013; Penner and Novakov, 1996].

Sensors

Sensor Effect is a physical mechanism, clearly indicating a measurand.

Sensor describes an arrangement to monitor the sensor effect, providing a correlating electrical signal - the **Sensor Signal**.

A **Sensor System** comprises the sensor, the analysis of the sensor signal, a housing and an user interface.

1.2.2. Deposition Mechanisms

Aerosols are dynamic structures, new particulates are formed, they change, stick together and grow, sometimes they dissolve and they deposit. Deposition is from very importance if aerosols are guided with tubing or pipes, where it is not desired its has to be known. For filtration on the other hand, deposition is maximized to remove particulates efficiently. Since for exhaust measurement sampling is required the first point is an issue. Here an overview shall be given and major dependencies pointed out. For particulates six different deposition mechanisms exist[Eastwood, 2008; Hinds and Kennedy, 2000]:

Sedimentation - Gravitational Settling

The deposition due to the gravitation force mainly affects particulates from roughly 1 µm upwards. For smaller particles other mechanisms are of more importance. It is a very important process in nature, for exhaust measurement it is mostly negligible. An approximation can be given with [Hinds and Kennedy, 2000]:

$$G = \frac{\rho_g d_p^2 C_c g}{\sqrt{Ku\ Pe}} \tag{1.1}$$

With G the gravitational settling parameter, ρ_g the density of the surrounding gas, d_p the particulate's diameter and g the gravitation constant. C_c the Cunningham slip correction factor, Ku the Kuwabara hydrodynamic factor and Pe the Peclet number are experimentally found empirical parameters.

Interception

An important assumption in fluid dynamics is that particulates follow stream lines. *Interception* describes the deposition because of the particulates spacial expansion. If a streamline converges to a surface close than one particulates diameter, it is deposited. This is e.g. a major process for filtration by fibers, but does not strongly affect exhaust sampling.

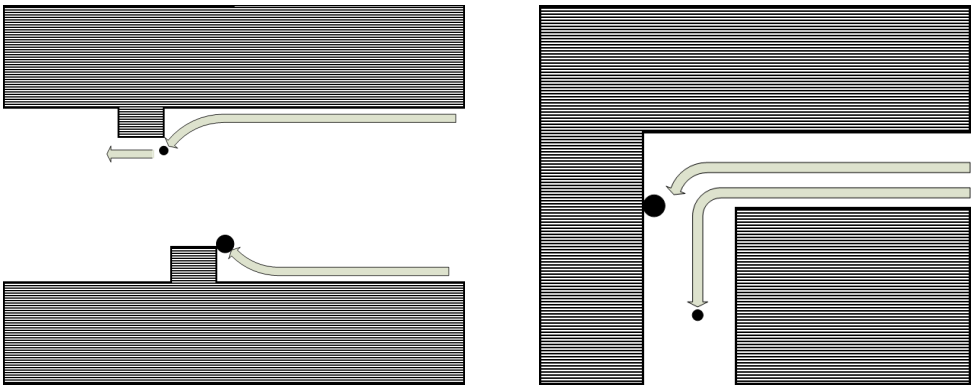

(a) Interception (b) Impaction

Figure 1.3.: Schematic representation of deposition by by interception at a barrier and impaction at a flow redirection.

Impaction

Considering mass and inertia, particulates can not follow stream lines strictly. *Impaction* thus describes deposition due to deviations from streamlines. This is described by the dimensionless Stokes number Stk, it is defined as [Hinds and Kennedy, 2000]:

$$Stk = \frac{\tau u_0}{d_f} \tag{1.2}$$

With τ the characteristic relaxation time the particulate needs to react to a change of the fluid flow (τ depends mainly on the particulates mass), u_0 the fluid velocity and d_f a characteristic dimension of the obstacle (e.g. a radius of curvature or a diameter of a fiber). For $Stk < 1$ particulates follow the stream lines. For exhaust sampling this process has to be considered by the usage of mostly straight tubing or pipes and the avoidance of narrowings and edges e.g. by tube connectors. For repeatability always a defined set of tubings and pipes has to be used.

Diffusion

Particulate movement due to Brownian motion is a very important deposition process for small particulates. It becomes the dominant process below 10 nm [Pratsinis and Kim, 1989], since the inertia of such small particulates is negligible. At these sizes the transition to the molecular regime is floating, since single molecules, like proteins, can be about that size or even bigger [Erickson, 2009]. The dominant deposition process caused by diffusion is a constant transport of particulates towards walls, which are functioning as a sink. In a flow also a constant aberrance of particulates from the stream lines is caused, thus increasing the probability for interception [Hinds and Kennedy, 2000]. The diffusivity of spherical particulates can be estimated with the Stokes-Einstein equation:

$$D = \frac{k_B T}{3\pi\eta d_P} \tag{1.3}$$

With D the diffusion coefficient, k_B the Boltzmann constant, T the temperature, η the viscosity and d_P the particulates diameter. Accordingly the

diffusivity rises with decreasing size of the particulates and reaches for d_P below 10 nm high values [Wei, Kittelson, and Watts, 2001]. Thus these small particulates spread efficiently in space and deposit onto walls of of e.g. tubes and pipes.

Electrostatic deposition

Electrostatic deposition can be a dominant mechanism, depending on the charge of the particles. The difficulty with this effect is that for the assessment of its impact the charge of the particulates has to be known. As a precaution a neutralization of the particulates should be done as described in section 2.2.8 and conductive tubes and pipes should be used to avoid static charges. This effect is utilized e.g. for electrostatic precipitators [Zhuang et al., 2000].

Thermophoresis

Also an effect which is hard to assess but sometimes very important, is the motion caused by temperature gradients. The fundamental effect is the difference in Brownian motion between a cooler and a hotter region. The faster motion in the hotter region is causing a net impulse towards the cooler region [Hinds and Kennedy, 2000]. For high exhaust temperatures and much cooler line walls the losses can be very high [Wei, Kittelson, and Watts, 2001] but it is neglected mostly [Hinds and Kennedy, 2000]. Aggravating is the size dependency, since smaller particulates are more diffusive as stated above [Eastwood, 2008]. It has to be considered by heating all possible obstacles for particulates.

1.2.3. European emission Legislation

Overview

The European emission politic is very comprehensive, since it comprises limitations of local concentrations as well as emissions at the pollution sources. The legislative frame for passenger cars, heavy duty vehicles and busses is given at the date of publication of this thesis by guideline

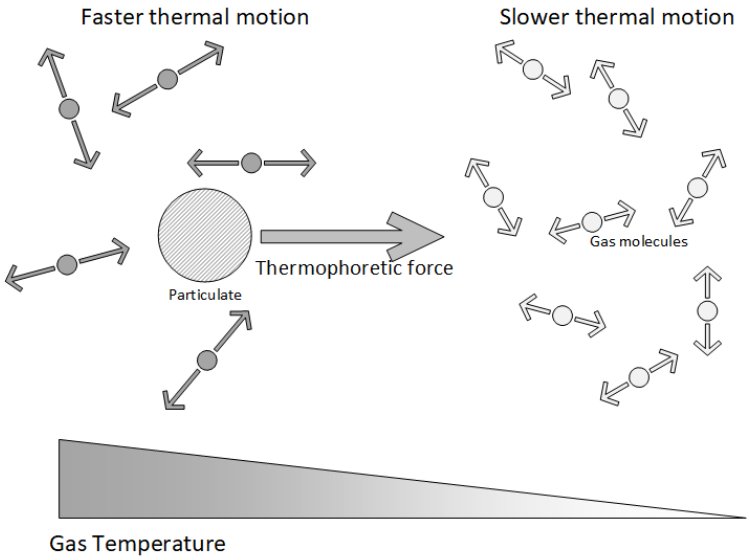

Figure 1.4.: Schematic representation of thermophoretical motion of particulates in a gas.

2007/46/EG (replaced 2020 by the edict (EU) 2018/858) and supplemented by edicts (EG) 692/2008, (EG) 595/2009, (EU) 566/2011, (EU) 459/2012, (EU) 427/2016 („RDE1“), (EU) 646/2016 („RDE2“), (EU) 2017/1151, (EU) 2017/1154 („RDE3“) and (EU) 2018/1832 („RDE4“). For two and three wheeled vehicles holds equivalent guideline 2002/24/EG with edict (EU) 168/2013.

The limits were updated every 4 to 5 years until today, always lowering the limits. The development is shown in figure 1.5 and the limits for the latest emission standard ”EURO 6d”, which will be valid from 2020, are listed in table 1.2.

The compliance with the legislative limits is checked with type approval tests, where one representative for every vehicle is tested for the emissions. All identical vehicles are then authorized for public road traffic. These procedures are critical, since deviations in performance of the measurement influence the result. Thus they were standardized by UNECE regulations R83 for passenger cars and R49 for heavy duty vehicles.

R83 prescribes the testing procedure in a detailed way, distinguishing between gasoline, diesel and hybrid vehicles. Since 2015 it also explicitly prohibits ”defeat devices” in reaction to ”Dieselgate”. It also prescribes the methodology for the particle measurement very detailed, what is of

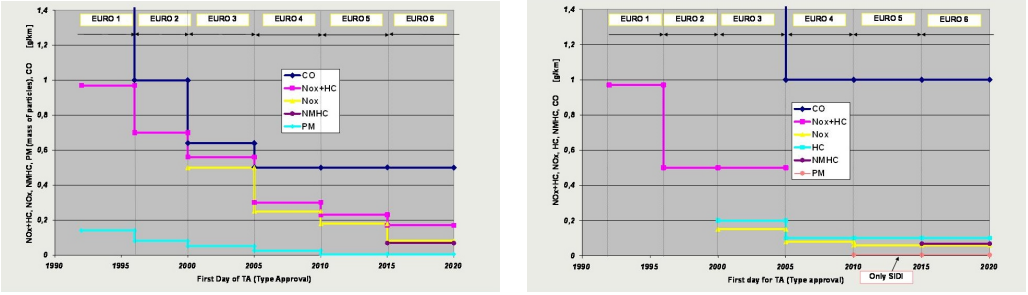

(a) Diesel (b) Gasoline

Figure 1.5.: Graphs of the development of the emission standards in Europe for passenger diesel and gasoline vehicles. CO. . . carbon monoxide, NOx. . . nitrogen oxides, HC. . . hydrocarbons, NMHC. . . not methane HC, PM. . . particulate mass. The PN limitation is not shown.

importance for this theses. A summary follows in the next section [Official Journal of the European Union EN, 2015].

The prescribed measurement technique is suggested by the Particle Measurement Programme (PMP), a program for development for particle measurement techniques in automotive exhaust, steered by the 2001 established working group of the UNECE transport division with the same name. It is an subgroup of the Working Party on Pollution and Energy (GRPE).

Particulate Emissions

Respective particulate emissions, particulate mass (PM) and particulate number (PN) are considered as measurands. The measurement equipment and its application are described in Appendix 4 for PM and Appendix 5 for PN, to Annex 4 in the R83 document.

The PM measurement is performed by gravimetric filter weighting (described in detail in section 2.2.1). The sample is drawn from a dilution tunnel (section 2.3.1), which simulates standardized environmental conditions to enable secondary particle formation. The sampled dilute exhaust has to be conditioned and the weighting has to be performed at standardized conditions.

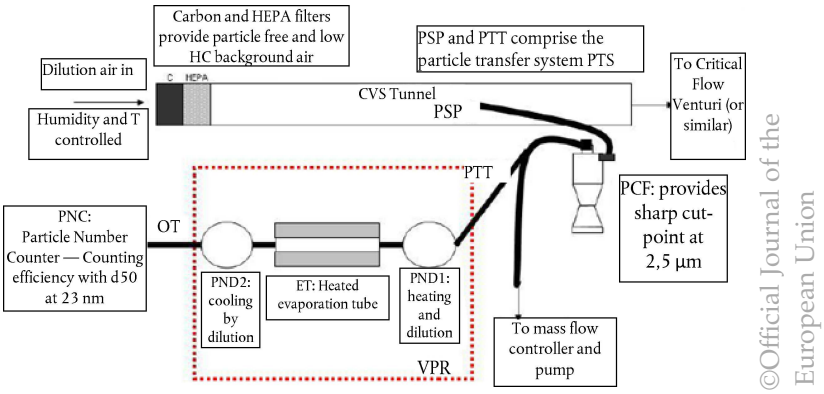

Figure 1.6.: Scheme of the recommended sampling system for PN measurement according to R83 [Official Journal of the European Union EN, 2015]. CVS... constant volume sampler, PSP... particulate sampling probe, PCF... particulate pre-classifier, PTT... particulate transfer tube, VPR... volatile partilce remover, PND... particle number dilutor, OT... outlet tube. The VPR comprises the parts within the dotted red rectangle.

PN is measured in a similar way, a scheme is shown in figure 1.6. Again the sample is drawn from a dilution tunnel by a sampling probe. The sample than shall pass a particulate size pre-classifier, a volatile particle remover (VPR - described in detail in section 2.3.2) and should than be measured by a well specified particle number counter (PNC). The sample should be diluted at 150 °C to 400 °C at least by factor 10 after the size pre-classification. At the PNC inlet again a gas temperature <35 °C should be reached, through cooling by further dilution of a factor 10 to 30. The size pre-classification should allow at least 99 % of 1 µm sized particles to pass and 50 % passing efficiency should be 2.5 µm to 10 µm. The VPR used should be able to remove 99 % of 30 nm particles from Tetracontane ($CH_3(CH_2)_{38}CH_3$) at an inlet concentration of $>1 \times 10^4\,\mathrm{cm}^{-3}$. The calibration and validation of the sampling system is prescribed as well as the PNC (see next section).

Particle Number Counter

The European regulation [Official Journal of the European Union EN, 2015] specifies, in compliance to the worldwide harmonized regulation [United Nations, 2014] requirements for allowed PNC devices. In summary the main points are:

- Full flow operation

- Maximum $\pm 10\,\%$ accuracy over the whole measurement range, down to $1\,\#/\mathrm{cm}^3$
- Linear response over the whole measurement range
- Counting efficiencies $(50 \pm 12)\,\%$ at $(23 \pm 1)\,\mathrm{nm}$ and $>90\,\%$ at $(41 \pm 1)\,\mathrm{nm}$

Until now these specifications can only be fulfilled by a Condensation Particle Counter (CPC - described in section 2.2.5).

1.2.4. Carbonaceous Aerosols - Soot - Black Carbon

Overview

Historically, soot was found as the first air pollutant in consequence of the high combustion of coal and wood in the industrialization era, peaking in the Great Smog of London in 1952 [Davis, Bell, and Bates, 2002; Penner and Novakov, 1996]. Further investigations than later revealed more subtle health effects triggered by carbonaceous air pollution than the imminent risk [Brook et al., 2010; Sauvain, Vu Duc, and Guillemin, 2003]. Also, lately evidence accumulates that BC emissions are the second biggest contribution of human made global warming [Bond et al., 2013]. Thus, in total a not negligible impact is caused by this kind of pollution.

As stated before, the term ”soot” comprises the carbonaceous fraction of exhaust particles. It is part of a carbonaceous aerosol, which arises from incomplete combustion of organic matter. In the environment, and also in automotive exhaust, particles appear in three distinguishable types, named ”nucleation mode”, ”accumulation mode” and ”coarse mode” (see fig. 1.8) [Eastwood, 2008; Giechaskiel, Maricq, et al., 2014]. The accumulation mode is mostly named soot in popular science. It consists from a core of persistent, nonsoluble (nonvolatile) Black Carbon (BC) covered by soluble (volatile) organic compounds [Bond et al., 2013]. As the name suggests the accumulation mode particles grow - accumulate - from primary core particles. These primary particles are much smaller than the formed aggregate, with a typical size range of $\sim$20 nm to 60 nm (see figure 1.7) [Eastwood, 2008]. Depending on the emission source, also sizes below 10 nm, e.g. from GDI engines, are possible [Dastanpour and Rogak, 2014; Karjalainen, 2014]. The number of primary particles in an aggregate spans from a few up to thousands, whereas the primary particle size does not correlate with the final

size of the agglomerated particle [Bond et al., 2013; Dastanpour and Rogak, 2014; Eastwood, 2008]. The agglomerated BC core is insoluble and with a vaporization temperature near 4000 K. As the name implies, it very efficiently absorbs visible light, with at least a mass cross section of $5\,m^2\,g^{-1}$ at 550 nm [Bond et al., 2013; Penner and Novakov, 1996].

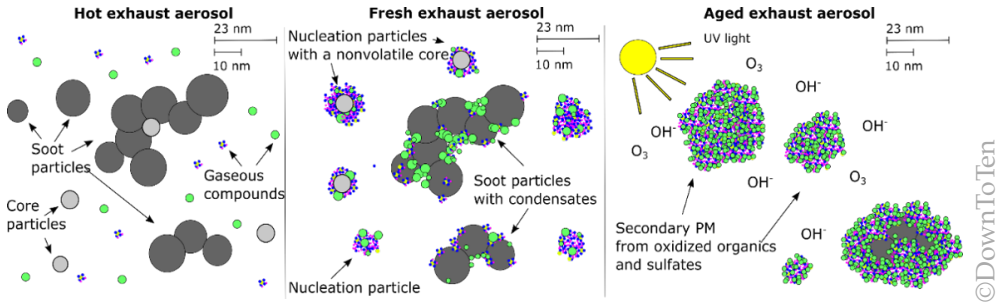

Figure 1.7.: Schematic representation of particles present in exhaust at different stages. The left figure shows the conditions in a hot exhaust, as it is inside of a tailpipe. The middle figure shows the condition of a cooled and diluted aerosol, as it is roadside. The figure on the right shows an aged exhaust aerosol, as present in an urban environment.

Nucleation mode particles consist of condensed volatile exhaust compounds (see fig. 1.2), as most studies suggest. Some evidence also suggest, that some are nucleation mode particles are solid or at least have a solid core [Eastwood, 2008]. The current legislation is considering only solid particle number emissions, thus influences or artifacts caused by nucleation mode particles are avoided by thermal treatment of the exhaust sample before measurement [Official Journal of the European Union EN, 2015].

Coarse mode particles are not directly emitted from the combustion engine, rather they are formed by the other two modes by accumulation and further growth at the walls of the pipe or tubing and a later drop off [Eastwood, 2008]. Coarse mode particles are in the size range of µm and are not of interest in the current legislation, before the measurement they are removed by a cyclone [Official Journal of the European Union EN, 2015].

Speaking of carbonaceous aerosols, the following discrimination is usual. Organic Aerosol (OA) comprises all carbon compounds with hydrogen and oxygen in the aerosol phase. It is formed by the volatile and soluble combustion products, the Primary Organic Aerosol (POA), which is also emitted by every BC source. The OA is thus the secondary aerosol of the POA. A scheme is shown in figure 1.9. Organic Carbon (OC) describes

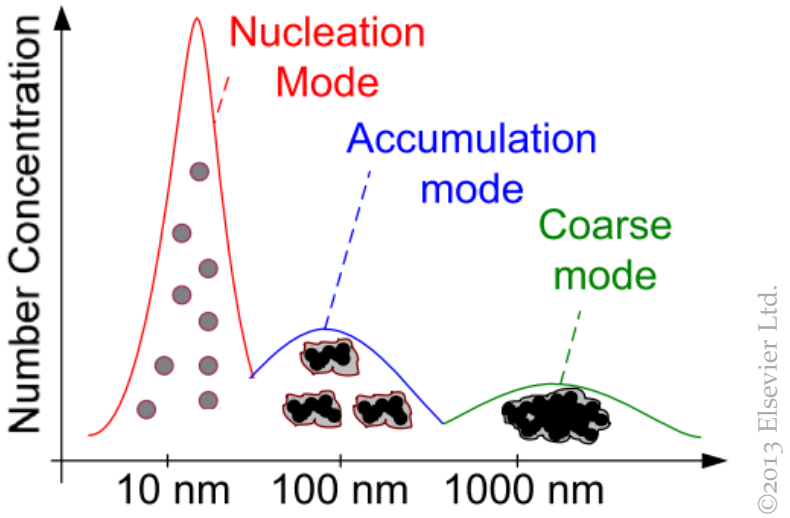

Figure 1.8.: Comparison of the size and contribution to exhaust PN concentration of the three types of carbonaceous particles.

the carbon mass within OA. BC and OA are forming together the total carbonaceous aerosol [Bond et al., 2013]. Sometimes the term brown carbon is used for BC with adsorbed OC components [Giechaskiel, Maricq, et al., 2014], what would best match the term "soot".

While BC is considered for its environmental impact [Bond et al., 2013; Jacobson, 2001], OC is found to be the cause for the health hazard which arises from carbonaceous aerosols [Haritash and Kaushik, 2009; Sauvain, Vu Duc, and Guillemin, 2003], since it includes Polycyclic Aromatic Hydrocarbons (PAH) and other hazardous and carcinogenic compounds [Öktem et al., 2005; Thomas Mckinnon and Howard, 1992].

Carbonaceous Aerosol Formation in Automotive Exhaust

The condition of the exhaust changes continually from the combustion in the cylinder until the tailpipe is reached and again drastic when it spreads into the environment [Eastwood, 2008; Giechaskiel, Maricq, et al., 2014]. Affected are mainly the volatile organic components and for diesel engines also the gaseous sulfuric acid, the water vapor content and especially the particulates. This has to be considered for measurements, since depending on the measurement position a different aerosol is sampled.

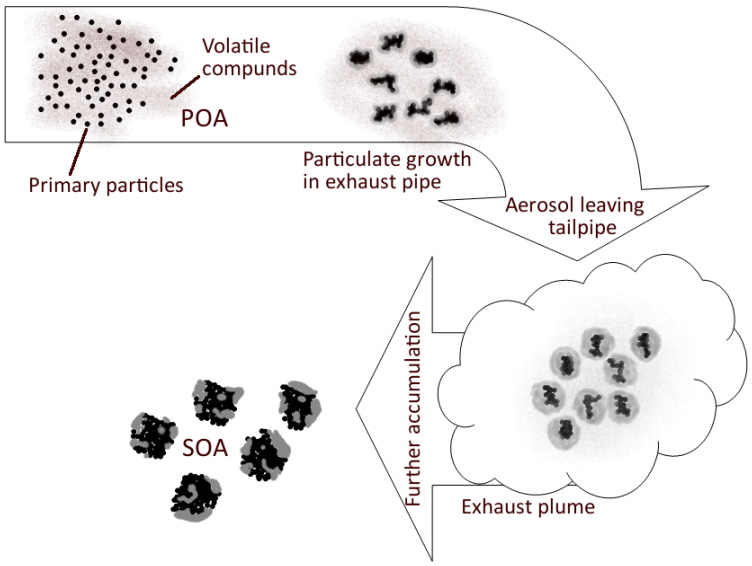

Figure 1.9.: Scheme of the process of carbonaceous aerosol formation. The POA is created by incomplete combustion, then particulates grow from the primay particles and a layer of volatile compounds is adsorbed. When the exhaust plume is formed by omission into the environment, condensation of volatile compounds is accelerated. From this particulates then the SOA is formed.

At the combustion in the at local fuel-rich regions also pyrolysis of the fuel and lubricants occurs, by what particles are formed. These primary particles, with a diameter up to 30 nm, then from aggregates already during the combustion. But up to 99 % of these black carbon particles are oxidized within the cylinder during the exhaust stroke. The remaining particles, already fractal shaped, then form with leftovers from fuel and lubricants the so called accumulation mode particles, consisting of the black carbon fractal particle covered with adsorbed volatile compounds of the exhaust. The particulate emission is then reduced by a particle filter for about 90 % and by an oxidation catalyst total hydrocarbons are further reduced, what means a reduction of PM. When the remained exhaust is leaving the tailpipe and confronted with a temperature drop of a few 100 °C and a dilution >1000 happens in less then 1 s, a local supersaturation of the volatile compounds occurs, what leads to further particle growth and formation of new particles. This secondary formation can be reinforced if a selective catalytic reactor (SCR) is part of the exhaust aftertreatment system [Eastwood, 2008; Giechaskiel, Maricq, et al., 2014].

Exhaust Particles, Secondary Aerosols and Environmental Impact

Depending to the ambient conditions the emitted particles contribute to the formation of SOA. Gaseous or volatile species in ambient air adsorb to the particles, thus deposition in the human respiratory tract becomes more efficient as in the gas phase [Shiraiwa, Selzle, and Pöschl, 2012].

Since hazardous components, like PAH or sulfuric compounds are also emitted by combustion engines, the formed secondary aerosol with present BC seeds becomes a health threat [Öktem et al., 2005]. Also, the SOA rises into higher atmospheric layers, where influences on earth climate are supposed, e.g. because the particles function as nucleation seeds for cloud formations. The SOA formation is a very efficient process, additionally it is pushed by photooxidation due to the solar radiation [Bond et al., 2013; Lee, Jang, and Kamens, 2004].

The small particles, present in the automotive exhaust system are not detectable in the environment at the emitted amount. Ultrafines reach background concentration within 150 m perpendicular to a road with a tenfold of concentration, PM_{10} halves its concentration within 100 m [Karner, Eisinger, and Niemeier, 2010].

The size of the emitted exhaust particles is also of interest from the regulative perspective. As stated above, in section 1.2.3, the PNC prescribed in the current legislation has to detect particles at 23 nm with 50 % efficiency. Thus, for certification measurements PN emissions until this size are regulated, emissions of particulates with sizes below about 20 nm are not considered at all (see fig. 3.2). Latest research shows that solid PN emissions in this regime are significant, thus a regulation for particulates $<$23 nm is expected in the future [Giechaskiel, 2019b; Giechaskiel, Joshi, et al., 2019; Giechaskiel, Lahde, et al., 2018; Giechaskiel, Vanhanen, et al., 2017; Leach et al., 2019]. Such a regulation might again focus on solid PN, as it is now, or might include also other types of particles. Nevertheless it will bring exciting challenges regarding measurement techniques and instrumentation [Giechaskiel, 2019a; Nakamura et al., 2019; Raza et al., 2018].

1.3. Problem Statement

An accurate determination of particulate emissions in automotive exhaust is of high interest for various reasons. First of all the environmental and health aspect, with knowledge of the exact emissions the observations in epidemiological and environmental studies can be interpreted more precisely. Further car manufacturers have to know the emissions of their engines to adjust it correctly and design an appropriate aftertreatment system, removing hazardous components in compliance with the legislative regulations. Also the legislator needs to know about the exact emissions to pass appropriate regulations. Heading the realization of such a measurement, five main problems have to be considered.

"How does the preconditioning of exhaust influence the measurement?"

The difficulty arises from the complexity of particle measurement and the conditions of the raw exhaust. Particle carrying aerosols react sensitively on manipulations of the ambient conditions. In section 1.2.3 the current legislative procedure of measuring particle emissions is outlined. The described procedure includes rough handling of the aerosol, causing changes of the particulate conditions. Since reliable PM and PN measurements in raw exhaust were not possible up to now, the actual conditions of the emitted carbonaceous aerosol are actually unknown.

"Is the standardization of losses sufficient?"

The legislative procedure was designed to assure reproducible conditioning of the exhaust gas, so a reproducible state of the exhaust gas at the measurement instrument is assured and also reproducible losses occur during the procedure. The influence of the conditioning system was characterized as good as possible, using cold and stable reference aerosols [Giechaskiel, Chirico, et al., 2010a], although the findings may not hold entirely for exhaust gas.

"Can raw exhaust be sampled directly?"

Because of the high temperatures, the aggressive compounds and the high humidity a direct sampling without preconditioning is not possible with available instruments. Also, if sampling of engine exhaust is required, particle number concentrations would be to high to be measured without dilution.

"How is an accurate measurement possible?"

On the other hand, the emissions per sample period of 1 s are very low, speaking of single particles cm^{-3} for a modern EURO 6d car. For a reliable measurement at such low concentrations a very accurate instrument is necessary.

"Can a new measurement fulfill the current constrains?"

In order to establish a new methodology of particle measurements in automotive exhaust, the guidelines of the current legislation have to be met. An enhancement can only be proven under the conditions the reference is operating.

Compendious research question

Since up to now it was not reliable possible to measure particulate emissions without prior influencing the sample. By characterizations of the sampling systems, the measurement is corrected towards the original exhaust state, but sill it could never be directly experimentally verified. Summarized two questions arise:

- *Is it possible to measure particulate emissions directly without an influencing preconditioning?*
- *Will the direct measurement and the measurement using preconditioning match?*

1.4. Scope

The aim of this work is to investigate possibilities for a direct measurement of particulate emissions in harsh environments, like existent in automotive exhaust. To reach this goal an understanding for the current measurement technology is necessary, but also for the particulates nature, their behavior and the interplay with ambient conditions.

Beginning with an overview of current particle measurement techniques for exhaust, also sampling and preconditioning systems, particle generators and instrumentation for particle classification are described.

The main topic of this thesis is the development and characterization of a High-Temperature Condensation Particle Counter (HTCPC), as an approach for direct and artifact free PN measurement of automotive exhaust. Findings regarding general CPC theory, describing material dependencies and involving the effect of capillary condensation, are discussed to bridge the technological gap between the HTCPC and established devices.

A setup for a in-situ Laser Induced Incandescence (LII) measurement system is presented as a complementary method for measuring PM in harsh environments.

1.5. Organisation of the thesis

This thesis is organized as a "Mantel" PhD thesis (§5 in the Curriculum for the Doctoral Programme in Technical Sciences [Graz University of Technology, 2012]), consisting of three publications and supplemental information. Within the thesis fundamentals and additional information is given to facilitate the understanding of the publications.

In chapter 2 state of the art techniques for particle measurement in exhaust, sampling and preconditioning systems and some general aerosol instrumentation, which was used for this work, is presented. General theoretical considerations and findings regarding the operation of CPCs are discussed in chapter 3, providing a deeper understanding of the instruments function. The development of the HTCPC is discussed in chapter 4. It includes two publications, describing the device, its characterization and application.

Section 5 comprises a further topic of this thesis, LII as an complementary approach to PN measurement, a suitable method for PM measurement in harsh environments.

The authors contribution is comprised in a short summary section at the end of every chapter. The relation to the state of the art is pointed out and an outlook of possible continuations is given.

The whole thesis is summarized and concluded in chapter 6.

2. Aerosol Instrumentation for Exhaust Particulates

2.1. General Remarks

Each of the in this chapter presented techniques could easily fill a scientists life. Here an overview of the possibilities of particulate instrumentation shall be given, thus for most techniques the descriptions will hold a basic level of complexity. CPCs, LII and sampling systems will be explained in more detail because of their importance for this thesis.

The selection of studied techniques is based on the state-of-the-art portfolio of automotive exhaust instrumentation. After a review of the techniques in the context of legislative compliant applications and with the aim to answer the research questions stated in section 1.3, an alternative concept of CPC technology was chosen as the main topic of the thesis and further a survey on LII, as an complementary PM measurement.

2.2. Measurement Techniques

2.2.1. Gravimetric Weighting

Gravimetric filter analysis is a widely used method for the determination of PM. An defined volume flow is lead over an High Efficiency Particulate Air (HEPA) filter, which captures 99.95 % of particulates bigger than 0.3 µm [Comite Européen de Normalisation, 2009]. The accuracy of the measurement is highly depending on the accuracy of the flow lead over the filter and the stability of the conditions while the filter is being loaded. Also very important are the conditions at the weighting and the reference weight. The

sample time has to be chosen appropriately for the measured concentrations and the sample flow, since enough mass has to be sampled for an adequate analysis. By usage of a size preselection before the filter loading, particle size distributions can be measured, e.g. $PM_{2.5}$ and PM_{10}.

This technique is used at various application fields like for cheap aerosol monitors as well as for high accuracy measurements.

According to the UNECE R83 [Official Journal of the European Union EN, 2015] the measurements has to be performed as follows (see figure 2.1): The sample has to be drawn from a thermally and flow regulated dilution (Constant Volume Sample - CVS) tunnel, which simulates standardized environmental conditions to enable the formation of the secondary aerosol particles, which are of interest. The sampled and diluted exhaust has to be $<52\,°C$ and all components used for aerosol leading shall be designed to minimize depositions. The sample should be drawn onto one single filter with an internal diameter of at least 12 mm, between 10 an 20 tunnel diameters downstream of the exhaust gas inlet. The size pre-classification should allow at least 99 % of 1 µm sized particles to pass and 50 % passing efficiency should be 2.5 µm to 10 µm. The sample flow has to be stabilized by more than $\pm 3\,K$ and has to be proportional to the total flow of diluted exhaust by more than $\pm 5\,\%$. The weighting should be done at $(22 \pm 3)\,°C$, $(45 \pm 8)\,\%$ relative humidity with the dewpoint maintained at $(9.5 \pm 3.0)\,°C$. Also calibration of the microbalance is prescribed.

2.2.2. Opacity Measurement

Opacity is the quantification of turbidity or haze, it is determined by the measurement of the transmittance of light through an aerosol (see fig. 2.2(a)). It can be described by the Beer-Lambert law [Baron and Willeke, 2001]:

$$T = \frac{I}{I_0} = e^{-s \cdot \sigma} \tag{2.1}$$

With T the transmission, I the detected intensity, I_0 the emitted intensity, s the extinction length and σ the extinction coefficient. $\sigma = \sigma_s + \sigma_a$ combines σ_s, the scattering coefficient, and σ_a, the absorbance coefficient, and is depending on the particulate number concentration c_n and the particulate

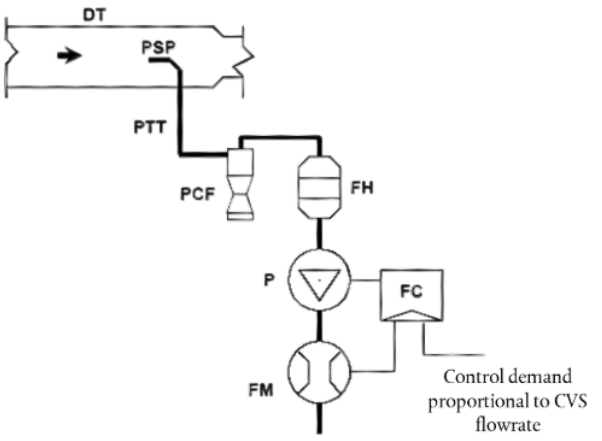

Figure 2.1.: Scheme of sampling system for PM measurement according to R83 [Official Journal of the European Union EN, 2015]. PCF... particulate pre-classifier, DT... dilution tunnel, FH... filter holder, P... pump, FC... flow controller, PSP... particulate sampling probe, PTT... particulate transfer tube, FM... flow measurement

size distribution d_p, $\sigma = \sigma(c_n,\ d_p)$. Effectively, only a determination of c_n is possible if d_p and the refractive index of the particles do not change during the measurement [Baron and Willeke, 2001].

For a reliable opacity measurement a sufficient particles have to be present in the light beam to detect a extinction. On the other hand for very high particle concentrations, the extinction coefficient changes because multiple particle scattering occurs. For modern cars the first case arises as a problem, since turbidity of the exhaust is measurable even at very high loads at all.

In Austria for passenger cars a measurement of the opacity is part of the mandatory §57*a* inspection according to UNECE R24 [United Nations, 1958] for licenses before EURO 6. For EURO 6 and later, currently inspection of the exhaust is done only by OBD sensors, but is likely to be replaced by a PN measurement in the next years.

2.2.3. Light Scattering

A refinement of the opacity measurement is the detection of scattered light instead of measuring the extinction of the primary beam, since only light which interacted with particles is detected (fig. 2.2(b)). Particles are

illuminated by a laser beam and a detector is placed in a certain angle to the optical axis. The light is partially absorbed and scattered by the particles and the scattered portion is the measurand in this technique. The scattering process is depending on the ratio between incoming wavelength and size of the particle, the light is interacting with. Depending on the process, the angular dependency of the scattering differs (see Table 2.1).

	Scattering regime	Angular dependency
$\lambda >> d$	Rayleigh	Dipole like
$\lambda \sim d$	Mie	Size dependent
$\lambda << d$	Geometric optics	Geometric optics

Table 2.1.: Scattering regimes for different ratios of the wavelength λ and the diameter of the particle d.

Light scattering techniques are used for diverse applications e.g. material analysis like Small Angle X-Ray Scatterig (SAXS), imaging methods like Computed Tomography (CT) or the here emphasized particle detection.

For measurements of particles by light scattering, a laser beam is directed onto a particle flow. For visible light, with $\lambda \approx 400\,\text{nm}$ to $650\,\text{nm}$, Mie scattering is occurring for particles up to about a few µm. Appropriate data analysis thus allows the measurement of mass concentration and the absorption coefficient (therewith the particulate number, as stated in section 2.2.2), with a calibrated instrument, a constant particulate number distribution and constant properties of the particulate ensemble. With these requirements, mass concentration and absorption coefficient are directly proportional to the scattered intensity [Axmann, 2014]:

$$c_C = \frac{C}{I} \tag{2.2}$$

$$c_{\sigma_a} = \frac{\sigma_a}{I} \tag{2.3}$$

With C the mass concentration, σ_a the absorption coefficient, I the detected scattered intensity and c_C and c_{σ_a} the conversion factors. For a measurement of C and σ_a the conversion factors have to be determined by calibration [Axmann, 2014].

Mie scattering also allows inspection of particle size, since the angular distribution of the scattered intensity is depending on it. In terms of a physical model the connection between the scattered intensity and the size of the scattering object can be given by the from factor $P(q)$. Basically, it describes the distribution of the scattered intensity in dependency of the scattering vector $q = \frac{4\pi}{\lambda} \cdot sin(\frac{\theta}{2})$, with θ the scattering angle. For light scattering experiments the dependency $P(q)$ to the scattering particles size can be modeled and by comparison of the measurement and the model the size can be determined [Ogendal, 2013]. The corresponding measurement is called Static Light Scattering (SLS). Depending on the particles shape the complexity of the modeling varies. The simplest case are spheres, like the droplets counted by a CPC, but also inspection of e.g. fractal aggregates is possible [Sorensen, 2001].

2.2.4. Optical Particle Counters

For an accurate PN determination, the counting of particles is necessary. In its easiest version, a very narrow particle carrying aerosol flow is lead through a light scattering setup (see section 2.2.3). These devices are called Optical Particle Counters (OPC - fig. 2.2(c)). The operation is limited by size and concentration of the particulates, since with decreasing size the scattered intensity also decreases and can not be detected anymore below a certain particle size. Advanced sensors cover sizes down to 100 nm [Heim et al., 2008], whereby the upper size is usually limited by a preceding size selection. The measurable concentration is from single particles upwards and limited at higher values. If particulates overlay when passing the light beam, their separation by inspection of the scattering signal is difficult. About 30 000 #/cm^3 can be counted reliably at a flow rate of 1 L min^{-1} [Brunnhofer et al., 2019]. Higher concentrations can be reached by advanced particle counting methods, or simply dilution of the sample. Dilution however increases the measurement uncertainty since it reduces the sample size, especially at low concentrations if counting experiments are analyzed according to Poisson statistics [Maierhofer et al., 2019].

OPCs are widely used like in environmental sensing or in industry e.g. for clean room monitoring. By evaluation of the scattered pulses also particle size determination, and by additional consideration of the particulates

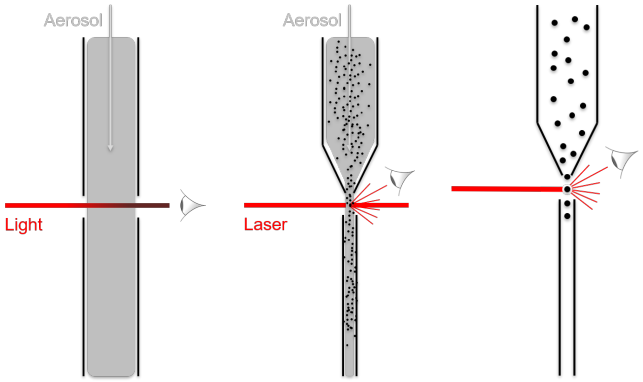

(a) Opacity Measurement (b) Light Scattering (c) OPC

Figure 2.2.: Schemes of the three mentioned optical measurement methods. The opacity measurement a) is a collective measurement at for turbid aerosols. Light scattering b) is a more sensitive method, enabling measurement even at low mass concentrations. With an OPC c) even single particle detecion is possible.

density, also a PM estimation is possible [Binnig, Meyer, and Kasper, 2007; Tittarelli et al., 2008].

2.2.5. Condensation Particle Counters

Determination of PN for particulates with sizes below the optical detection limit using an OPC is possible by a preceding particulate magnification. This is done by controlled condensational growth of droplets around the original particulates in a supersaturated vapor (the process of nucleation is described detailed in section 3.1). The whole setup comprising the magnification stage and the OPC is called Condensation Particle Counter (CPC) or Condensation Nuclei Counter (CNC).

CPCs are well established devices for measuring PN concentrations in aerosols [McMurry, 2000; Sem, 2002; Wang et al., 2010]. These in general simple devices were studied and developed by various groups all over the world, evolving it to a reliable high-tech instrument [Kuang et al., 2012; Stolzenburg and McMurry, 1991]. The application field covers clean room monitoring [Zhang and Liu, 1991], atmospheric [Wehner et al., 2011] or ambient measurements [Seipenbusch, Binder, and Kasper, 2008] and classification of automotive exhaust [Giechaskiel, Maricq, et al., 2014]. Therewith

also covering a big bandwidth of measurable concentrations and particle species. Specialized instruments are available for every application, even hand-held devices [Hämeri et al., 2002] are available.

For a controlled condensation a defined supersaturation is necessary, therefor a certain volume flow of a saturated vapor from a heated working fluid is created in the so called saturator. It is dimensioned in a way that the vapor is uniformly tempered at the outlet. From there the vapor is lead, passing a thermal insulation, into the cooler condenser. By the cooling of the vapor, the amount of substance which can be in the vapor phase at equilibrium conditions decreases and a supersaturated vapor arises. Particulates present in the supersaturated vapor serve as nucleation seeds and trigger droplet growth. This process is often called "particle activation". The length of the condenser and thus the remaining time of the droplets in the supersaturated vapor defines the end size of the droplets. That way particulates from ∼nm can be magnified to easily detectable ∼µm droplets. The original size, or actually volume, of the particulate does not influence the end size of the droplet, since the share of the particulates volume to the one of the droplet is negligible. For instance the ratio of the volume from a sphere with the diameter of 100 nm to one a with 1 µm diameter is 1:1000, whereas the ratio of the diameter is 1:10. The minimum size of activated particles is set by the supersaturation, see section 3.1 for details.

Inside the condenser usually a wick is placed, a porous material which enhances with its high surface the 100 % vapor saturation. Usual working fluids are n-Butanol or n-Isopropanol at operating temperatures between 10 °C to 30 °C for the condenser and 30 °C to 40 °C for the saturator. The actual geometry of the device differs between the single devices and is optimized for the contemplated application.

CPCs enable reliable single particle counting of particles down to 1 nm [Kuang et al., 2012], what is certainly close to the regime of single molecule sizes. The plausibility of these developments shall not be discussed here, just the possibilities emphasized. The concentration range which can be covered is limited the same way as for OPCs, at some concentration more than one particle at a time passes the laser beam regularly and single particle detection is not possible any more. The measurable concentration can be extended by dilution of the sample, but the measurement uncertainty is thereby increased.

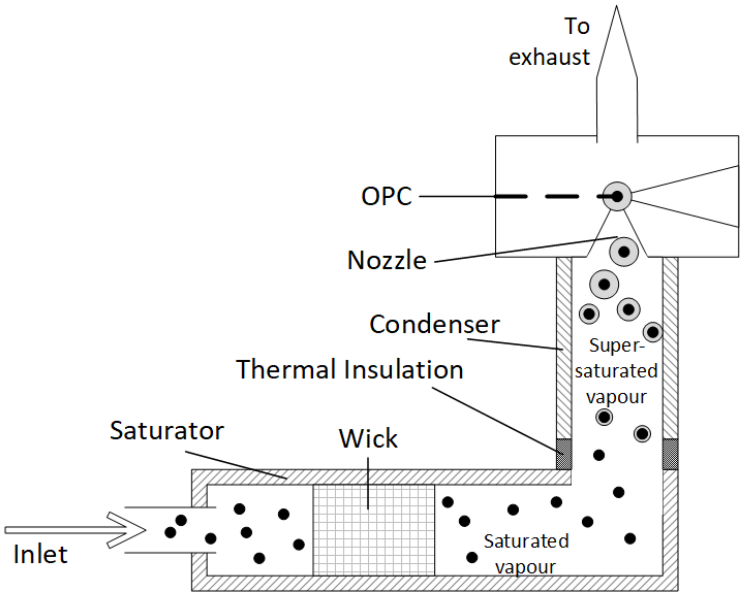

Figure 2.3.: Functional scheme of a CPC. The particulate carrying aerosol is entering the saturator where it is mixed with a saturated vapour. The mixture is lead into the cooler condenser where the vapour condensates onto the particulates, growing them to an optically detectable size.

A special version of a CPC is the MAGIC water CPC [Hering, Stolzenburg, et al., 2005], using water as working fluid. Since for water vapor the mass diffusion happens faster then thermal diffusion in air, this device follows another concept. The device consists from a conditioner, a growth tube and an OPC. A particle carrying sample aerosol is lead into the conditioner, which is held at higher temperatures as the sample aerosol. Because of the high mass diffusivity of water, the vapor condenses on the cooler particulates before the heat flux heats the particles up. In the warmer growth tube the particles grow further in a saturated water vapor.

2.2.6. Photoacoustic Spectroscopy

Photoacoustics describers the detection of an acoustic signal at photonic (optical) stimulation [Bell, 1880]. By periodic illumination of a particulates by a laser, a certain portion of light will be absorbed. The warming of the particulate causes a rise of the temperature of the surrounding gas, thus generating sound waves. The frequency of the periodic illumination defines the frequency of the acoustic signal. By measurement of the intensity of the

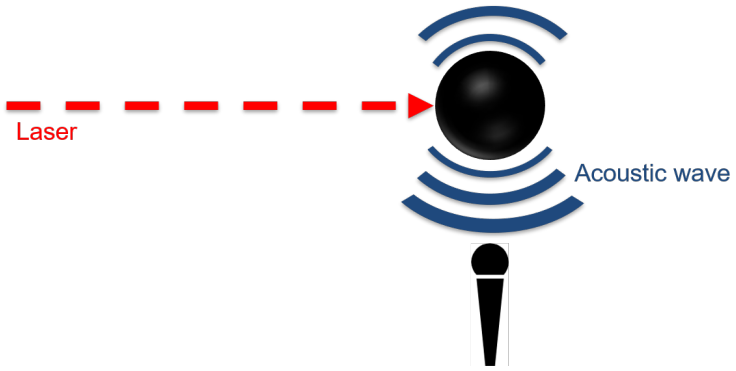

Figure 2.4.: Principle of the photoacoustic spectroscopy. By periodic heating, detectable sound waves are created.

acoustic wave, the mass fraction can be determined. Thus, the denomination Photoacoustic Spectroscopy (PAS). By choice of a spectroscopic wavelength, the method can be adopted to various gases and particle species.

For particulate emissions a BC measurement can be realized very efficiently, since the absorption coefficient is very high. By usage of a laser beam in the near infrared the cross sensitivity to other compounds of the exhaust is minimized. Appropriate design of the measurement cell and thus adjustment of the resonant frequency of the cell, concentrations of $1\,\mu g\,m^{-3}$ can be measured [Schindler et al., 2010]. Strictly a separation of the contribution of BC and other absorbing materials in the exhaust, like ashes or some gases, is not possible [Eastwood, 2008]. Thus the quality of the measurement is contingent on a calibration using particulates from a combustion (see section 2.4.1).

PAS is currently one standard technology for measuring PM in automotive exhaust. Since it allows miniaturization, also devices for on road measurements are available. These devices are called Portable Emission Measurement Systems (PEMS) [Rubino et al., 2010].

2.2.7. Laser Induced Incandescence

Related to PAS is the Laser Induced Incandescence (LII) technique. It bases on the same principle, namely thermal stimulation and the detection of a response. LII uses a laser energy that high, that particulates are heated to incandescence. The detection is hence not acoustic but optical [Vander

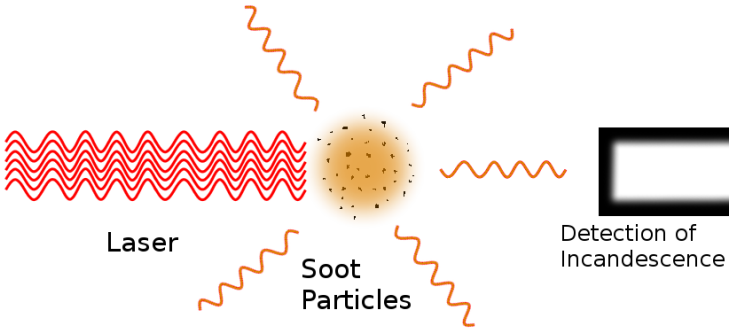

Figure 2.5.: Scheme of LII. By a high power laser a bunch of particulates is heated and its glowing is detected.

Wal and Weiland, 1994]. At such high laser energies, typically MW/pulse, spectroscopy is not feasible any more. Also the specimen has to have the required temperature resistance for incandescence. Thus this technique is somehow predestined for BC measurement in exhaust gases, since no cross sensitivity to any gaseous compound is possible and any volatile particulate evaporates [Zizak, 2000]. On the other hand, for a reliable analysis of the measured LII data some assumptions regarding critical influences have to be done. Like the uniform heating of the particles regardless their sizes, a constant incandescence and no influence on the particulate by the measurement [Eastwood, 2008]. Hence, the physical model used for evaluation is very important for a reliable LII measurement. The LII process is described in more detail in section 5.

The handling of this technique requires advanced technology. The laser pulses are typically of ns duration with an pulse energy of mJ, what results into MW of power [Wainner and Seitzman, 1999]. Since repetition rates of 10 Hz and higher are of interest to resolve engine load changes adequately, a special laser module is required. The incandescence signals, which have to be detected are of ∼100 ns duration and magnitudes lower than the excitation energy. Thus very sensitive detectors are required, which are 100 % shielded from the excitation wavelength. Further fast electronics are necessary to process the short pulses and perform the extensive analysis in real time. Nowadays these technologies are available and a realization of a LII system for automotive exhaust can be realized [Kupper, Pulko, et al.,

2019].

Nowadays LII is mostly used for scientific purposes, e.g. to inspect the formation and sizing of primary particles in flames [Wainner and Seitzman, 1999], for measurements of particulate concentrations or particle synthesis [Schulz et al., 2006]. Commercialized systems are available for environmental measurements of BC and also for aviation exhaust measurement, but are not widely established.

2.2.8. Measurement of Electrical Charge

Since particles can carry carry an electrical charge, this can be utilized for measurement techniques, whereat the charging mechanism itself requires the same attention as the detection. For the measurement of exhaust particulates photoelectric and diffusion charging is of importance. The first method charges particulates by irradiation of particulates. Electrons were emitted according to the photoelectric effect, thus a positive charge remains (also called photoionization). The electrons are captured by gas atoms, turning them into negative ions which can be precipitated by a weak electrical field [Baron and Willeke, 2001; Eastwood, 2008; Nishida, 2018]. At the second method ions attach to particulates by diffusion, thus charging the particulates. Therefor ions have to be created e.g. by an radioactive source or an electric (corona) discharge [Eastwood, 2008; Siegmann and Siegmann, 2010]. Exhaust gas particulates usually already carry charges when they are emitted. These charges would bias an electrical measurement, thus they have to be removed before the charging with a so called neutralizer. Therefor the particulates have to be mixed with bipolar ions e.g. produced by a corona discharge [Hinds and Kennedy, 2000] or by photoionization without a the removal of the negative gas ions [Eastwood, 2008].

The charged particulates then can be evaluated in different ways. In general the charge signal carried by the particulates correlates with their active surface area [Siegmann and Siegmann, 2010]. By considering the charge distribution of the particles in the measured aerosol [Fuchs, 1963; Wiedensohler, Lütkemeier, et al., 1986], PN can be measured by these devices. For exhaust gases the following measurements are of interest:

- **Sampling** on a conductive filter allows the measurement of the charge by an electrometer and subsequent filter weighting [Baron and Willeke, 2001].
- By a **Faraday cup electrometer** the equalization charge is measured with an electrometer when the charged particulate is passing through [Hinds and Kennedy, 2000; Siegmann and Siegmann, 2010].
- A **Electrical Low-Pressure Impactor (ELPI)** is a cascade impactor (see section 2.3.3) whereby the deposited current is measured in real time, measuring size distributions [Marjamäki et al., 2000].

2.3. Sampling and Preconditioning

Measurement instruments, as described in section 2.2, accept samples at certain temperature and volume flow and can handle certain amounts of particulates. If a sample of automotive exhaust are drawn, it has to be conditioned for the measurement because of the high temperatures, particulate concentrations and existing volatile compounds. By inconsiderate handle of particulate carrying aerosols size depending high losses can occur, thus the preconditioning procedure has to be realized consciously, for a representative and reproducible measurement.

2.3.1. Exhaust Dilution

Whether the measurement is stationary at a testbed or mobile at a vehicle different systems are applicable, also depending in which state of the exhaust particulates should be at the measurement, different dilution techniques have to be used.

Dilution Tunnel/Constant Volume Sampler

When the exhaust leaves the tailpipe and forms the known plume, the conditions change drastically. The temperature drops for a few 100 °C and a dilution >1000 happens in less than 1 s [Eastwood, 2008]. Thereby the volatile compounds of the exhaust condensate on the already existing particulates or nucleate to particulates smaller 100 nm. The so formed aerosol

is different regarding PN and size distribution compared to the exhaust before leaving the tailpipe. For an minimization of the environmental impact the aerosol spreading into the environment has to be known. Thus by a dilution tunnel standardized conditions are constructed for an reproducible measurement [Giechaskiel, Maricq, et al., 2014; Hooftman et al., 2018].

The sampled exhaust is lead by a so called transition line into the dilution tunnel. This transition line should be conditioned and held at a justifiable length to minimize deposition of particulates (see section 1.2.2 for details). The UNECE regulation regarding emissions for type approvals of vehicles addresses this point explicit [Official Journal of the European Union EN, 2015], since the influence on the sample can be immense if the possible deposition mechanisms are considered insufficient or inconsequent [Wei, Kittelson, and Watts, 2001].

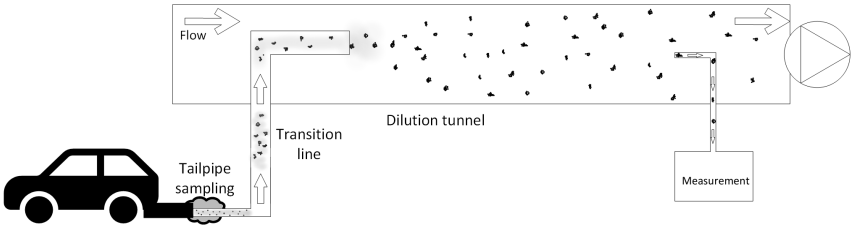

Figure 2.6.: Schematic representation of a diltution tunnel.

The dilution tunnel itself can be realized in different ways. First, the full exhaust flow can be sampled, or just a portion. Further, on one hand the dimension can differ and on the other hand the kind of dilution. Both influence the formation of the aerosol and the measurement and is thus regulated by the UNECE regulation [Official Journal of the European Union EN, 2015]. The prescribed method is the Constant Volume Sampler (CVS) dilution tunnel, where the total flow through the tunnel is held constant, so the sample flow is proportional to the exhaust flow. Other methods are a constant dilution ratio, what requires the knowledge of the sample flow, or a constant dilution flow, what is realizable easy but gives an undefined dilution [Eastwood, 2008].

Rotating Disc/Chopper diluter

A disc with cavities rotates at a certain speed and transports with the cavities exhaust from a sample line into a dilution line. The dilution is thus given by

the size of the cavity, the rotating speed and the flow in the dilution line. That way dilution ratios between 1:10 and $1:10^4$ are possible without influencing the size distribution under 1 µm, above the inertia of the particulates causes impaction inside the cavity [Hueglin, Scherrer, and Burtscher, 1997]. By the systematic of "shoveling" the exhaust into the dilution flow, discrete samples are taken from the sample flow creating a batch-wise measurement [Eastwood, 2008].

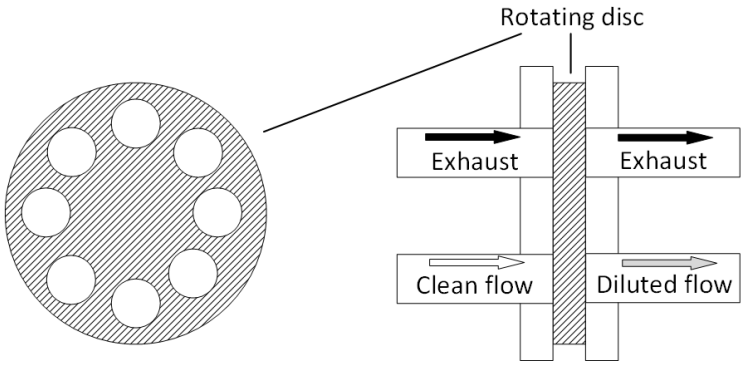

Figure 2.7.: Schematic representation of a rotating disc dilutor. Exhaust is transported into the clean flow by the rotation of the disc.

A system can be realized very compact, thus also suitable for mobile applications. Further the diluter itself can be made from temperature sustainable materials and heated for a minimization of thermophoretic deposition (see section 1.2.2 for details).

Porous Tube diluter

A porous tube is placed concentric inside a pipe. Exhaust is lead through the inner porous tube and into the space between the outer pipe and the inner porous tube the dilution gas is leaded. The dilution gas passes through the porous tube, dilutes the exhaust and by its flow it keeps the particulates away from the walls. Typical dilution ratios are 10 to 30, with an minimal influence on the size distribution, for small as well as for µm sized particulates [Mikkanen et al., 2010].

Because of its simplicity a miniaturization is possible and since for operation just the dilution flow is needed, also mobile applications are possible. A drawback of this method is the poor mixing of the aerosol with the dilution

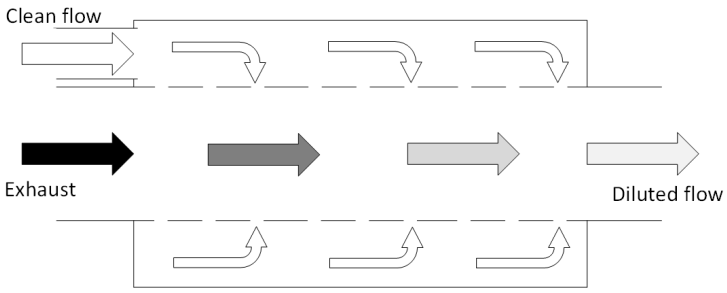

Figure 2.8.: Schematic representation of an porous tube dilutor.

gas, leading to an uneven particle distribution over the cross section of the dilutor.

Ejector diluter

A Venturi nozzle operated with a dilution gas and exhaust at the intake, provides a constant dilution. Again, because of its simplicity miniaturization is possible. For its operation the dilution flow is needed and also the device has to be heated to prevent condensation [Eastwood, 2008]. This kind of dilution is quite rough, influencing the particulates with the turbulent flow after the nozzle and by the temperature drop because of the expansion. The heating prevents condensation of volatile compounds but deposition of particulates occurs inside these diluters, what influences the flow and thus the dilution ratio should be monitored [Ntziachristos, Giechaskiel, et al., 2004].

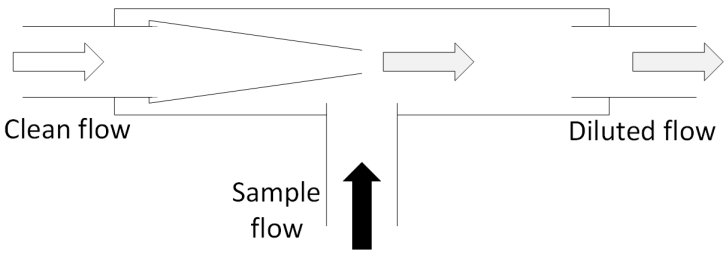

Figure 2.9.: Schematic representation of an ejector disc dilutor.

Such devices are commercially available with dilution ratios of 1:50 [Dekati Ltd., 2019a] or up to 1:225 for a tandem setup [Dekati Ltd., 2019b].

2.3.2. Removal of Volatile Compounds

As stated in section 1.2.4, automotive exhaust consists from primary particles and volatile organic compounds (VOC), the primary organic aerosol (POA). Depending on the conditions the exhaust experiences, a different secondary aerosol is formed from the solid and the volatile fraction. Also it was found that volatile compounds cause artefacts in PN measurements, leading to an overestimation of small particulates [Zheng et al., 2011]. Thus, for an reproducible measurement the solid particulates can be measured after an removal of the volatile compounds. Further, the current legislation also limits only the solid PN [Official Journal of the European Union EN, 2015].

Evaporation Tube/Themodenuder

The simplest approach for removal of volatile compounds is by evaporation though heating [Kreidenweis, McLnnes, and Brechtel, 1998]. This technique origins from environmental sciences and is applicable, if by the evaporation not again a saturated vapor is created, which would condensate again after cooling down. This is the case for most environmental aerosols, but not for automotive exhaust sampled from the exhaust pipe. For this application after the evaporation tube a "adsorber tube" is added, which is actively cooled and equipped with an adsorbing material, like activated charcoal [Burtscher et al., 2001]. Such a device was commercialized as "Themodenuder" (TD) [Dekati Ltd., 2007]. For its usage high losses for small particulates have to be considered, because of thermophoretic and diffusional losses (see section 1.2.2 for details). For an adequate heating and cooling it has to be operated with a flow rate of $2.5\,\mathrm{L\,min^{-1}}$, thus arises a calculated penetration efficiency of 35 % and 75 % for 5 nm and 100 nm sized particulates. Also still measurement artifacts cause by semi-volatile particulates can occur [Swanson and Kittelson, 2010].

Catalytic Stripper

Diluted exhaust is lead through catalytic material heated to 300 °C, thus removing volatile compounds by oxidation and/or adsorption [Abdul-Khalek and Kittelson, 2010]. The penetration efficiency for 5 nm and 100 nm

sized particulates was determined to 10 % and 70 % for a flow rate of 10 L min^{-1}. Thus the losses of nonvolatile particulates are higher then for the TD, but the removal of volatile compounds is more efficient. It completely prevents the occurrence of artifacts down to 3 nm [Swanson and Kittelson, 2010]. A comparison with a PMP compliant APC, shows a higher removal of volatile particulates for the CS also for particulates below 23 nm [Zheng et al., 2011].

Volatile Particle Remover according to UNECE R83

The Volatile Particle Remover (VPR) is a system in compliance with the requirements of UNECE regulation R83 for particulate emissions of passenger cars, described in section 1.2.3 [Official Journal of the European Union EN, 2015]. Also see figure 1.6.

It can consist e.g. from two ejector diluters (see section 2.3.1), with an evaporation tube in between. The first ejector diluter is operated with an dilution ratio between 9 to 15 heated to 150 °C, the evaporation tube is heated to 300 °C and followed by the second unheated ejector diluter. Losses are expected low because of the rapid cooling at the dilution [Giechaskiel, Chirico, et al., 2010b].

Realized another way, it can consist from a rotating disc diluter (see section 2.3.1), heated to 150 °C, followed by an evaporation tube and a porous tube diluter (see section 2.3.1) [Giechaskiel, Cresnoverh, et al., 2010a; Zheng et al., 2011]. Such a system was commercialized in the Advanced Particle Counter (APC) by AVL List GmbH [AVL List GmbH, 2019].

The VPR achieves the specification of the R83 [Giechaskiel, Chirico, et al., 2010b], but evidence suggests, that the PMP suggested VPR leads to an insufficient removal of volatile compounds for particulates below 23 nm[Swanson and Kittelson, 2010; Zheng et al., 2011].

2.3.3. Size Selection

Impactor

Taking advantage of the particulates inertia, a efficient deposition is possible (the process of impaction is described in section 1.2.2). By a adjustment of flow velocity and a abrupt change of the flow direction, e.g. by the flow towards a plate, particulates below a certain mass pass the obstacle whereas particulates with higher mass are deposited. A size selection is possible according to the aerodynamic diameter.

Its application is generally feasible down to very small sizes, what is used e.g. for particulate sampling [Marple, Liu, and Whitby, 1974] or as a cascade within the ELPI [Marjamäki et al., 2000]. A usual application is also a coarse preselection of ”big” particulates.

Cyclone

Not exactly an impactor, but also basing on the particulates inertia is the cyclone. By forcing the aerosol into a helical movement by a accordingly formed vessel, due to the centrifugal force particulates above a certain mass are deposited.

Such a device is currently prescribed by R83 for preselection of coarse particulates as the pre-classifier.

Differential Mobility Analyzer

By passing a flow of charged particulates trough a transverse electrical field, a separation according to mass and charge, thus according to their *electrical mobility*, will happen. Taking advantage of this, within an Differential Mobility Analyzer (DMA) charged particulates are led between a cylindrical grounded housing and a negative electrode in its center. By varying the voltage of the electrode 10 kV to 10 000 kV, the mobility diameter of particulates reaching the outlet can be set, thus a size selection performed [TSI Inc., 2019a].

The DMA was commercialized by TSI Inc. It has to be operated in combination with the Electrostatic Classifier, a support device for the DMA, which provides the necessary flows and the charging ("neutralization", since the overall charge is zero) of the particulates [TSI Inc., 2019c]. DMAs and electrostatic classifiers are widely used in aerosol science.

Scanning Mobility Particle Sizer

A electrostatic classifier and DMA followed by a CPC gives a setup capable of measuring the number concentration of particulates in aerosols. The combination is called Scanning Mobility Particle Sizer (SMPS) [TSI Inc., 2019d]. Also the SMPS is an established and widely used instrument in aerosol science.

2.4. Particle Generators

For testing purposes of particle measurement techniques defined test aerosols are indispensable. Novel instruments have to be characterized under controlled conditions, so a calibration can be done. For the calibration again defined test aerosols are needed. The controlled production of airborne particles with certain properties is an art in itself in aerosol sciences. Here the devices used within thesis will be presented, one of them an own built spark generator.

2.4.1. Combustion Aerosol Standard

Combustion generated particulates come along with the POA, what requires a different treatment as pure solid particles. For laboratory examinations with exhaust instrumentation a combustion generated test aerosol has to be used. The Combustion Aerosol STandard (CAST) is simplified a diffusion flame burner with fine-tunable flows of Propane, Air and Nitrogen thus stable incomplete burning can be practiced. Thereby and by quenching of the flame, big amounts of soot can be produced and by change of the settings the size distribution and mass emission can be influenced [Jing, 1999]. The reproducibility of the aerosol is sometimes an issue of the CAST,

with regular maintenance and cleaning the stability should be within 10 % regarding the mode diameter and a factor two for the concentration [Moore et al., 2014].

2.4.2. Spark Particle Generators

Taking advantage of spark erosion, particles can be generated from any solid conductive material. By placing two electrodes from the same material vis-à-vis and applying a AC high voltage, particles are formed from the electrode material [Mäkelä et al., 1992].

When two conductive parts, here the electrodes, are placed vis-à-vis and the difference of the electrical potential is high enough, an electrical breakdown occurs even if a nonconductive medium like air is in between. The electrons have to overcome the resistance of the medium and the work function (the enery needed to remove an electron from a solid - typically some eV), what requires high field strength. When the current is flowing through the air, it is ionized along the path of the electrons - a plasma is generated. This is called a gas discharge. Depending on the power of the electron current, different conditions are taken. The most efficient particle generation is achieved by a spark discharge, rather than by a stable electric arc. Driven by impact ionization a multiplication of charge carriers happens, thus more arrive the anode then left the cathode. Therefor typically some mA of current and kV voltage are needed at a few cm of distance between the electrodes in air.

The erosion of the electrode material is caused by the release of atoms from the electrode material through the delivery of more energy than the bonding energy of the atom is. This is done thermally and electrically - through heat and a present electric field. The contributions change with the power, at very high powers the thermic effect prevails, the atoms are sublimated directly. This applies for a stable electric arc. At lower powers the electrical field provides the necessary energy, thus the necessary applied voltage for a spark discharge is very high ($\sim$kV) and for the sustainment of a electric arc is very low ($\sim$V).

As a consequence of the erosion, atoms are brought into the gas phase. Caused by thermophoresis and the concentration gradient a mass transport away from the electrodes occurs. With falling temperatures the vapor will

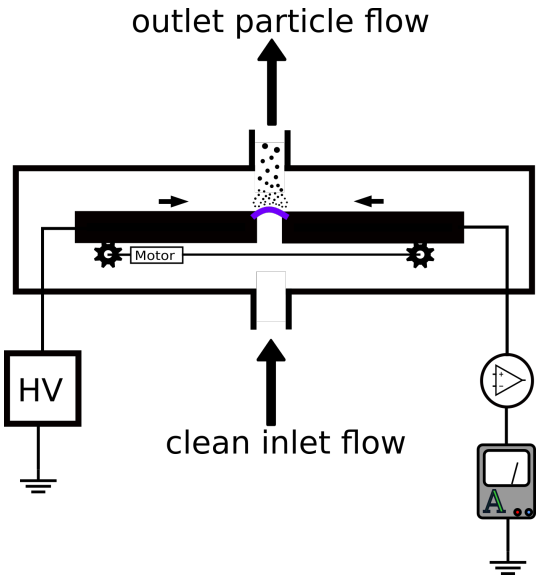

Figure 2.10.: Scheme of a spark particle generator.

condensate to droplets and after the temperature falls below the melting point further coagulation leads to fractal particles. If oxygen is present during this process, oxidation is very likely. For prevention the particle generation can be done in an inert gas atmosphere.

The electrical current can be used as a control parameter. If it is held constant at a fixed electrode distance and applied voltage, a constant erosion and therewith a constant particle generation is possible.

Realization of a Spark Generator

Within this thesis a spark particle generator was realized. A commercially available XP-Power FS60P-12 high voltage (HV) module was used for generation of the necessary high voltage. By applying a input voltage between 0.7 V to 12 V proportionally a high voltage between 0.2 kV to 6 kV with a power between 0 W to 10 W is available at the output. Two electrodes were connected to the HV output and placed vis-à-vis with ∼0.5 cm space in between. When the module is switched on, a spark between the electrodes produces a short circuit at the modules output. The chosen HV module has a short circuit detection, thus the electrical current is interrupted every time

a spark occurs. Therewith spark discharges with the chosen HV module occur with a frequency of about 50 Hz.

For safety reasons the setup was built into a plastic container with a safety switch, prohibiting operation with the opened box (Fig. 2.11(a). The electrodes were mounted with 3D printed, isolating parts, which were attached to a thread rod for adjustment of the distance between the electrodes. A chamber was 3D printed to include the ends of the electrodes and enabling a continuous flow of air or an inert gas for reproducible particle generation.

The spark particle generator can be equipped with different electrodes. Until now experiments with zinc and graphite (see figure 2.11(b) for the size distribution) with a filtered airflow were done. The generated size distributions were stable for hours of operation at a fixed input voltage and distance.

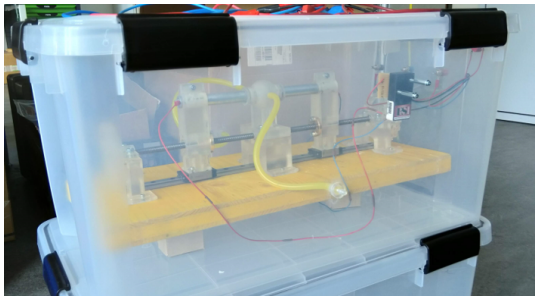

(a) Photography of the plastic container with the spark particle generator.

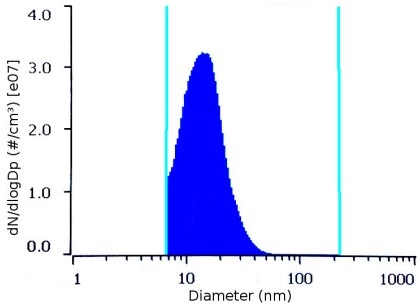

(b) Size distribution of generated particles from graphite electrodes.

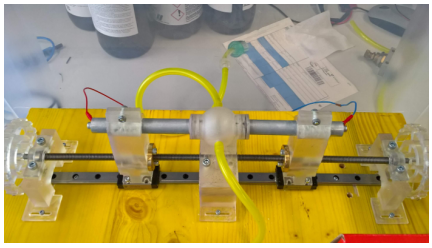

(c) The spark particle generator equipped with zinc electrodes.

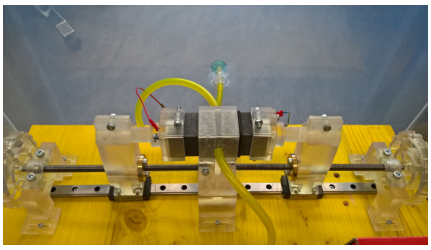

(d) The spark particle generator equipped with graphite electrodes.

Figure 2.11.: The realized spark particle generator.

Systematic variations of the input voltage and the distance between the electrodes caused marginal changes of the size distribution. This remarkable

behavior is probably due to the internal short circuit protection of the HV module used.

2.4.3. Heated wire/furnace generators

A simple and established way of particle generation is through thermal sublimation. With an efficient surface to mass ratio, wires are convenient. The heating can be done by direct resistive heating of the wire, if the material allows it, or the wire can be heated by a furnace. As described above, the sublimated vapor will condensate with falling temperatures to droplets and after the temperature falls below the melting point, coagulation leads to fractal particles [Peineke, Attoui, and Schmidt-Ott, 2006]. Again, if oxygen is present during this process, oxidation is very likely, for prevention the particle generation can be done in an inert gas atmosphere.

Such a device was commercialized by GRIMM Aerosol with the "7860 WOx Generator" [GRIMM Aerosol, 2019].

If a tube furnace is used for the heating of the wire, it is sometimes treated as a separate kind of particle generator. This holds especially if metal particles are generated and a lager area, or maybe a second area is heated, so the forming particles are sintered to spheres [Scheibel and Porstendörfer, 1983].

2.4.4. Electrospray generators

A sample solution is charged within a vial and is being pushed by a pressure difference through a capillary. A high voltage electrical field at the capillary exit pulls the charged solution out of the capillary, forming droplets that are mixed with a filtered gas. This produces a sheath flow, which transports the droplets into a neutralizing chamber (see section 2.2.8) to neutralize the highly charged droplets [TSI Inc., 2002].

Electrospray generators are used widley since they produce a very monodisperse size distribution. Thus they are also used for creating particulates from emery oil, which are recommended by legislation beside combustion generated paricles for CPC calibration [Grob et al., 2014].

Such a device was commercialized by TSI Inc. as the "ELECTROSPRAY AEROSOL GENERATOR 3482" [TSI Inc., 2019b].

2.5. Summary and Outlook

In this chapter a review of state-of-the-art measurement techniques for particulate emissions in automotive exhaust is given. The authors contribution to CPC technology is presented in chapters 3 and 4 and to LII in chapter 5.

In section 2.4.2 the realization of a spark particle generator within the scope of this thesis is described. The setup was done with low effort and cost-efficient to prove the feasibility of the concept using a commercial HV module and with graphite and zinc electrodes. A systematic characterization was not possible within the time frame of this thesis, thus a full characterization of the produced particulates in dependency of the current, the space between the electrodes and the spark frequency should be the first next step. It may also be repeated with an inert carrier gas like N_2 instead of air. Further investigations could involve different electrode materials, where the usage of two electrodes of different materials at a time could especially give interesting particles with interesting properties.

3. Condensation Particle Counter Theory

3.1. Condensation Theory

The process of condensation can be described by various theories. Very common and widely known for the description of the formation of droplets from a vapour is the classical nucleation theory (CNT). Although it is a very simplified approach and insufficient for a detailed description, it is widely used for rough estimations and as a benchmark for more sophisticated, newer theories and experimental investigations [Dillmann and Meier, 1989; Gránásy, 2000; McGraw, Wang, and Kuang, 2012; Vesala et al., 1997; Winkler, Vrtala, and Wagner, 2008; Yu, 2005].

In nature formation of droplets from vapour happens almost exclusively with particulates as so called *nucleation seeds* (sometimes also *condensation seeds* or *condensation nuclei*) [Seinfeld and Pandis, 2006]. This heterogeneous nucleation is utilized within a CPC in a controlled manner.

3.1.1. Classical Nucleation Theory

CNT describes homogeneous droplet formation and growth in a pure vapour. The minimum size a particulate has to have to trigger condensation and droplet growth can be described by thermodynamic considerations:

Nucleation treats the physical transition between liquid and gaseous state of matter and in a closed system always the state of matter with the lowest free enthalpy (Gibbs-Energy) is stable. The considered system shall be isobar and isotherm. In a gas constantly clusters of molecules form and decay again, if a cluster remains stable and grows further a droplet is formed. Thus, the

change of the free enthalpy for an droplet forming can be written as the sum of the effort for the surface creation and the gain from the volume:

$$\Delta G = 4\pi r^2\sigma - \frac{4}{3}\pi r^3 \Delta g_u \tag{3.1}$$

With ΔG the change of free enthalpy (Gibbs-Energy), r the radius of the droplet, σ the surface tension and Δg_u the change of specific enthalpy. $\Delta g_u = \rho RT \cdot ln(S)$ with ρ the density, R the ideal gas constant, T the temperature and S the saturation ratio. As stated above, equation 3.1 consists from two terms, one for the creation of surface $4\pi r^2\sigma$, depending on the droplet radius to the power of two, and one for the gain of volume $\frac{4}{3}\pi r^3 \Delta g_u$, depending on the droplet radius to the power of three. If the system is not saturated ($S < 1$) the volume terms contribution is positive, since g_u is positive, hence a stable droplet is impossible (see figure 3.1 on the left). For a supersaturated system ($S > 1$) the volume terms contribution becomes negative. Until a certain r is reached, the surface term still rises faster then the volume term drops (figure 3.1 on the right). The total free enthalpy starts to drop from a certain droplet size on, from this critical radius r^* the droplet is stable.

Mathematically r^* can be derived from equation 3.1 by finding its maximum turning point, so $\frac{\partial}{\partial r}\Delta G = 0$. Therewith the critical radius $r^* = r_0$ or *Kelvin* radius r_K (sometimes Kelvin diameter $d_K = 2 \cdot r_K$) can be calculated:

$$r^* = r_0 = r_K = \frac{d_K}{2} = \frac{2\sigma}{\Delta g_u} \tag{3.2}$$

Alternative approach

The Kelvin radius can also be derived from considerations regarding the saturation vapour pressure. It is defined as the partial pressure of a vapour from a liquid, necessary for mass equilibrium between the liquid and the gas phase. Hence, the liquid will evaporate until the saturation vapour pressure is reached. For droplets, because of the curved surface, a higher partial pressure is necessary to prevent evaporation. The necessary partial pressure decreases with increasing droplet diameter (thus increasing radius of curvature). This is called the *Kelvin effect*. If the droplets grow above a certain

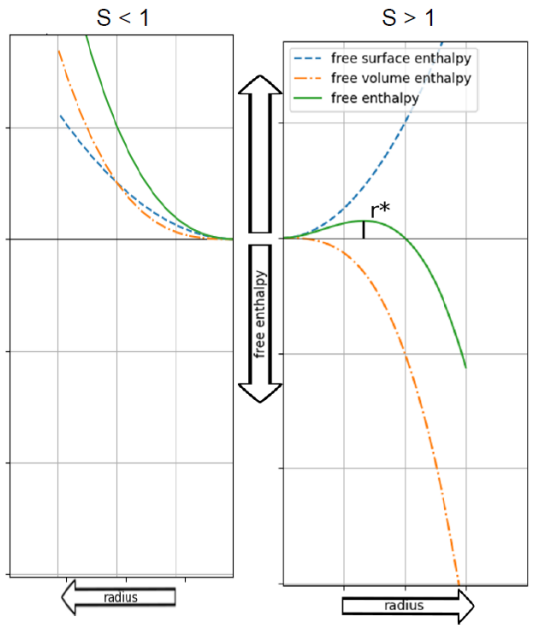

Figure 3.1.: The free enthalpy for the transition from gas to liquid for a supersaturated and a not saturated, isobar and isotherm system. Separately shown are the contributions of surface growth and volume gain.

size, the present vapor pressure suffices to prevent evaporation. The necessary saturation ratio for mass equilibrium is given by the *Kelvin equation* [Baron and Willeke, 2001]:

$$S = e^{\frac{4\gamma M}{\rho R T d_K}} \tag{3.3}$$

With γ the surface tension and M the molecular weight.

3.1.2. Heterogeneous Nucleation

In the simplest approach, basing on CNT, an insoluble particulate bigger than d_K serves as a condensation seed and triggers droplet growth. This approximation is feasible, since in a supersaturated environment small particulates are covered by a liquid layer adsorbed from the surrounding vapor [Baron and Willeke, 2001]. The energy barrier for heterogeneous nucleation on a spherical surface can be derived by geometrical considerations [Antti, 2006]:

$$\Delta G_{het} = \frac{1}{2}\Delta G_{hom} \cdot f(\cos\theta, \frac{r_p}{r^*}) \tag{3.4}$$

With $f(\cos\theta, \frac{r_p}{r^*})$ the contact parameter (generally $f < 1$), a dimensionless parameter depending on the contact angle θ, the present particles (droplets) radius r_p and the critical radius r^*.

The experimental investigation of the process of heterogeneous nucleation is challenging, because of the complexity of the process and the difficulty of a stable initial situation. Anyhow, a constricted verification of the classical theory is possible by measurement of the nucleation rate within an expansion chamber, where the predictions were found to match the experimental values inside the measurement uncertainty [Winkler, Vrtala, Steiner, et al., 2012].

Still the description of the heterogeneous nucleation process by the classical theory is insufficient, what was proved impressively by the detection of heterogeneous nucleation for cluster sizes below the critical size, a decade ago [Winkler, Steiner, et al., 2008]. New approaches are developed, including substantial findings which were gained since the first theories were postulated. One such approach is e.g. the Mean First Passage Time (MFPT) for nucleation barriers [McGraw, Wang, and Kuang, 2012].

An inspection of the heterogeneous nucleation process could be possible by a Small Angle X-Ray Scattering (SAXS). Efforts in this topic are in the early stages, but very promising [Bauer et al., 2019]. Investigations regarding SAXS on aerosols were also done within this thesis - see section 3.4 for details.

3.2. CPC Counting Efficiency

In contrast to the theoretical picture described above, not all particulates bigger than r^* trigger droplet growth, just like not all particulates below r^* do not. The size dependency of the activation probability is called *counting efficiency* (or sometimes *detection efficiency*) and has to be characterized for every CPC, since it differs from device to device [Wiedensohler, Orsini, et al., 1997].

The counting efficiency of a CPC depends mainly on the supersaturation profile in the condenser, which is influenced mainly by the geometry of the device, the flow conditions and the set temperatures of satruator and condenser [Ahn and Liu, 1990a; Ahn and Liu, 1990b; Sem, 2002; Sutugin and Fuchs, 1970; Wiedensohler, Orsini, et al., 1997]. The actual slope of the counting efficiency curve is rather softly decaying than forming a sharp cut off at the critical diameter (see figure 3.2 for a scheme). For an easier classification of CPCs it is usual to determine the size with 50 % counting efficiency, which is called d_{50} or *"cut-off point"*. Additionally to the d_{50}, also the steepness of the curve is critical for measurements of particulates with sizes in the non-linear region. Thus, this was regulated for certification and type approval measurements by legislation. Currently the counting efficiency has to be (50 ± 12) % at (23 ± 1) nm and >90 % at (41 ± 1) nm [United Nations, 2014].

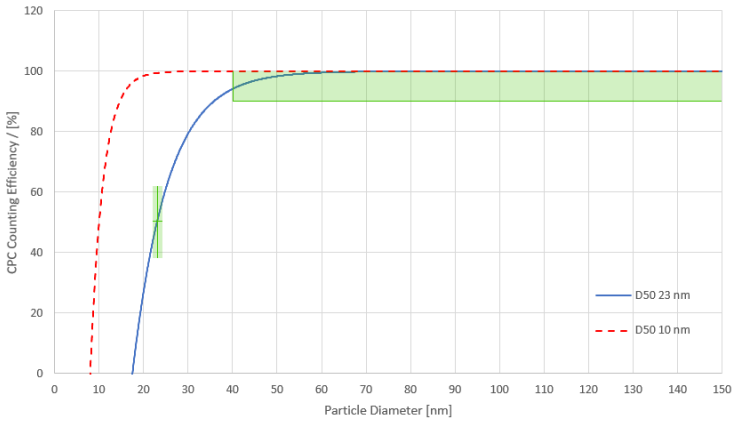

Figure 3.2.: Calculated counting efficiency curves for a d_{50} at 23 nm (blue line) and 10 nm (red, dotted line). The marked regions represent the current legislative requirement on the counting efficiency. The calculation was performed using the "two-parameter formula" [Stolzenburg and McMurry, 1991]

CPCs with a cut-off below 23 nm can be realized. To the lower end experimental devices activate particulates down to 1 nm [Kuang et al., 2012]. In this context the question for a reasonable cut off size arises, since the transition from small particulates to single molecules is floating and not sharply defined. Nevertheless latest investigations on automotive particulate emissions suggest that a not negligible fraction of solid particulates is emitted below 23 nm [Giechaskiel, Vanhanen, et al., 2017], thus a shift of the legislative requirements to a d_{50} at 10 nm is expected [Bainschab et al., 2017;

Baltzopoulou et al., 2018].

A more detailed treatment of CPC cut off characteristics in dependency of device properties would exceed the scope of this thesis. Further the influence on the counting efficiency by the interplay between the measured particulates and the CPC working fluid shall be discussed.

3.2.1. Particulate Influences on the Counting Efficiency

Heterogeneous nucleation is influenced by the properties of the nucleation seed and the vapour material. There are physical influences like the vapour saturation, the particulates size or the particulates morphology. As described above, these factors are addressed mostly by nucleation theories. But heterogeneous nucleation is also influenced by chemical properties of the nucleation seed and the vapour material, like polartiy, solvation, diffusivity or surface energy. These chemical influences have been found to be very distinct and are of special importance for the operation of CPCs [Giechaskiel, Wang, et al., 2011; Magnusson et al., 2003]. Established working fluids like n-Butanol or Isoporpanol, as all alcohols, are chemically reactive substances, thus their behavior as a working fluid differs for different particulate materials*.

Magnusson et al., 2003 performed a systematic investigation on the critical parameters for nucleation. They examined numerous chemical substances for their nucleation behavior and by considering their chemical properties they derived correlations between certain properties and the aptitude as a CPC working fluid. They found a strong correlation between a decreasing Kelvin diameter and with a rising surface tension for most materials. For n-alcohols, the trend was found to be inverse.

3.2.2. Investigations on material influences

Based on the work of Magnusson, in a preliminary study to this thesis n-Decane was identified as a promising potential CPC working fluid out of 88 screened substances [Kraft, Reinisch, and Bergmann, 2016]. Considered were

*Comment of Prof. Reinhold Niessner at the IAC 2018 (St. Loius, USA) to the presented experimental data of the author.

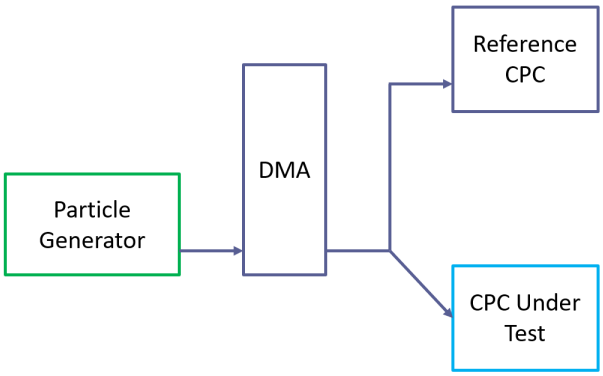

Figure 3.3.: Schematic of the experimental setup for the investigations on the material influence of the working fluid.

only chemical inert substances, which were further assessed for diffusivity, dielectric constant, vapor pressure, Kelvin diameter, hygroscopicity and commercial availability. n-Decane comprises the most favourable mixture of properties and since it is non reactive the condensation behavior should be the same for particulates from different materials.

This hypothesis was roughly investigated within this thesis. The same CPC, an *AVL 10 nm CPC* provided by AVL List GmbH, was operated with n-Butanol and n-Decane to avoid influences due to the device and a factory calibrated TSI 3790 automotive CPC was used as a reference. The setup consisted from a particle source, followed by a size selection unit (TSI 3082 EC + TSI 3082 DMA). Afterwards the flow was split and lead into the reference device (TSI 3775 CPC) and into the CPC under test (Fig. 3.3). Therewith the counting efficiency for the CPC under test was measured at 10 nm, 23 nm, 30 nm, 40 nm and 90 nm for different particle sources (see table 3.1).

Measurements were done for one set of all particle materials for the AVL CPC with one working fluid and the TSI 3790 for comparison. Because of low concentration issues at small sizes, the CPCs under test were not connected in parallel, but were tested one after another. The counting efficiency of one size was measured for TSI and the AVL CPC, for all particle generators. Afterwards the working fluid of the AVL CPC was changed. Also the wick was changed and the device was flushed three times with the new substance. Then a rough calibration was performed, where the counting efficiency of the AVL CPC was adapted to the TSI 3790 using WOx particles with the TSI

Tested CPCs	Particle Materials	Generator
AVL CPC Decane	Spark Soot	Spark Particle Generator (see section 2.4.2)
AVL CPC Butanol	Combustion Soot	Jing MiniCAST
TSI 3790 Butanol (Factory Calibration)	WOx	GRIMM 7860 WOx Generator [GRIMM Aerosol, 2019]
	NaCl	TOPAS Atomizer
	ZnO	Spark Particle Generator (see section 2.4.2)

Table 3.1.: List of tested CPCs and the used particle materials.

3775 as a reference. The measurement for every CPC and every particulate material was repeated five times. The data can be found in Appendix A.

By a comparison of the data from the AVL CPC using n-Butanol and the TSI 3790 (Fig. 3.4) small deviations of the counting efficiencies are present, but the trend of the behavior is the same. For different materials a different counting efficiency is clearly visible. NaCl particulates were not activated efficiently, the two kinds of soot and the WOx particulates were in the same regime and for the ZnO a chemical reaction with the n-Butanol vapour can be assumed.

Different is the behavior with n-Decane (Fig. 3.4(c)). The counting efficiency does almost not change for particulates from different materials. WOx, ZnO and soot from combustion show nearly similar counting efficiencies and the NaCl and soot from spark generation are within $\pm 5\,\%$ deviation. As stated above it is assumed that due to the chemical inertness of n-Decane the activation of particulates is independent of the particulates material. Because the particulates physical properties are not known beside the aerodynamic diameter, the material influence can not be isolated. The deviations in the counting efficiency left, might be due to physical properties of the particulates but it can not be distinguished by the present data.

This investigation should be seen as a rough survey into this topic to hedge the functionality of the HTCPC in a comprehensive way. A detailed

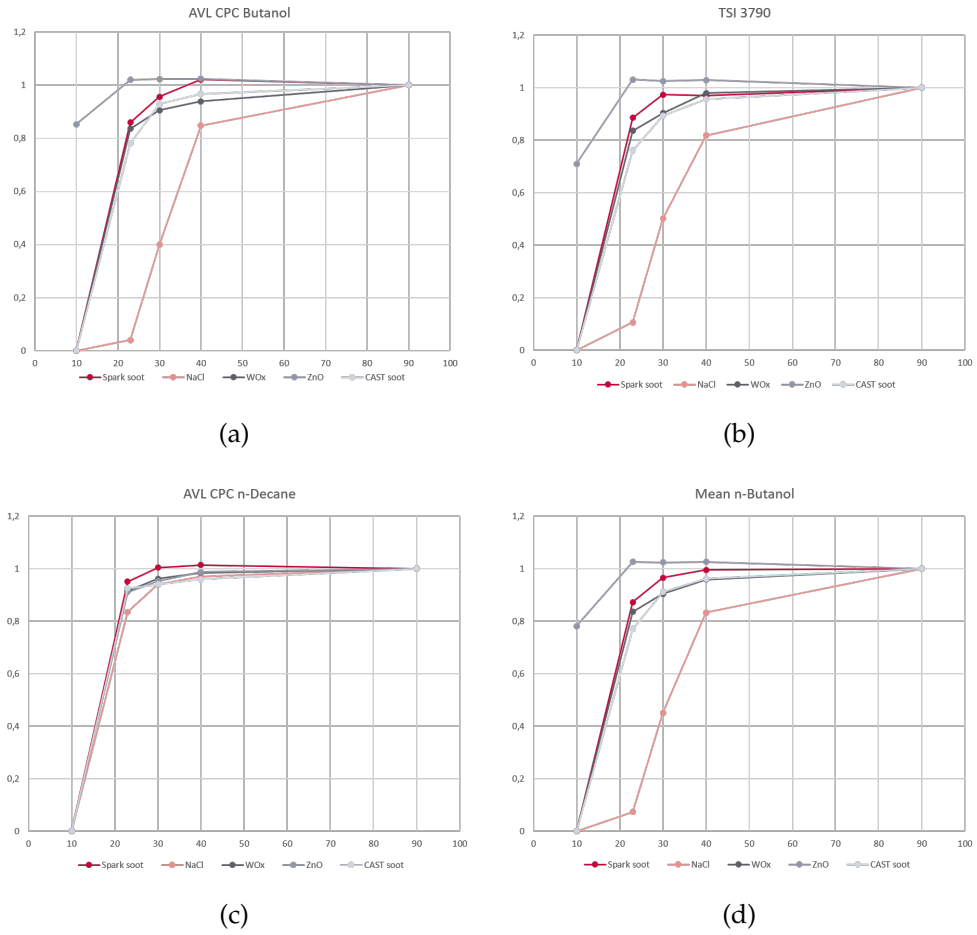

Figure 3.4.: Measured counting efficiencies for the AVL CPC using Butanol (a), the TSI 3790 (b) the AVL CPC using n-Decane c) and the mean of all measurements with n-Butanol d). The occurred differences between a) and b) are due to the influence of the CPC housing since the material influences are same for both devices.

examination of the nucleation process and its influence would go far beyond the scope of this thesis, although it is inseparably linked.

3.3. Capillary Condensation

The heterogeneous nucleation process is strongly influenced by an effect called *capillary condensation*. It describes condensation of vapour below the saturation vapour pressure [Evans, Marconi, and Tarazona, 1986]. Fractal particles are, without preceding treatment, covered by a layer formed by volatile substances from the ambient [Baron and Willeke, 2001]. This layer can be removed by proper treatment using a VPR (see section 2.3.2 for details). If now such a "stripped" particle should be measured by a CPC, again a first layer of working fluid vapour would adsorb when it enters the saturator. Thus, the particulate activation is actually a growth process of a droplet, since the interface to the vapour is already given by the adsorbed working fluid vapour. That way particles below the critical size according to CNT, are detected.

Capillary condensation on fractal particulates is promoted by the conditions in the slits formed by the primary particles. From the short range van der Waals forces present at these nanoscopic structures, adsorption of vapour molecules is reinforced. The liquid layer inside forms a meniscus and grows until an equilibrium is reached, which is depending on the capillary size, the vapour pressure and the specific adhesive forces between the materials. The speciality arises from the increased availability of van der Waals forces due to the geometric conditions, the vapour pressure above the meniscus, following the Kelvin effect by trend, and the form of the meniscus, which is depending on the capillary shape and the adhesive forces. A detailed and accurate description of capillary condensation is a field of research since nearly a century [Evans, Marconi, and Tarazona, 1986]. Until now it did not find its way into aerosol science, although the difference between an fractal shaped and an spherical particulate is significant under this point of view.

Heading a calculation on capillary condensation, suitable for fractal particulates, already available theories can be used. Some have been developed for sorption hysteresis [Cohan, 1938], regarding the adhesive forces of the liquid [Derjaguin, 1940] or even for unitary approaches [Evans, Marconi,

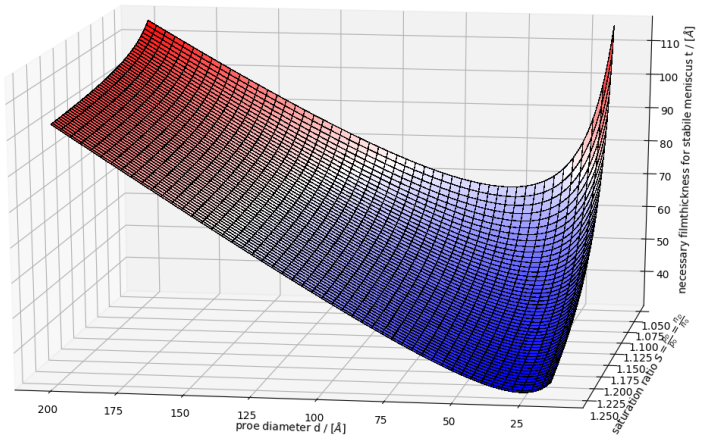

Figure 3.5.: The stable film thickness at the wall of a capillary t in dependency of the saturation ratio $S = \frac{p_0}{p_D}$ (attention inverted) and the pore diameter d

and Tarazona, 1986; Philip, 1977]. The calculation follows [Broekhoff and Boer, 1967], by usage of the approach for two spheres from [Philip, 1977]. The result is equation E.4 and is shown in figure 3.5. The resulting model can be transferred in a boundary case into the classical Kelvin equation. Details regarding the calculation can be found in Appendix E.

Figure 3.5 shows, that thermodynamic equilibrium for a stable liquid layer is possible below total saturation. The saturation ratio is written $S = \frac{p_0}{p_D}$ in compliance to [Broekhoff and Boer, 1967]. Thus e.g. 1.250 equals 80 % saturation. The stable film thickness rises with the saturation ratio and the pore diameter. This agrees with the observation that fractal particulates in a saturated vapour are covered by a nm film of liquid [Baron and Willeke, 2001] and are thus growing according to homogeneous nucleation theory.

3.4. Small Angle X-Ray Scattering - SAXS

For the examination of particles by scattering experiments, the size of the target has to be about the wavelength to receive size and shape dependent scattering. The particles which are of interest for automotive exhaust are in the size range from 10 nm to 100 nm, thus for scattering experiments X-rays are necessary.

SAXS describes scattering experiments, as briefly described in section 2.2.3, using X-rays [Glatter and Kratky, 1982]. The denomination "small angle" arises from the fact, that the scattering is detected only at small angels - up to an angle of about 7° to 10°. At lager angles the technique is calles Wide Angle X-ray Scattering (WAXS). Small angle scattering (SAS) experiments are not bond to X-rays, also neutrons are a common source for SAS experiments [Feigin and Svergun, 1987].

For the performance of SAXS experiments specialized equipment is necessary. A first experiment was done at the SAXS beamline at the ELETTRA synchrotron in Trieste. particles from a WOx generator (see section 2.4) were used, since the high atomic weight of Tungsten is beneficial. Since X-ray beam has to be held in vacuum, because it would be diffused in air, the particles were lead through a capillary with 1 mm diameter. Unfortunately no useful data could be gained from these measurements, the only contribution which could be identified in the signal was from the quartz capillary.

With an revised setup experiments in cooperation with the Faculty of Chemistry and Chemical Technology were done on a tabletop SAXS device (see figure 3.6(a)). By design of a measurement cell and minor modifications to one of the SAXS cameras (see figure 3.6(b)), which was already prepared for measurements on flowing fluids, to enable aerosol flow, measurements became possible. Findings from the first experiments were considered at the design of the new cell. First, the volume was bigger to achieve a larger interaction volume between the beam and the particles and second the windows to the cell were made from conductive Kapton to prevent static charges and thus deposition of particles. The cell itself was made from copper grounded by the SAXS device.

To put it simply, the measurement cell was a slit, milled into a copper block with drillings for the aerosol in- and outlet. On the front and backside a Kapton foil was clamped airtight by stainless steel parts (see figure 3.6(c)). The aerosol inlet was on the top, wile two outlets were on both sides of the cell, leading to an common exhaust also at the top of the cell.

The necessary amount of particles in the beam to create an detectable scattering signal was estimated by two independent approaches. First, the scattering signal was calculated on an absolute scale basing on [Orthaber, Bergmann, and Glatter, 2000]. Second, basing on the assumption that mmol of concentrations can be detected by SAXS [Ahner et al., 2010], the necessary

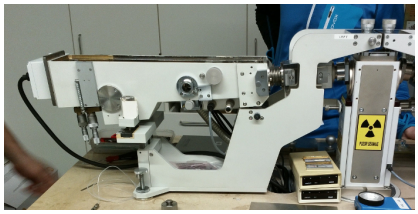

(a) SAXS camera front view

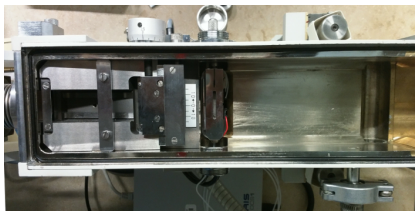

(b) SAXS camera top view with fluid flow cell

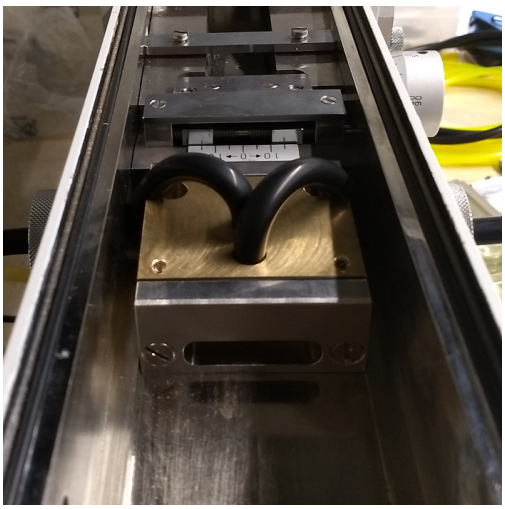

(c) SAXS measurement cell for aerosol experiments

Figure 3.6.: The SAXS tabletop device at the FKKT and the aerosol measurement cell.

mass concentration and further the molar concentration was calculated. Both approaches lead to the result that 10×10^{10} #/cm^3 to 10×10^{13} #/cm^3 are necessary.

Unfortunately these activities could not be pursued. Due to a lack of resources and time, since the main topic of this thesis should not have been disregarded. Although it is an promising field of research, which was studied lately also by other groups [Bauer et al., 2019; Yon et al., 2018].

3.5. Summary and Outlook

In this chapter first the theoretical aspect of the functionality of a CPC is explained by a short review of classical homogeneous and heterogeneous nucleation theory. Subsequently, the behavior of a real CPC is explained and the term *counting efficiency* is discussed in regards of particle and material influences. The discussion continues with capillary condensation as a proposal for an extension of theoretical descriptions and SAXS for experimental validation. The purpose of these activities was to gain a fundamental understanding for CPCs in regards of physical theory and application, so the HTCPC development could be performed at highest possible quality.

That the counting efficiency of CPCs is influenced by different particles working fluids is widely known in the aerosol community and a constant topic of research. The authors contribution to this research are the measurements presented in section 3.2.2, where the counting efficiency for n-Decane and n-Butanol as CPC working fluids for different particle species was investigated. To describe the differences due to particle morphology, in section 3.3 a model for capillary condensation on fractal particles was designed. As a method for an experimental proof for the theoretical considerations, in section 3.4 the utilization of SAXS for examination of aerosols was investigated.

The work could present the base for a distinct approach of CPC characterizations. In regards of capillary condensation modeling, a continuation towards combination with CNT would be favorable to enable a d_K for fractal particles - a kind of $d_{K,CPC}$. In-situ SAXS measurements on aerosols would give the possibility to measure the particles fractal dimension and size before leading them to a CPC, thus enable a detailed characterization of the CPC. In a more developed stage even in-situ SAXS measurements within the condenser of a CPC might be done to study the condensation behavior at different operating points and for different particles. For SAXS measurements the way may be long to find its way into aerosol science, but as the feasibility was already proven for synchrotron beamlines (as stated above), the next step in regards of measurement with tabletop devices would be an increase of the number of particles in the illuminated volume (not concentration per unit volume) to increase the scattering signal.

4. High Temperature Condensation Particle Counter

4.1. Objective and Organization of this Chapter

The development of the HTCPC aimed to address two research questions of the thesis: *"Is it possible to measure particulate emissions directly without a influencing preconditioning?"* and *"Will the direct measurement and the measurement using preconditioning match?"*, stated in section 1.3.

The difficulty from which these research questions is arising, is the complexity of measuring particulates in automotive exhaust. The mixture of gases and condensed matter, created by the combustion of fuel, is lead at barely defined conditions through the exhaust aftertreatment system and released from the tailpipe with a rough temperature drop and a high dilution very fast. Further the conditions of the combustion change with the load of the engine, therewith the composition of the exhaust and the transformations it undergoes until reaching the environment [Eastwood, 2008]. Now, if exhaust is sampled from at a arbitrary position at the exhaust system or a CVS and is then preconditioned for a measurement system, many variables are linked to the reproducibility of such a measurement. Still, the sampling and preconditioning systems were designed to minimize the influence on the exhaust, even possibly freeze its state by adequate dilution and are extensively characterized in regards of particulate losses [Giechaskiel, Chirico, et al., 2010a]. Although these systems are very high sophisticated, there are still differences in the measurements caused by application [Zheng et al., 2011], devices with different measurement techniques [Giechaskiel, Maricq, et al., 2014] or the kind of used preconditioning system [Swanson and Kittelson, 2010].

A PN measurement system without preconditioning and a very short sample line, which could handle the high temperatures and thus keep the volatile compounds in the gas phase and resist abrasive exhaust compounds, would minimize the possible influences on the measurement drastically. Furthermore it would allow a characterization of established PN sampling and preconditioning systems on exhaust for the first time. Thus, also an improvement of the calibration of established devices would be possible. A HTCPC is such a measurement system, it could mark the next step in exhaust measurement.

Organization of this chapter

The work on the HTCPC is presented in two journal papers, integrated in the chapter. The first paper (section 4.2) deals with the general principle and the realization of a stable HTCPC. It comprises the design and conceptualization of the device, our considerations and activities regarding the identification of a suitable working fluid and the design of a high temperature optics module. We provided the general proof of concept, a characterization of the counting efficiency, revealing compliance with the current PNC requirements (see 1.2.3) and the proof for long-term durability on automotive exhaust. The second paper (section 4.3) describes improvements on the already verified device, to facilitate measurements on automotive exhaust. Therefor the optics module was significantly improved and prepared to be combined with CPC counting electronics provided by AVL. We dealt with the wick material and the device was completely redesigned to a mixed-flow HTCPC. With the redesign we introduced an inherent dilution concept, enabling direct sampling of raw exhaust and a steady operation.

To support the HTCPC development also a setup for static light scattering was built to examine the droplet size, activities in this regard are is presented in section 4.4.

The development of this HTCPC was also topic of the master thesis of Michael Kügler [Kügler, 2018] and Michael Gleichweit [Gleichweit, 2019], both works were accompanied and guided by the author of this thesis.

The literature research on high temperature working fluids, presented in Paper I (section 4.2) was done by Martin Kraft from SAL GmbH (former

CTR AG).

The HTCPC as presented in this chapter is intellectual property of AVL List GmbH, patent applications have been submitted before any publication. The issued patents are listed in section .

4.2. High-Temperature Condensation Particle Counter Using a Systematically Selected Dedicated Working Fluid For Automotive Applications

Section 4.2 was published as *M. Kupper, A. Boies, M. Kraft, and A. Bergmann (2019), "High-Temperature Condensation Particle Counter Using a Systematically Selected Dedicated Working Fluid For Automotive Applications"* in the journal Aerosol Science and Technology. DOI: *10.1080/02786826.2019.1702920* [Kupper, Kraft, et al., 2019]

Abstract

A stable high-temperature condensation particle counter (HTCPC), operating above 170 °C was realized. First a dedicated working fluid was identified in a two-stage process, consisting of a pre-selection based on relevant substance properties and a subsequent experimental evaluation. A prototype for experimental evaluation of the concept was designed and built, supported by CFD simulations considering the properties of the working fluid. The surface tension of the working fluid was measured at different temperatures, revealing higher values than predicted and a specific adhesion to graphite. With a especially developed high-temperature optics module, the proof of principle was verified. Calibration measurements have been performed against an automotive grade CPC. The operation in compliance to the legislative requirements for particle number counters was successfully proven.

Introduction

Condensation particle counters (CPCs) are well established devices for measuring particle number (PN) concentrations in aerosols [McMurry, 2000; Sem, 2002; Wang et al., 2010]. These simple apparati were studied and developed by various groups all over the world, evolving them to reliable and established instruments [Barmpounis et al., 2018; Hering, 2018; Kuang et al., 2012; McMurry, 2000; Stolzenburg and McMurry, 1991]. Applications range from clean room monitoring [Zhang and Liu, 1991] to atmospheric [Wehner et al., 2011] or ambient measurements [Seipenbusch, Binder, and Kasper, 2008] to classification of automotive exhaust [Giechaskiel, Dilara, et al., 2008] due to the large range of measurable concentrations and particle species. Specialized instruments are available for every mentioned application and even hand-held devices [Hämeri et al., 2002] are available. Apart from some exceptions, like the MAGIC water CPC [Hering, Stolzenburg, et al., 2005], the majority of CPCs are using n-Butanol or Isopropanol as a working fluid and operating at 20 °C to 40 °C. In 2013 Nick Collings et. al. proposed new concept of a CPC operating at high temperatures around 150 °C [Collings, Rongchai, and Symonds, 2014], for direct and artifact minimized PN determination of engine exhaust as alternative to the corresponding legislative regulations [Giechaskiel, Cresnoverh, et al., 2010b]. The current particle number counter (PNC) requirements according to the solid particle number emission legislation require a limit of detection of less than 100 #/cm^3 of the PNC, which can hardly be fulfilled by other high temperature capable devices like. e.g. ELPI, or diffusion charger based methods [United Nations, 2014]. By modifying a commercially available CPC they demonstrated the principle operation for two siloxanes as working fluids and the necessary cut-off requirement for the european PN measurement regulation [European Commission, 2008]. The general concept of a high-temperature CPC (HTCPC) was proven a possible new application field, e.g. enabling direct measurements of hot exhaust without preconditioning or measure close to flames without influencing the particle formation. Despite the proof of concept, no long-term stability of the device was reported and after Collings work no further research on HTCPCs has been reported to our knowledge. The Collings et al. concept used an existing optical particle counter (OPC, TSI 3034), which requires further development for high temperature operation.

This work deals with the realization of an optimized HTCPC explicitly designed for high temperature operation. Our study comprises a dedicated saturator and condenser design, supported by CFD simulations, an extensive study on different working fluid candidates and the development of a high-temperature OPC. We placed special emphasis on long-term stable operation and enabling measurements in accordance with european PN measurement regulation. Furthermore the approach of a high temperature CPC would allow to extend the size range covered by regulatory guidelines from 23 down to 10 nm, without the risk of counting artefacts caused by nucleation mode particles due to sampling. Thus, the high temperature CPC might pave the way to a robust alternative to the existing PMP protocol [United Nations, 2014].

Materials and Methods

The study comprises the identification of an appropriate working fluid, the design of a HTCPC embodiment and a dedicated high-temperature optics module.

Working Fluid

The long-term stability of HTCPC operation requires a working fluid that is thermally stable, has applicable vapor pressures at high temperatures and is widely available. A dedicated working fluid was identified from a wider pre-selection of possible candidates belonging to various classes of chemicals. The surface tension of the chosen working fluid was measured. Using the specific material parameters of the substance, CFD-simulations were performed to optimize the HTCPC design. The device was built and its function evaluated experimentally.

Identifying a suitable working fluid is a crucial part of the realization of a HTCPC. Collings et al. selected their working fluid by an empirical approach [Collings, Rongchai, and Symonds, 2014]. They evaluated six substances and tested four in operation with their HTCPC device: a perfluorinated polyether, a polyphenyl ether, tetramethyl tetraphenyl trisiloxane and pentaphenyl trimethyl trisiloxane. A sufficient counting efficiency was reported with the two siloxanes. Based on the results of Collings et al,

Class	Scanned substances
Carboxylic acids	4
Alcohols	1
Ethers	2
Glycols and glyocol ethers	4
Aliphatic hydrocarbons	7
Aromatic hydrocarbons	7
Amines	3
Ketones	1
Esters	11
Others	7

Table 4.1.: Investigated potential high-temperature CPC working fluids, sorted by classes. The full list can be found in Appendix C.5.

we performed for a systematic study on possible working fluids for high temperature application.

Preselection
Based on criteria favorable for a CPC working fluid, which were e.g. identified by Magnusson et al. [Magnusson et al., 2003], a preselection of potential working fluids was done. In total 46 substances out of 10 substance classes were chosen (see Table 4.1). To evaluate the potential of the candidate substances to act as a working fluid, an adapted classical nucleation theory (CNT) approach according to Magnusson et al., 2003 was applied. The nucleation criteria found in their work are basing on a derivation of an explicit solution for the saturation ratio from the CNT.

To find nucleation criteria from the CNT equation, Magnusson et al. set the nucleation rate to $1\,\#/\mathrm{cm}^3\mathrm{s}$ and to obtain an explicit solution for the saturation ratio, they replaced the product of the saturation ratio and the saturation vapor pressure by the partial pressure. Insertion into the Kelvin equation leads them to the following expression for the Kelvin diameter d_K:

$$d_k = \frac{\sqrt{6RT \ln \frac{2MN_A^3 \sigma p^4}{\rho^2 \pi R^4 T^4}}}{2\sqrt{\sigma}\sqrt{N_A \pi}} \tag{4.1}$$

with the gas constant R, the temperature T, the molecular weight M, Avogadro's constant N_A, the surface tension σ , the partial pressure p and the density ρ. Magnusson et. al. state that "σ is the strongest factor that influences the theoretical d_K as expressed by the CNT". From equation 4.1 it follows that d_K is directly proportional to $\sqrt{\frac{ln(\sigma)}{\sigma}}$, so fluids with a higher surface tension should give a smaller Kelvin diameter. Basing on experimental evaluation they conclude that a high surface tension in combination with a low molecular weight will generally have a small Kelvin diameter, whereas they saw a dominant influence of the surface tension. Additionally, a correlation with the dielectric constant was shown and explained by the relationship between the surface tension and the dielectric constant [Papazian, 1971]. The found correlations can be seen as a general trend and applied with varying success to different classes of chemicals. Iida, Stolzenburg, and McMurry, 2009 states the same result, the surface tension has the dominant correlation with the activation efficiency.

The potential working fluid candidates were classified by these parameters. As additional other important substance properties we included: melting point, boiling point, dissociation temperature, flash point, ignition point, density, vapor pressure, viscosity, polarity, estimated consumption, diffusivity, toxicity, corrosivity, solvation and price. The substances were classified by selection criteria listed in Appendix C.2. The properties were taken from literature [Haynes, 2012; *infotherm.com* 2015; Kirk et al., 2007; Marrero and Mason, 1972; Poling, Prausnitz, and O'Connel, 2001; VDI-Gesellschaft, 2005; *webbook.nist.gov* 2015], but for many substances very few experimental high-temperature data was available. In the cases the values were available for lower temperatures, linear extrapolation to higher temperatures were performed. If data were not available, they were calculated from regression equations found in literature [Haynes, 2012; *infotherm.com* 2015; Kirk et al., 2007; Marrero and Mason, 1972; Poling, Prausnitz, and O'Connel, 2001; VDI-Gesellschaft, 2005; *webbook.nist.gov* 2015]. The table used for the preselection can be found in Appendix C.5.

Degradation experiments
To test the most promising working fluid candidates under operational conditions, a dedicated vessel with four equal containers, each with a volume of 40 mL, was manufactured from aluminium. Three tests were performed. First the vessel was sealed tightly and heated for 8 h to 250 °C with 20 mL

of one substance in every container. Second, a piece of silicon carbide (SiC), as a candidate for a wick material, was placed into the container with the substance and again heated for 8 h to 250 °C. Finally the container were filled with the working fluid candidates and additionally with 200 µL water and again heated for 8 h to 250 °C, to test for hydrolysis.

Surface tension measurement
Since the surface tension was considered as the crucial parameter for the nucleation behavior and for none of the considered substances measured values at high temperature were available, measurements for the found working fluid (the working fluid is presented in section 4.2) were done. By the pendent droplet method the bulk surface tension was measured. Therefore a aluminium capillary with an outer diameter of 1.5 mm was attached upright to the side of a heated aluminium block so that ∼1 cm protruded from the bottom. Solid pieces of the working fluid were held to the hot capillary, so the melted working fluid flew down to the tip of the capillary, forming a droplet. The droplet was photographed with a digital camera and the pictures were analyzed using the open source "Opendrop" software [Berry et al., 2015] The measurement was done between 80 °C and 220 °C in steps of 20 °C. The temperature of the aluminium block was controlled by a PID algorithm (Pt100) and restive heating. For every temperature setting the system was held for about 10 minutes to assure a uniformly temperature distribution in the capillary and the droplet. It was assumed that the capillary and the droplet take the temperature from the heated aluminium block, since the free part if the capillary and the droplet had a small mass and the thermal conductivity inside the material can be considered much higher than losses due to convection and radiation.

Second the contact angle on a graphite substrate was measured between 80 °C and 220 °C in steps of 20 °C to investigate the material influence. The temperature of the graphite was controlled by a PID algorithm (Pt100) and restive heating. The setup was in a cubic box with 10 cm edge length and an opening for a digital camera, to ensure homogeneity between the setup and the surrounding air. Graphite was chosen to estimate the specific adhesion forces between the working fluid and soot. The nature of the used graphite was inspected with an scanning electron microscope (SEM, Figure C.1) before the experiment and was identified as natural, crystalline graphite.

Flow design

The wick is a core element of the HTCPC. It is a porous material placed inside the saturator (location 6, Figure 4.1a) and is in contact with the working fluid. By capillary forces it soaks completely and its high surface enables fast saturation of the passing aerosol with vapor from the working fluid. We used a cylinder from cordierite ceramics, originally used as a substrate for diesel particulate filters. The particle flow does not pass through the wick, since high losses can be expected. Therefore the HTCPC followed a mixed-flow design [Stolzenburg and McMurry, 1991] whereby the aerosol is injected separately (location 9) from the saturated vapor stream (location 8). Nitrogen was chosen as carrier gas to guard against oxidation of the working fluid, catalyzed by the wick material.

The HTCPC prototype was designed with a horizontal saturator containing the wick and a vertical condenser [Agarwal and Sem, 1980]. The device is thus shaped like a "L" (Figure 4.1(b)). It was manufactured mainly from aluminium, except where noted. The saturator is in total 6.5 cm long and contains one wick from NGK cordierite ceramics with cylindrical shape, 4 cm long and 2.5 cm in diameter. The wick fills the inner diameter of the saturator completely, enabling a flow with a honeycomb structure with a cell density of 400 /inch² ($\triangleq 15.75\,\mathrm{mm}^{-2}$) and 0.2 mm wall thickness. The flow is led through an elbow and a 3 cm insulation made from Polyether ether ketnoe (PEEK) into the 8.5 cm long condenser, on whose end a nozzle with 1.8 cm length and a 500 µm outlet aperture is attached. To bypass the wick with the particle flow, a capillary with an inner diameter of 0.7 mm was introduced through the elbow, so that the particles enter directly into the condenser.

The filling of the working fluid into the saturator was controlled by means of an optical filling level monitor, a heated magnetic valve and an external heated tank.

CFD simulations regarding the flow and the droplet growth were performed with Ansys Fluent 16.0.1 using a density-based implicit solver with the pseudo-transient solution method. The fluid calculation uses the ideal gas model and considers the fluid as a mixture of two gases, whereas air was considered as one gas and the working fluid vapor as the second. The mass fractions of the gases in the fluid were calculated continuously, considering

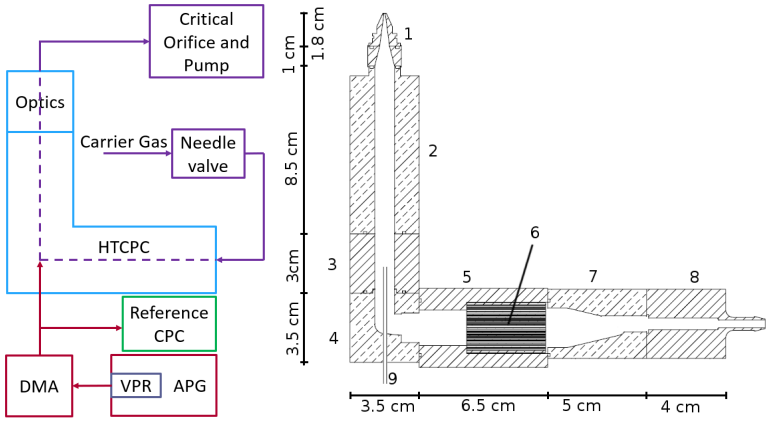

Figure 4.1.: Schematics of the HTCPC setup. a) flow diagram of the operation, b) scheme of the used HTCPC device. (1) nozzle, (2) condenser, (3) PEEK-insulation, (4) elbow, (5) saturator, (6) wick, (7) saturator inlet, (8) PEEK carrier gas inlet, (9) particle flow inlet.

condensation at the walls and evaporation at the completely wetted wick. Thermal dependency of material properties was also considered in the simulation (see Appendix C.3).

The material properties of the working fluid are crucial input parameters (they are listed in Appendix C.3), since they influence the calculation in many ways like the saturation, the thermal diffusion of the vapor or the nucleation. The flow was set to 1 L min^{-1} at standard conditions - 1013 Pa and 273.15 K. For the simulation the temperature of the saturator was 210 °C, the temperature of the condenser was 190 °C. The Kelvin diameter and the droplet growth were calculated by post processing, using the resulting parameters from the simulation for the steady state. All simulations were full 3D, using the original manufacturing CAD files without the capillary since just the general flow through the device was studied. The design was revised basing on the simulation results and was not simulated again.

Optics Module and Characterization

Two types of experiments were performed. First, for a fundamental proof of principle it was tested if particle activation (heterogeneous nucleation) occurs. Second the counting efficiency was measured.

For reliable measurements also the counting of the droplets must happen at high temperatures, since cooling over large temperature differences would cause a high supersaturation and therewith homogeneous nucleation becomes very likely. Performing optical measurements at about 200 °C requires a design which differs from typical OPCs, since no electronic components would stand the heat. For these studies an "*open module*" was developed for first experiments and inspection of the process. For the second set of experiments a dedicated high-temperature counting module was developed, designed to optimize the collection of scattered light in the high temperature environment.

Open Optics Module
The open module carries no optical components (thus "*open*") beside optional plane-parallel windows and allows optical measurements above the nozzle up to an angle of 23° in the horizontal plane of the beam (see Figure 4.2a). It was constructed from aluminium and surrounds the nozzle completely. The aerosol is lead upwards into exhaust removal. The purpose of it is to keep the aerosol flow at operational temperatures after leaving the nozzle and allow optical measurements like static light scattering (SLS). The optional plan parallel windows prevent disturbance by unwanted flows. Direct ejection of the hot saturated aerosol into ambient temperatures through the nozzle would create a very high supersaturated working fluid vapor and therewith bias the measurement. Also, for our working fluid, which is presented in section 4.2, the emerging fog solidifies at ambient temperature and starts to settle. The scattering on the solidified droplets would prevent any reliable optical measurement if not heated. For our optical measurements a 635 nm laser (Thorlabs CPS635) was aligned in such a way that it passed right above the nozzle at the end of the condenser. The scattered light was detected by a movable detector (avalanche photo diode - Thorlabs APD 120 A2/M) at different angles to inspect the angular dependency of the scattering.

Counting Optics Module
The counting optics module (see Figure 4.2b) was realized again with a 635 nm laser (Thorlabs CPS635). To improve the laser beam profile four adjustable shades were used to remove the dispersed light from the focused beam. The emerging beam was lead to the optics module by three mirrors, so repositioning was possible without moving the laser itself. A cylindrical lens (Thorlabs LJ1636L1) attached to the optics module focused the beam

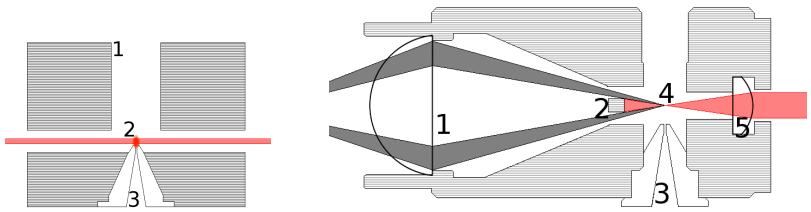

Figure 4.2.: Schematics of the (a) high-temperature cap and (b) the counting optics module. (a): (1) aerosol outlet, (2) scattering event, (3) nozzle of the HTCPC, the observation is possible by a drilling perpendicular to the drawing. (b): (1) collecting lens for the scattered light, (2) beam dump, (3) nozzle of the HTCPC, (4) scattering event, (5) cylindrical collimating lens.

right above the nozzle at the end of the condenser. The distance of the lens to the nozzle was twice the focal length of the lens. By focusing the laser beam the interaction time of the droplets with the laser beam is minimized and the intensity of the scattering maximized. The beam is then dumped into a blackened rod. A converging lens (Thorlabs LA1951) attached at the other end of the module collected the scattered light and directed it onto an avalanche photo diode (Thorlabs APD 120 A2/M) which was placed away from the heated module right into the focus of the lens. The distance of the scattering event and the detector was chosen to twice the focal length of the lens. The diode signal could either be collected by an oscilloscope (Tektronix MDO3024) for adjustment and inspection or be connected to counting electronics supplied by AVL List GmbH, providing a pulse count per second in real time with dead time correction.

Scattering Measurements
For the first experiments the open module was attached to the top of the condenser. Experiments were performed using pressurized air. The total flow through the device was $0.6\,\mathrm{L\,min^{-1}}$, set by a Vögtlin red-Y mass flow controller (MFC) at room temperature and driven by the gas flow from the laboratory pressurized air system. The exhaust was removed by laboratory ventilation.

The scattered light was inspected within a masters thesis with dedicated a setup for detection of static light scattering (SLS). The detected scattering was, as expected, angular dependent Mie-scattering, originated by the

working fluid droplets [Kügler, 2018].

Calibration Measurements
The second part, regarding the performance of the HTCPC, was done with the counting optics module (Fig. 4.2b). The linearity and the detection efficiency were measured to evaluate the performance of the HTCPC. A critical orifice was used to set the flow to $1\,\mathrm{L\,min^{-1}}$ at the outlet of the optics module. The critical orifice was heated to 60 °C, to prevent plugging by solidification of n-Eicosane. The flow was verified at this temperature. The flow through the capillary was controlled indirectly by a needle valve and flow meter at the carrier gas inlet. By a fixed overall flow given by the critical orifice, the difference between the overall flow and the carrier gas flow is the particle sample flow.

The saturator, condenser and the optics module were wrapped into glass wool for thermal insulation and to facilitate thermal stabilization. The operational temperatures were 205 °C saturator, 170 °C condenser and 215 °C for the optics.

The linearity was measured with an AVL 10 nm CPC (factory calibration, AVL List GmbH) as a reference. Soot particles with polydisperse size distribution were generated with an AVL particle generator (APG, AVL List GmbH). The aerosol of the APG passed an internal volatile particle remover (VPR) and was then diluted by an internal dilution bridge. The dilution was set to 32 stationary points between $0\,\#/\mathrm{cm^3}$ to $30\,000\,\#/\mathrm{cm^3}$ in 4 independent test series, for every point data was collected for 30 s.

The detection efficiency was measured also with an AVL 10 nm CPC (factory calibration, AVL List GmbH) as a reference and a TSI 3082 differential mobility analyzer (DMA, TSI Ltd.) for selection of particles with the same mobility diameter (see Fig. 4.1(a) for the flow diagram). Soot particles were again generated with an APG, by usage of the internal VPR and the internal dilution bridge. Particles were mobility selected with a DMA after the APG and afterwards the flow was lead subsequently into the HTCPC and the reference CPC. The size dependent counting efficiency was measured at 10, 20, 23, 30, 40, 50, 60 and 80 nm. Data was collected for 60 s for every size, the whole series was repeated 3 times. The measurements of the HTCPC and the reference were done subsequently for every set point.

Long Term Durability
To test the long term durability against engine exhaust, measurements at two chassis dynamometer at the Institute of Internal Combustion Engines and Thermodynamics of the Technical University of Graz were done. Six types of tests were conducted with varying test cycles. The total time of operation was 450 min whereas in total 223 min a test was driven. The flow through the device and the sample flow were not switched off between the test runs. The tests were done within an ordered measurement campaign, thus details of the tested vehicles must not be published. Measurements were done at a motorcycle equipped with a 1 L gasoline engine and a passenger car, also equipped with a 1 L gasoline engine. With the motorcycle two WMTC cycles were driven and with the car an IUFC, an ERMES and a RDE cycle*, followed by some constant points. The tests at one vehicle were done on one day in a row and both vehicles were tested within a week. The HTCPC was not serviced in between.

The sample position was at the transition line which transports the exhaust from the tailpipe to the dilution tunnel. The sample was drawn at ambient temperature with a Tygon tube to the particle flow inlet of the HTCPC, as carrier gas nitrogen was used. The sample position and the tube were at room temperature. Reference data from the other particle number counting devices available at the chassis dynamometer must not be published since it was an ordered measurement campaign. As a reference device the DownToTen system was installed, a loss optimized sampling system for sub 23 nm exhaust particles, equipped with a 10 and a 23 nm CPC [Bainschab et al., 2017].

Results and Discussion

Working Fluid

From the preselection (described in section 4.2) four promising candidates were selected for further evaluation: Palmitic Acid, n-Eicosane, Dibenzyltoluene and Dibutyl Sebacate (see Table 4.2).

*The "RDE cycle" is a standardized route in Graz for measurements with portable emission measurement systems, for comparison a according test is also used at the chassis dynamometer.

Degradation experiments
As shown in Figure 4.3 the investigations showed a significant thermal degradation and gas formation for Palmitic acid even with the sole substance in the vessel. Also, the aluminium was attacked rigorously. In contrast, with n-Eicosane no material change was observed at all three tests. A spectroscopic analysis of the n-Eicsane heated in the vessel, showed no decomposition products. Dibenzyltoluene turned from its original transparent appearance into a yellowish color at all three tests, but no additional influence from water or the SiC was observed. Dibutyl Sebacate also indicated thermal resulting in formation of solid particles, floating in the mixture of the original substance and other degradation products.

Property	Dibenzyltoluene[1] $C_{21}H_{20}$	Dibutyl Sebacate[1] $C_{18}H_{34}O_4$	Palmitic Acid[1] $CH_3(CH_2)_{14}COOH$	n-Eicosane[2] $C_{20}H_{42}$
Melting Point / [°C]	-34	-9.2	62.5	36.4
Boiling Point / [°C]	390	356	351	344
Flaming Point / [°C]	210	178	206	100
Ignition Point / [°C]	450	365	-	232
Vapor Pressure (25 °C) / [mPa]	49	-	-	1
Dielectric Constant / [-]	-	4.54	2.42	2.08
Estimated Consumption / [mL h^{-1}]	2	-	5	8
Kelvin Diameter (125 % saturation) / [nm]	27.36	-	25.07	25.25

Table 4.2.: Parameters of the four final working fluid candidates. Values from [1] VDI-Gesellschaft, 2005 [2] Poling, Prausnitz, and O'Connel, 2001

As a result of the selection experiments, n-Eicosane ($C_{20}H_{42}$), an aliphatic hydrocarbon, was selected as the dedicated working fluid. As a saturated and acyclic hydrocarbon its high boiling point, the high vapor pressure at operational temperatures (1532 mPa at 200 °C) and its classification as non-hazardous according to the chemical data sheet, made it in combination with the commercial availability at high purity the most desirable working fluid. As a paraffin n-Eicosane further combines many favorable properties from which chemical inertness should be emphasized. Therewith unwanted chemical reactions with the specimen are very unlikely, even at the high operating temperatures. As already stated before, to guard against oxidation catalyzed by the wick material, nitrogen was used as carrier gas.

Having assessed the working fluid feasibility based on bulk properties, there are still influences on the CPC operation which must be assessed relating to the nucleating and growth potential with a CPC. Two things should be pointed out here explicitly, first the chemistry between the particle functioning as nucleation seed and the working fluid and second the morphology

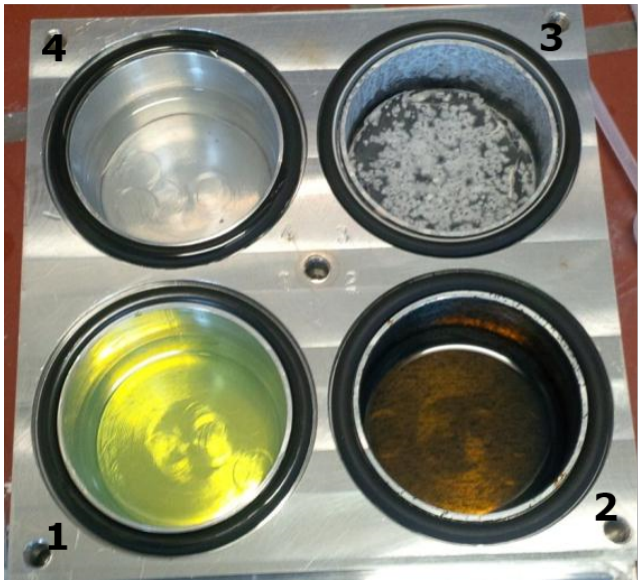

Figure 4.3.: The vessel for experimental evaluation of the temperature stability of the four final working fluid candidates after being heated to 8 h to 250 °C. 1 Dibenzyltoluene, 2 Dibutyl Sebacate, 3 Palmitic Acid and 4 n-Eicosane

of the particle. These influences are dominant and differ between particle species [Giechaskiel, Wang, et al., 2011]. The specific behavior has to be checked within a measurement campaign, so it can be considered for reliable CPC operation.

Surface Tension Measurements
For the surface tension measurement, the digital photography taken at the pendent droplet experiment were evaluated using the "Opendrop" software [Berry et al., 2015]. As input parameter the density of the material is required by the program, the values were taken from literature [Poling, Prausnitz, and O'Connel, 2001]. The measured surface tension values are shown in figure 4.4 (see Appendix C.4 for the values). The measurement gave values higher than the regression formula from literature [VDI-Gesellschaft, 2005]. The deviation of the measurement to the literature data is between 10 % to 15 %. As discussed in section 4.2, a higher surface tension causes a smaller Kelvin diameter d_K. According to Magnusson et al., 2003 this reduces the calculated value for d_K from the HTCPC simulation (presented in the next section) about 7 %.

The measurement of the contact angle of n-Eicosane on a graphite surface demonstrated complete wetting, since every droplet of n-Eicosane deli-

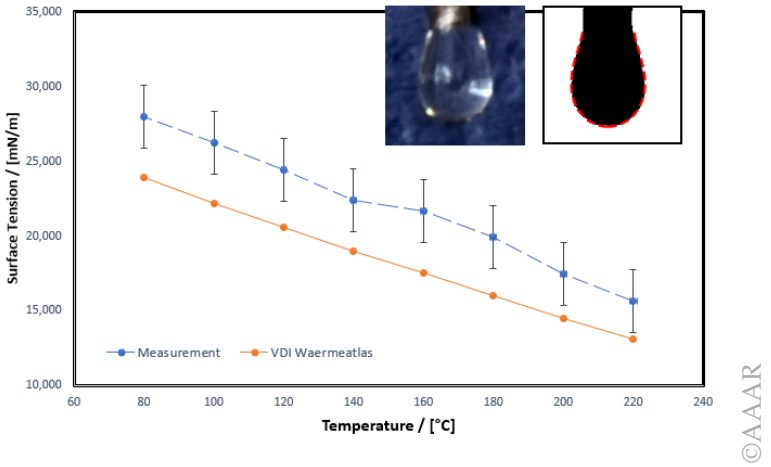

Figure 4.4.: Measured surface tension of n-Eicosane in dependency of the droplet temperature, for comparison plotted with surface tension data from literature [VDI-Gesellschaft, 2005]. In the upper right corner an example is given for the picture evaluation. Left the original picture for the droplet at 220 °C is shown, right the evaluated shade of the droplet. The dashed line is the result of the "Opendrop" software.

quesced on the graphite surface. Even with the setup open in the lab with the graphite heated to about 50 °C no contact angle could be observed. This behavior can be explained on one hand by the low surface tension of n-Eicosane compared to the surface energy of the graphite surface, but it also indicates high adhesion forces between the liquid and graphite. Thus efficient particle activation for soot is very likely. The specific adhesion forces cause the formation of a first layer of n-Eicosane on a soot particle in a supersaturated vapor, for much smaller sizes than the Kelvin diameter [Fletcher, 1958]. Since soot is a fractal particle, this process is enhanced by capillary condensation [Philip, 1977]. For a covered particle the interface to the vapor is completely given by the working fluid film and therewith the nucleation behavior follows CNT very close. Though, particles in automotive exhaust are not only soot. The interplay of different particle materials with n-Eicosane might result in material specific differences for the counting efficiency of the HTCPC.

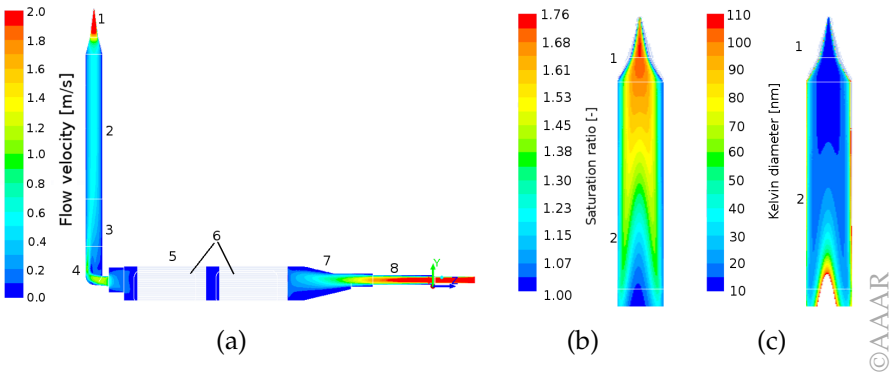

Figure 4.5.: Results of the Ansys Fluent simulation of the HTCPC geometry. (1) nozzle, (2) condenser, (3) PEEK-insulation, (4) elbow, (5) saturator, (6) wick, (7) saturator inlet, (8) PEEK aerosol inlet, (9) carrier gas inlet. a) Flow profile inside the HTCPC geometry, a flow separation is visible at the elbow. A particle flow inlet (pos. (9) in Fig. 4.1(b)) was not considered. b)The saturation ratio inside the condenser of the HTCPC. Very high values of nearly 180 % saturation were calculated for the set temperature difference of 20 °C. c)Basing on the simulation results, the homogeneous Kelvin diameter was calculated. For the high supersaturation region an activation of 10 nm particles is possible. In subfigures b) and c) the condenser was stretched in diameter for better readability.

Flow design

The flow dynamics within the original HTCPC design were investigated by CFD for typical operational flow rates (1 L min^{-1} total) and temperatures (temperature difference of 20 °C). The results in Fig. 4.5 show a laminar flow at the inlet and through the honeycomb structure of the wick. At the elbow a flow separation is predicted although the flow remains laminar through. The saturation of the wick was revealed to be very good. Modeled with a completely wetted honeycomb structure, after approximately 10 mm of the first wick 100 % saturation of the gas is reached in the simulation. In consequence of these results, one wick was removed and the elbow was redesigned to minimize the flow separation, the revised design is shown in Figure 4.1(b). The temperature of the gas in the condenser does not reach the condenser temperature, anyway a very high saturation of almost 180 % is predicted for a δT of 20 °C. Considering the results of the surface tension measurements, the values of the calculated Kelvin diameter d_K has to be reduced by 7 % to ∼9 nm.

Optics Module and Characterization

Examination of the condensation behavior brought distinct results. At fixed operating temperatures, scattered light from droplets could be observed above the nozzle. If a HEPA filter was attached to the particle inlet, the scattering vanished. This proves heterogeneous nucleation on particles introduced into the device. As already mentioned, the scattered light was inspected by a SLS setup with a masters thesis [Kügler, 2018] to characterize the droplets. The droplet diameter were found in the regime 4 µm to 8 µm [Kügler, 2018].

The intensity of the scattering can be taken as an estimator for the supersaturation, since the droplets grow bigger, the time to pass the laser beam increases and thereby increase the scattered intensity at a fixed flow rate. Changing the temperature difference between saturator and condenser influenced the observed scattering. Lowering the temperature difference caused a decrease of the intensity. Increasing the temperature difference also increased the scattered intensity, since the final droplet size and therefore the scattered intensity is dependent on the supersaturation.

Using the counting optics module, the scattered light was inspected with an oscilloscope (Fig. 4.6) and analyzed offline. Peaks were again only visible if particles were in the aerosol stream. The peak width was found to be about 200 ns (FWHM), which matches with a flow of 1 L min^{-1} and a nozzle diameter of 1 mm the approximated droplet size of a few µm at the given size of the laser focus. With the efficient light collection of the counting optics module, the APD reached saturation for every peak, which facilitates the counting but makes the peak intensity inspection impossible.

Calibration Measurements

The result of the linearity check is shown in figure 4.7. For all four test series the response to changes in the particle concentration of both devices is very similar over the whole concentration range. The coefficient of determination gives $R^2 = 0.9907$, calculated with Pearson's formula of the correlation coefficient. By trend the HTCPC slightly overestimates the concentration.

The measured detection efficiency on soot particles in dependency of the particle mobility diameter is shown in Figure 4.8. The data is normalized to the measurement at 90 nm and corrected size dependent for losses in the particle supply and the capillary according to Baron and Willeke, 2001;

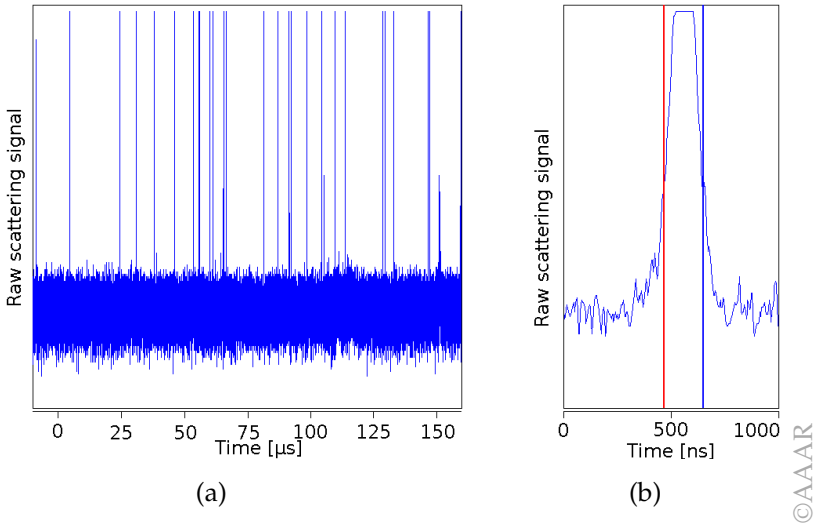

Figure 4.6.: Raw signal of the detected scattered light above the HTCPC nozzle. Every peak in the graph is one droplet passing the laser beam. If no particles were in the aerosol no peaks, no peaks were present in the signal. a) 400 µs of raw data, multiple peaks are visible, b) magnification of 1 µs, the FWHM of the peak is about 200 ns.

Hinds and Kennedy, 2000. The counting efficiency curve of the reference device - the AVL 10 nm CPC - was considered for deriving the HTCPC counting efficiency. The legislative requirements for PNC according to Annex 5 of the GTR 15 [United Nations, 2014] prescribes a detection efficiency of (50 ± 12) % at (23 ± 1) nm and >90 % at (41 ± 1) nm. For all three measurements the requirement at 23 nm is fulfilled and two measurements also fulfill it at 41 nm. The detection efficiency at 23 nm is at the lower end for all three measurements, thus fine tuning of the efficiency curve to reliably match the requirements by adaptation of saturator and condenser temperature is possible. This was not done within this study, since the possibility of a compliant measurement device was clearly proved.

It shall be noted that the observed working fluid consumption was about twice as the considered 8 mL h^{-1} for the simulation.

Long Term Durability
After 450 min of total operation and 223 min exposure to undiluted automotive exhaust, the HTCPC was functioning unrestricted. For automotive grade CPC that corresponds to at least 45 000 min of operation (dilution > 100). Inspection of the wick and the remaining working fluid showed no

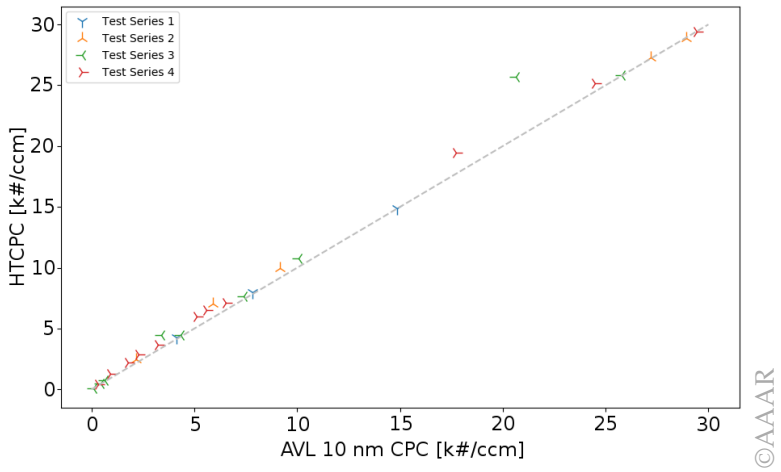

Figure 4.7.: Results of the linearity of the HTCPC to an 10 nm AVL CPC. 32 stationary points were measured in 4 test series (measurements). R^2 = 0.9907. Saturator temperature 205 °C, condenser temperature 170 °C.

residue of chemical interaction with the exhaust.

The particle count was in correlation with the reference devices and a drift was not indicated, thus long term stability of operation is given. The integrated particle count over two complete cycles gives a ratio of 1.25 between the HTCPC and the reference CPC with legislation compliant counting efficiency for the first and one of the later cycles. Data from the particle number counting devices available at the chassis dynamometer must not be published since it was an ordered measurement campaign. For proper PN measurements a calibration procedure for high temperatures has to be developed.

Conclusion

The feasibility of our optimized HTCPC was proven. With systematic investigations we identified n-Eicosane as the best candidate for a high temperature working fluid. The measurements of its bulk surface tension gave in mean 7 % higher values than predicted by the regression formula from the literature what results in a smaller d_K. Measuring the contact angle on a graphite surface revealed specific adhesion forces between the two substances, making it even an even more desirable working fluid for automotive exhaust. The mixed-flow design of the HTCPC enables a continuous laminar flow

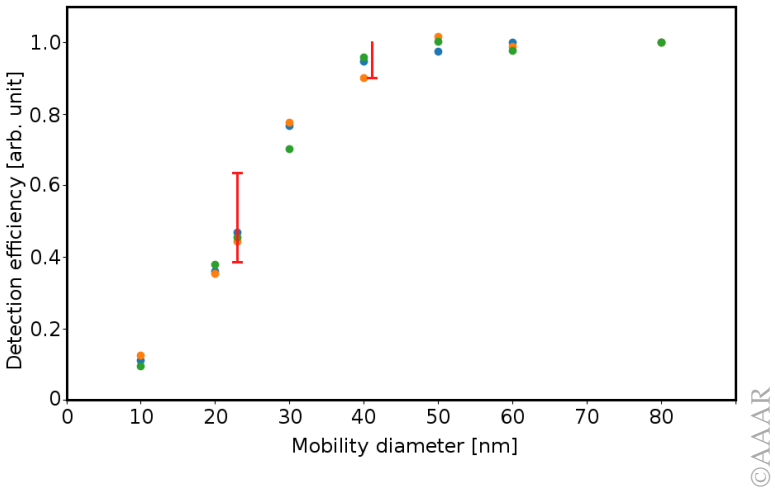

Figure 4.8.: Results of three detection efficiency measurements of the HTCPC for soot from a APG, corrected for diffusional losses in the capillary. Marked span covers GTR 15 requirements. Every point is the mean value of 60 s sampled data. Saturator temperature 205 °C, condenser temperature 170 °C.

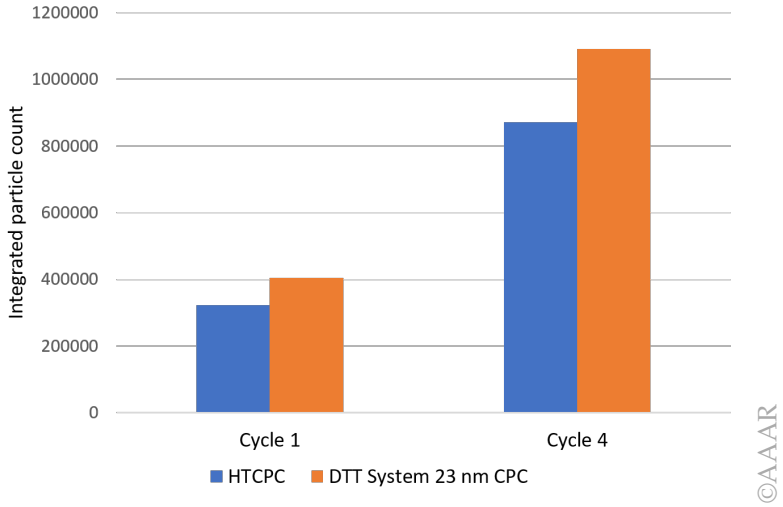

Figure 4.9.: Integrated particle counts from two driven cycles from at the testbed. The ratio of both values is 1.25 in both cases.

through the device and thus minimizing particle losses. As carrier gas nitrogen is used to prevent oxidation of the working fluid, catalyzed by the wick. With an open optics module we inspected the operation of the device and characterized the droplet growth. With our especially developed high temperature counting optics module, operating at 215 °C, we proved CPC operation at high temperatures. Calibration measurements were done using

soot particles from an APG and revealed a linear behavior and a counting efficiency compliant to the current legislative requirements. By measurements on automotive exhaust for 223 min and a total operation time of 450 min, the long-term stability of the device was verified.

Acknowledgement

This work was done within the Competence Centre ASSIC - Austrian Smart Systems Research Center, co-funded by the Austrian Federal Ministries of Transport, Innovation and Technology (bmvit) and Science, Research and Economy (bmwfw) and the Federal Provinces of Carinthia and Styria within the COMET Programme.

This work was supported by AVL List GmbH.

4.3. A High-Temperature Condensation Particle Counter Optimized for Engine Exhaust

Section 4.3 will be published as *M. Kupper, M. Kügler, M. Gleichweit, M. Kraft, M.Koch and A. Bergmann, "A High-Temperature Condensation Particle Counter Optimized for Engine Exhaust"* in the journal MDPI Sensors.

Abstract

A stable high-temperature condensation particle counter (HTCPC), operating above 170 °C was optimized for measurement on automotive exhaust. A dedicated wick for high temperature application was identified in a two-stage process, consisting of a pre-selection based on relevant substance properties and a subsequent experimental evaluation in combination with the working fluid. A prototype for experimental evaluation of the concept was designed and built, supported by CFD simulations considering the properties of the working fluid and the wick. An optimized high-temperature optics module was developed and verified for reliable CPC operation.

Introduction

Condensation particle counters (CPCs) are well established devices for measuring particle number (PN) concentrations. They cover a broad field of application [McMurry, 2000] for environmental sensing, science and industry [Giechaskiel, Dilara, et al., 2008; Hillemann et al., 2014; Seipenbusch, Binder, and Kasper, 2008; Wehner et al., 2011; Zhang and Liu, 1991], and are even the prescribed devices for measuring PN in automotive exhausts in compliance to European legislative guidelines, according to UNECE regulation 83 for passenger cars [Giechaskiel, Maricq, et al., 2014; Official Journal of the European Union EN, 2015]. So a lot of groups all over the world made these, in general simple devices, the content of their research[Barmpounis et al., 2018; Kuang et al., 2012; McMurry, 2000; Stolzenburg and McMurry, 1991]. Water CPC [Hering and Stolzenburg, 2005; Hering, Stolzenburg, et al., 2005] Although specialized devices for various applications have been developed of the years, the underlying CPC concept remained essentially unchanged. Butanol is used as working fluid, requiring room-temperature operating temperature. For aerosols of elevated temperatures, such as from combustion engines, this entails a major drawback: the aerosol temperature has to be significantly reduced, resulting in substantial changes of the aerosol properties through condensation [list possible changes]. An obvious solution to this problem was presented in 2012 by Rongchai and Collings, who introduced a high-temperature (HT) CPC approach for automotive exhaust measurements above 150 °C.

Here, we present a revised and optimized mixed-flow high-temperature optical particle counter (HTOPC) for operation above 170 °C, which we characterize by ...[list what was done]. Our design, which builds on a previously presented HTCPC prototype using n-Eicosane as a working fluid, is optimized for engine exhaust measurements and includes significant improvements of the wick material, as well as a reasonable realization of the mixed-flow principle. Of central importance is the development of a high temperature optical particle counting unit that shows stable operation at 230 °C. We demonstrate that this design is capable of long-term operation and very high particle concentrations. By systematic investigations on wick materials and the working fluid behavior an optimized flow concept is presented, including an inherent dilution. All components as well as the whole device have been extensively characterized, revealing stable and reliable

operation. Our HTOPC setup thus complies to the European legislative guidelines for measurements on automotive exhaust gas.

Materials and Methods

Description of the HTCPC
The HTCPC was designed as a "mixed-flow" CPC, where the saturated vapor is created with a particle free gas and the particles were injected directly into the condenser [Stolzenburg and McMurry, 1991]. A scheme is shown in Figure 4.10. The saturator was aligned horizontally and the condenser vertically. The particles were injected through a dedicated injection nozzle, designed for optimized distribution of the particles into the supersaturated region. The flow concept is described in more detail in section 4.3.

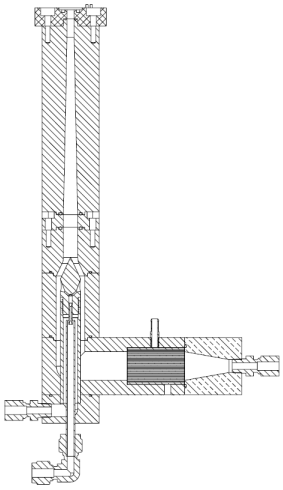

Figure 4.10.: Scheme of the used HTCPC device.

The saturator is in total 10 cm long and has space for one wick with cylindrical shape, 4 cm long and 2.5 cm in diameter. The wick is filling the inner diameter of the saturator completely, enabling a flow with a honeycomb structure. The cell density and wall thickness differs between the tested wicks. The flow is led through an elbow and a 1.5 cm insulation made of PEEK into the 14.5 cm long condenser. The inner diameter of the condenser constricts continuously from 1 cm to 0.7 cm. At the end a nozzle with 1.8 cm length and a 500 µm outlet aperture is attached. The particle carrying aerosol

is lead through a capillary with a diameter of 0.7 mm into the injection nozzle, where the flow is distributed uniformly into 8 partial flows and mixed with the supersaturated gas.

Working fluid
In a previous work n-Eicosane was identified out of 46 candidates as the best candidate for a high temperature working fluid (see section 4.2). It is a saturated, aliphatic, long-chained hydrocarbon ($C_{20}H_{42}$), and belonging to the paraffins. Thus it is non-toxic, thermally stable and chemically inert. With its high boiling point and high vapor pressure it combines a lot of favorable properties for a CPC working fluid.

Unfortunately thermal degradation of n-Eicosane occurs by the presence of oxygen. Long term operation is possible if an inert gas like N_2 is chosen as carrier gas and the particle carrying sample aerosol is injected after the wick. But also this procedure does not prevent degradation completely. We found experimental evidence, that the wick material is mainly influencing the degradation process. The degradation product was examined with an optical microscope.

Long-term operation showed thermal degradation, catalyzed by the cordierite wick used at the time. The reaction is very likely an oxidation, since in the selection process durability tests at 250 °C were done with exclusion of Oxygen. For all tests no evidence for degradation was found for n-Eicosane, even if a catalyst was present. Thus, for a long term stable HTCPC an adapted operation mode using will be presented.

Wick Materials
For a reliable operation, a suitable combination of wick material and working fluid is needed, ideally damping the decomposition of the working fluid and still provide a sufficient saturation. Considerations suggest a porous, temperature durable material without catalytic components which could be available easy at the desired dimensions at high quantities. Therefor we considered IBIDEN FRAUENTHAL MK20 cordierite ceramic, IBIDEN FRAUENTHAL HT ceramic, IBIDEN FRAUENTHAL NT ceramic and porous aluminum as potential candidates, NGK cordierite ceramic and silicon carbide (SiC) diesel particulate filter were also tested for comparison (Figure 4.11), since wicks from NGK ceramics were used until now and SiC is known catalyst. The material properties are listen in Table 4.3. Also taken into account were cords for candle wicks and glass wool but were not

	FT HT	FT cordierite	FT NT	aluminum	NGK	SiC
Cell density / [cm^{-2}]	200	400	400	320	400	400
Wall thickness / [mm]	0.37	0.11	0.5	0.23*	0.11	0.31

Table 4.3.: Material parameters of the tested materials. FT ... FRAUENTHAL, *... cells round, thinnest location, uncertainty of wall thickness ± 0.01 mm

evaluated because of their cumbersome handling and because of the satisfying performance of the other evaluated materials. Graphite was refused due to its low free volume and compared behavior observed at the other materials at the given geometry it can't be expected to reach a satisfying vapor saturation.

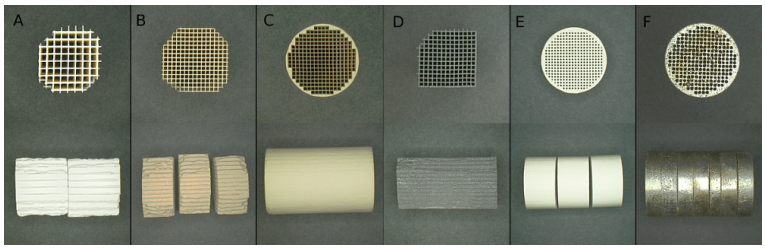

Figure 4.11.: Photographs of the tested wicks before usage: A) IBIDEN FRAUENTHAL HT ceramics, B) IBIDEN FRAUENTHAL cordierite ceramics, C) NGK cordierite ceramics, D) SiC diesel particulate filter, E) IBIDEN FRAUENTHAL NT ceramics, F) porous aluminum.

Experimental Methods

To test the materials for their suitability, they were used as a wick in the HTCPC setup. The tests were performed with the HTCPC prototype, one wick was inserted in the saturator, then the device was heated up to 210 °C for the saturator and 190 °C for the condenser and after reaching operation temperatures n-Eicosane was filled into the saturator. A total flow of 0.6 L min^{-1} was enabled through the device for 18 h. It was assured, that the wick was always wetted and the volume flow was constant. After every performed test, the embodiment was disassembled and cleaned, also fresh n-Eicosane was used every time.

This procedure was performed for silicon carbide (SiC), NGK cordierite, FRAUENTHAL cordierite and FRAUENTHAL HT ceramics for air and high pure nitrogen (N2) as carrier gas. FRAUENTHAL NT ceramics and porous aluminum were excluded during the testing procedure due to poor performance. The four tested materials were also examined by X-ray fluorescence

spectroscopy (XRF) to determine the chemical composition. Analysis with XRF for the degratdation prodcus of the working fluid was refused since the light H and C atoms are not detectable this technique.

Flow Design
For the flow concept of the HTCPC was designed on one hand to assure a uniformly saturated vapor, a laminar flow and a high supersaturation. On the other hand sampling of high particle concentration was considered by an inherent dilution system and an optimized distribution of the sampling aerosol in the saturator is assured by a injection nozzle.

Simulations
CFD simulations were performed using Ansys Fluent 16.0.1 with a density-based implicit solver with the pseudo-transient solution method. The fluid calculation is using the ideal gas model. The fluid inside the HTCPC was considered as a mixture of two gases, whereas nitrogen was considered as one gas and the working fluid vapor as the second. The mass fractions of the gases in the fluid were calculated continuously, considering condensation at the walls and evaporation at the completely wetted wick. Thermal dependency of material properties was also considered in the simulation. The flow was set to $1\,\mathrm{L\,min^{-1}}$ at the outlet. The temperature of the saturator was 210 °C, the temperature of the condenser was 190 °C. The Kelvin-diameter d_K was calculated by post processing, using the resulting parameters from the simulation for the steady state. All simulations were full 3D, using the manufacturing CAD files.

Flow concept
The main flow of the particle free carrier gas should enter the saturator and pass the wick so a saturated atmosphere of working fluid vapor is created. The vapor is then mixed with the particle carrying sample aerosol shortly before the insulation between the saturator and the condenser (Fig. 4.12), by a distribution nozzle. The nozzle is designed for a laminar mixing of the saturated vapor and the sample aerosol. The flow inside the nozzle is split into 8 channels, distributing the sample aerosol uniformly around the top of the nozzle.

The inherent dilution of the sample aerosol is realized by a capillary with an inner diameter of 0.7 mm and a length of 18 mm which is leading the sample flow from the sampling line to the injection nozzle. The dilution ratio is set by the pressure difference between the inner of the HTCPC and

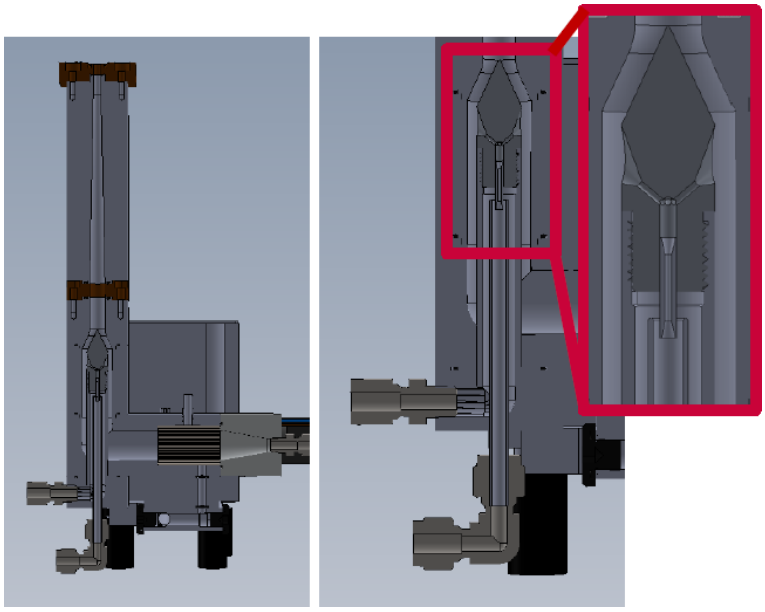

Figure 4.12.: Scheme of the flow design of the HTCPC.

the sampling line. The principle is shown in Figure 4.12. The sample line transports 1 L min^{-1} from the source (e.g. particle generator or exhaust pipe) at ambient pressure towards the capillary. Due to the pressure difference between the sample line and the carrier gas a certain amount of the sample aerosol is extracted from the sample line, the rest is lead further to the exhaust. The pressure difference is set by a needle valve at the carrier gas inlet, since the total flow through the HTCPC is fixed by a critical orifice.

The condenser continuously narrowing to improve the temperature distribution within the aerosol, since n-Eicosane has a very low temperature conductance.

Optical Particle Counter

Determination of the particle count rate takes place in the optical particle counter (OPC), which consists of the laser source (Fig. 4.13, part 2), the scattering chamber (15), the imaging lens system (8, 11) and the detector (12). The particle beam enters the scattering chamber through a nozzle (7) with 0.57 mm in diameter and traverses a light sheet that is generated by the laser. Scattered light from the particles is collected by the lens system and imaged onto the detector. In order to prevent condensation of working fluid on the optical elements and walls, the temperature of the scattering chamber has to exceed the condenser temperature. In our case, the scattering

chamber of the high-temperature OPC (HT-OPC) is operated >15 °C above the condenser temperature, thereby being designed to reach 235 °C. The laser and detector, in contrast, must not exceed a temperature of 40 °C, causing challenges in terms of thermal insulation and misalignment due to thermal expansion.

In the following we first describe improvements of the presented HT-OPC design with respect to a previous version, before we discuss details of the light sheet generation, signal collection and thermal management [Gleichweit, 2019]. Measurements characterizing the performance of the HT-OPC are presented in Sec. 4.3.

Improvements to previous setups
Based on experiences with a previous design (4.2), we developed a new optics unit with the following improvements:
(i) A commercial diode laser module with integrated optics for collimation and formation of the light sheet is used. Alignment mechanics (Fig. 4.13, parts 1, 4, 5) for position and tilt angle enable precise positioning of the light sheet above the nozzle. All crucial parameters to align the light sheet position can be tuned precisely while the active components are operated at room temperature.
(ii) A variable position of the imaging lenses (8, 11) provides flexibility in the lens design and focal lengths, and allows to choose between microscope-like and 2-f imaging configurations. With the microscope-like configuration we increased the light collection efficiency by 54%, corresponding to an NA increase from 0.24 to 0.45.
(iii) In the microscope-like configuration the region between the objective lens (8) and the ocular lens (11), called tubus in a microscope, provides room for a beam trap (9, 13) and an optical band pass-filter (10). In order to reduce stray light within the optical path which generates background on the detector, a mirror (9) is used to reflect the main beam towards a proper beam dump (13). Placing the beam trap at this position further allows for convenient size and position optimization, further increasing the collection efficiency of signal light. The optical filter (10) transmits the laser wavelength and blocks black body radiation emanating from the hot surfaces inside the scattering chamber (15).
(iv) The scattering chamber (15) can be opened in order to monitor the beam path, which facilitates beam alignment through the OPC but is not necessarily required.

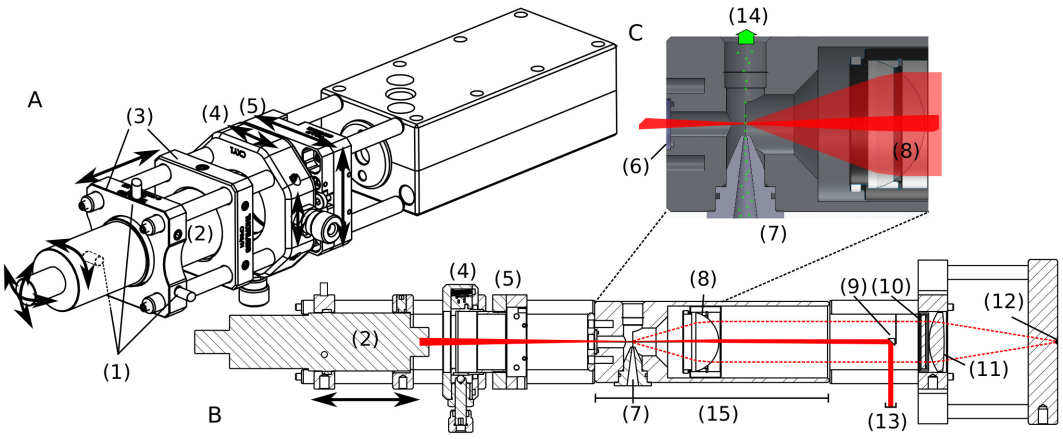

Figure 4.13.: Scheme of the high temperature OPC module. A: isometric drawing of the laser side. B: vertical cut though the whole module. C: close up of the laser-particle interaction region. (1) custom made tripod cage plate (2) laser (3) laser retainer (4) XY-Translator (5) slip plate positioner (6) laser window (7) nozzle (8) objective lens (9) prism mirror (10) optical bandpass filter (11) ocular lens (12) detector (13) beam dump (14) particle flow (15) scattering chamber. The red dotted line and shaded region indicate scattered light.

Light sheet generation

The smallest possible height of the light sheet is required for a short particle-laser interaction time and, correspondingly, a high particle count number. To achieve this, we use a commercial laser module[†] that includes focusing optics with fixed focal length which leads to a working distance of (95.05 ± 0.05) mm. It provides a 2.4 mm broad beam with 21 µm in height in the focal region. The laser source and the detector (both <40 °C) are connected to the hot scattering chamber by a stainless steel rod system (Thorlabs 30 and 60 mm cage system) in order to provide sufficient mechanical stability and thermally decouple them from the scattering chamber (15) (>200 °C). The laser module is mounted on a tripod system (1) that allows for vertical and horizontal tilt, while x-, y- and z-alignment is achieved via the combination of laser retainer (3), slip plate (5) and x-y-stage (4). With these five degrees of freedom the laser beam can be guided precisely along the central axis through the scattering chamber, with the smallest vertical diameter of the light sheet placed exactly above the nozzle and the outgoing beam hitting the prism mirror (9) and beam dump (13). The focused laser beam enters the scattering chamber through a MgF_2-coated glass window[‡] (6), which influ-

[†]Schäfter and Krichhoff 5LT-100-2 and 55CM-660-23-M01-A8-C-6, 660 nm, 23 mW.
[‡]Edmund Optics 32947 Window B270, Thickness (1.15 ± 0.05) mm.

ences the light sheet dimensions. The light sheet height, as measured with a knife edge beam profiler, increases from $(20.9 \pm 0.5)\,\mu m$ to $(22.2 \pm 0.2)\,\mu m$, the working distance from $(95.05 \pm 0.10)\,mm$ to $(95.50 \pm 0.10)\,mm$, and the Rayleigh range of the focus region is extended from $(1080 \pm 50)\,\mu m$ to $(1250 \pm 30)\,\mu m$. However, all these alterations are within an acceptable amount.

Signal light collection
Scattered light from the interaction region, indicated by dashed lines and shaded region in Fig. 4.13, , is collected by a plano-convex lens (Fig. 4.13, part 8, Thorlabs LA1951) that is placed at focal-length distance to the nozzle and thus acts as objective lens. The collimated light is focused onto the detector (12) by the ocular lens (11, Thorlabs LBF254-040). The employed detectors are described in Sec. 4.3, under Light Collection Characteristics. This microscopy-like configuration provides room in the tubus region between the two lenses for additional elements: a prism mirror (7, 3x3 mm^2) is used to reflect the primary beam, which is also collimated in this region, towards a distanced beam dump (13). This minimizes both the stray light caused by the intense primary beam and the loss of scattered signal light. An optical band pass filter[§] (8) is used to block thermal radiation emanated by the scattering chamber and other background. By switching from the 2f to the microscope-like setup the numerical aperture was increased from NA = 0.243 to 0.447. Together with an optimized beam trap size, this promises a higher light collection efficiency.

Thermal considerations
The scattering chamber is heated with conventional cartridge heaters to a temperature of up to 235 °C. At these temperatures MgF_2 is one of the few conventionally available anti reflection coatings. This high temperature operation of the scattering chamber brings strain and distortion into the setup. The design is based on considerations regarding thermal expansion, thermal induced strain, temperature management and resilience during heating-cooling cycles. The consequence of thermal deformation of the mounting system was estimated based on an unbalanced temperature distribution in the stainless steel rods, causing a tilt of the laser source. By a temperature difference between 0 °C to 50 °C between the upper and the lower rods, a shift of the laser focus point vertical to the optical axis between 0 µm to

[§]Thorlabs FBH660-10, center transmission wavelength 660 nm, FWHM 10 nm

150 µm can be expected [Gleichweit, 2019]. Such a shift causes a drift of the collected signal light on the active detector surface, thus a sustainable alignment and a homogeneous temperature distribution is critical for operation. A uniform temperature distribution after a heat-up phase of 12 min of the scattering chamber was verified with IR-camera measurements, wherefore one chamber side panel was painted matt black (Appendix, Figure D.1). The HTCPC was found to retain alignment after several heating-cooling cycle.

For further optimized long term operation the scattering chamber is wrapped with fiberglass fabrics for better temperature stability and homogeneity. Passively cooled heat sinks[¶] had to be applied to the slip plate and cage plate adaptor to keep the laser, IR-filter and detector close to ambient temperature.

Results and Discussion

Working Fluid and Wick Material

With the degradation of n-Eicosane, the originally limpid fluid changes its colour from yellowish to orange brown to dark brown and black. Also it becomes more viscous with proceeding degradation. Very sustainable remains in form of a black or dark brown film were left by this process at the inside of the HTCPC. It can just be removed by application of rough forces, like scratching or rasping. The wick present was covered by a layer of degradation products on the part which has contact to air. Inspection with an optical microscope revealed a continuous layer of grains, arising from the degradation (Fig. 4.14). Thereby the porosity of the material is reduced and the surface sealed, comprising the functionality as a wick. Pure n-Eicosane would form a smooth white surface.

Since n-Eicosane is a long chained hydrocarbon ($C_{20}H_{42}$), it is very likely that the observed reaction is a cracking of the long molecule into shorter hydrocarbon chains. This processes are usually observed at much higher temperatures and pressures. Nevertheless, catalyzed by some materials even under the absence of oxygen such a reactions are possible. Further the

[¶] 2x Seifert WA208, 75 mm x 54 mm x 31.6 mm, thermal resistance 2.2 K/W; 1x ABL Components 515AB0500MB 50 mm x 88 mm x 25 mm, thermal resistance 2.5 K/W; 1x AVC O4523DC, 84 mm x 70 mm x 35 mm, thermal resistance >1 K/W.

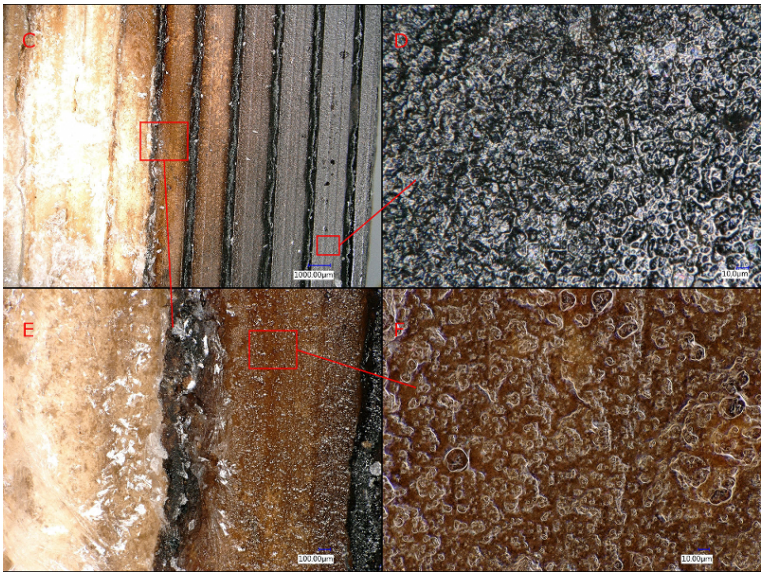

Figure 4.14.: Inspection of the degradation products of n-Eicosane on the surface of a wick from IBIDEN FRAUENTHAL HT ceramics.

degradation process was not very efficient, since with a continuous even with air flow the first indication appear usually after a few h.

It can be assumed, that the reaction happens in the liquid state of n-Eicosane rather than in the vapour. Degradation products were just found if liquid n-Eicosane was present, in the gas path as well as in the deposition trap before the ejector pump just pure white n-Eicosane was found. Also, since the liquid working fluid changed its appearance progressive, components who already reacted were probably degraded further.

The thermal degradation process at the HTCPC can be minimized by usage of N_2 as carrier gas, but is still depending on the used wick material. The experiments showed that porous aluminum and IBIDEN FRAUENTHAL NT ceramic are not suitable candidates because of rather bad saturation behavior. The necessary supersaturation for a sufficient droplet growth with these two materials could not be reached with the located operation tempertaure. Therefore they were not examined further. The long term test were performed with IBIDEN FRAUENTHAL HT ceramic and IBIDEN FRAUENTAL cordierite ceramics as potential candidates, NGK cordierite ceramic and silicon carbide for comparison.

Silicon Carbide

The tests with the SiC wick and air as the carrier gas showed in comparison to the other materials the strongest degradation of n-Eicosane. The remaining working fluid in the saturator was of dark yellow to orange brown colour. The surface of the wick was partly covered with a very sustainable, dark brown to black glazing. This layer probably prevents the operation as a wick, since no vapor can be disposed through it. Further some channels were completely clogged by the degradation products of n-Eicosane, hindering the flow of the carrier gas.

Contrary, the test with N2 as carrier gas showed almost no degradation of the working fluid after 18 h, although slight but distinct darkening of the wick was visible on the side the carrier gas approached. This is probable due to residual oxygen which was bonded inside the material.

NGK Cordierite Ceramics
For the test with air as carrier gas very strong degradation of the working fluid was observable. The surface of the wick was hevily stained and covered with a layer of degradation products of n-Eicosane. As for the SiC, also here some channels were completely clogged. The remaining working fluid was of dark yellowish colour with brown streaks.

The usage of N2 as carrier gas reduced the degradation of n-Eicosane strongly, but still degradation was observable at a distinct degree. The wick was clearly stained and the remaining working fluid was of a yellowish colour. This observation was astonishing, since the degradation was assumed to be an oxidation. Thus it was assumed further, that it can be prevented with the exclusion of Oxygen. The observed degradation under N2 atmosphere could be explained with the assumption, that the material retains high amounts of oxygen within its crystal lattice. Also even high-pure (99.9 %) Nitrogen contains very small amounts of other gases, one of them Oxygen. By operation for 18 h by a flow of 0.6 L min^{-1}, an amount of Oxygen is passing the wick which can not be neglected. The decomposition could be catalyzed more efficient by this material due to its composition, since it contains higher amounts of Iron and Titanium than the other materials (Tab. 4.4).

IBIDEN FRAUENTHAL Cordierite Ceramics
Again, for air as carrier gas heavy degradation was observable. The degree of degradation and the observed consequence were very similar to those from the test with NGK ceramics with air.

If N2 was used as carrier gas, almost no changes could be observed. The wick was slightly stained, but clearly less than the SiC under N2 atmosphere. The working fluid appeared completely limpid.

IBIDEN FRAUENTHAL HT Ceramics

The test with air as carrier gas brought also for this material heavy degradation of n-Eicosane, but the least distinct in comparison to the other materials tested with air. The wick was still heavily stained and covered by decomposition product of n- Eicosane, and the remaining working fluid was of yellowish colour (Fig. 4.15). From this it appears that the HT ceramics is the weakest catalyst from the materials tested.

Figure 4.15.: Pictures of the IBIDEN FRAUENTHAL HT ceramics wick after 18 h operation with air as carrier gas. Views: A) front, B) side, C) bottom and D) top

After testing the test with N2 the only observable change was a slight darkening at the top of the wick. This is probably due to the residual oxygen which was stored inside the material. The working fluid showed no sign of degradation at all, appearing completely limpid.

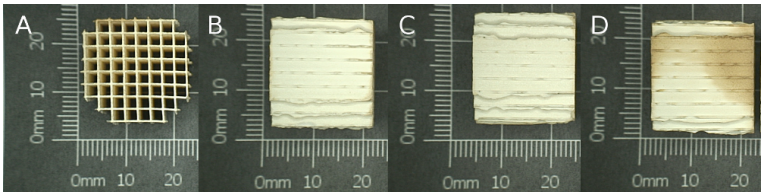

Figure 4.16.: Pictures of the IBIDEN FRAUENTHAL HT ceramics wick after 18 h operation with mixed flow using N2 as carrier gas. Views: A) front, B) side, C) bottom and D) top

XRF Analysis

The results of the XRF analysis are listed in table 4.1. The SiC diesel particulate filter showed mostly Si and small amounts of Sr and Al. Carbon is not detectable with the used technique. The analysis of the IBIDEN FRAUENTHAL MK20 ceramics revealed aberrations from the data sheet. Found were a slightly higher proportion of Si and no Mg although 9 % were

stated. It contained about twice as much K, Ti and Fe as the HT ceramic samples and the NKG cordierite ceramics contains even higher amounts of Ti and Fe. This explains the increased catalytic activity, since Fe is a known catalytic active element and Ti a known carrier element that supports the catalytic component by increasing the surface area [Farrauto, Dorazio, and Bartholomew, 2016; Kügler, 2018].

Element	FT HT	FT MK20	NGK	SiC
Al	62.1 %	35.5 %	36.1 %	1.4 %
Si	34.2 %	57.2 %	54.6 %	94.4 %
K	1.4 %	2.8 %	0.4 %	0.1 %
Fe	1.1 %	2.6 %	5.4 %	0.4 %
Cl	0.4 %	0.4 %	0.4 %	0.2 %
Ca	0.4 %	0.5 %	0.3 %	0.2 %
Ti	0.3 %	0.6 %	2.0 %	0.0 %
Sr	0.0 %	0.0 %	0.0 %	3.2 %
Ga	0.0 %	0.2 %	0.0 %	-
Ni	-	0.0 %	0.3 %	0.0 %
Cr	0.0 %	0.0 %	0.1 %	0.0 %

Table 4.4.: Results of the XRF analysis of the four materials tested in the long term test [Kügler, 2018]. FT HT...IBIDEN FRAUENTHAL HT ceramics, FT MK20...IBIDEN FRAUENTHAL MK20 cordierite ceramics, NKG...NGK cordierite ceramics, SiC...Silicon carbide diesel particulate filter. -...not detected

Conclusion Working Fluid and Wick Material

The degradation after 18 h of operation was the strongest for the SiC, followed by about the same for the two cordierites, whereas the NGK cordierite showed clearly strong degradation under the N2 atmosphere. For the IBIDEN FRAUENTHAL HT ceramic the degradation was the lowest.

All experiments with air as carrier gas resulted in a breakdown of the HTCPC due to thermal degradation of the working fluid. The time of possible operation differs if different wicks were used, what suggests an influence on the process.

The two cordierite ceramics showed the most degradation of n-Eicosane, what is not especially surprising, since the material is a known catalyst and is actually used as a particle filter for diesel engines (DPF). Anyway, the effect was much smaller as with full flow operation on air, even after 18 h

operation was still possible. Although the coating of the wick itself was weakly distinct, the color of the working fluid during operation became very dark. Same was observed with SiC, but with a weaker effect. Pleasant surprising was, that operation with the FRAUENTHAL HT ceramics showed no change in color of the working fluid, no observable coating of the wick and almost no change in color. The happened reaction can be lead back to two circumstances: first, even high purified N2 gas contains some ppm of oxygen and second the wick was stored in ambient air, so oxygen was bonded into the porous material.

Flow Design
The results of the simulation of the dilution concept is shown in Figure 4.17 and listed in Table 4.5. The resulting pressures for the 0.7 mm x 18 mm are in a feasible regime. These pressures could be set experimentally and the uncertainty of the pressure measurement propagates not too much onto the flow setting.

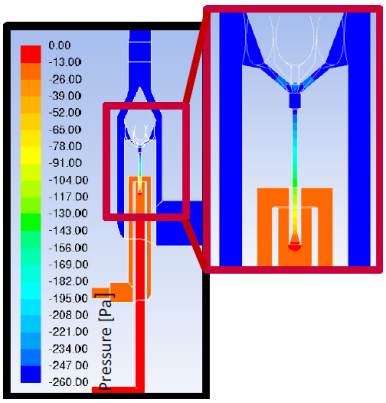

Figure 4.17.: Results of the simulation of the flow concept.

Further the simulation resulted a good mixing behavior of the vapor and the sample aerosol (Fig. 4.18) and predicts a very high saturation of about 140 %, resulting in a d_K of about 20 nm for the set temperatures. In the previous work (section 4.2) the simulation resulted a d_K under 10 nm, which could not be proven experimentally. The geometry of the condenser was revised for this prototype, considering the thermal conductivity of n-Eicosane.

The total flow was around 0.9 L min^{-1} to 1 L min^{-1} and with the MFC at the carrier gas inlet the flow was set to 0.1 L min^{-1} lower than the total flow. The difference of 0.1 L min^{-1} between the carrier gas and the total flow thus had to be the sample flow.

0.7 mm **x** 18 mm	DR	Sample Line / [Pa]	Carrier Gas / [Pa]
	1:5	0	-244
	1:10	0	-539
1 mm **x** 15 mm	DR	Sample Line / [Pa]	Carrier Gas / [Pa]
	1:5	0	-46.7
	1:10	0	-100.9
no capillary	DR	Sample Line / [Pa]	Carrier Gas / [Pa]
	1:5	0	-10.4
	1:10	0	-14.1

Table 4.5.: Simulation results for the dilution ratio of the inherent dilution of the HTCPC. Dilution ratio for different pressure difference between the sample line and the saturated flow, for two different capillaries and if no capillary was inserted. DR. . . dilution ratio

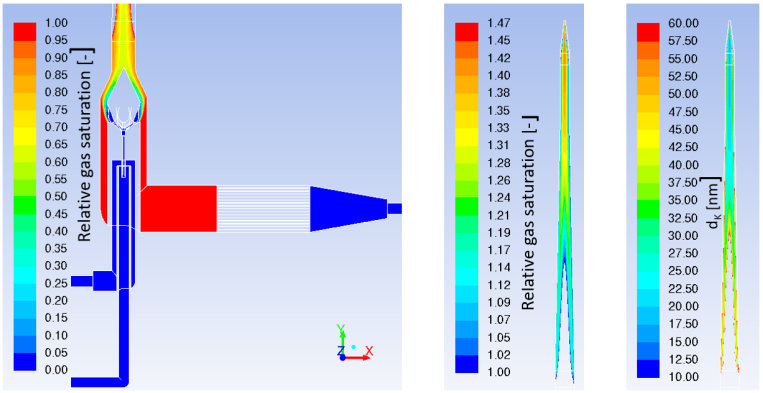

Figure 4.18.: Results of the simulation of the saturation and the Kelvin diameter d_K.

For the calculation of the PN concentration the flow values are needed and critical.

Optical Particle Counter

In the final characterisation process of the HTCPC it is crucial to know the HT-OPC's measurement range and mechanical constrains. In this section we describe the performance of the HT-OPC in terms of signal quality, counting efficiency, linearity, maximum count rate. With the knowledge of the dimensions of the beam interacting with the particles and pulse duration of the detected scatter peaks the particle flow rate can be estimated and the other way around.

Light collection characteristics

Inspection of the signal was performed with two different detectors: either an avalanche photo diode (APD, Thorlabs APD120A/M) or a regular photo diode (PD, Hamamatsu S5971, 100 MHz, PIN-type) on a detector board dedicated for CPC operation, provided by AVL List GmbH. The APD delivers up to 1.8 V at 50 Ω impedance load and is read with a storage oscilloscope at 2.5 GS/s. The PD is sampled by an ADC at 50 MHz with 8175 a u resolution. The power of the laser source (up to 23 mW) is adjusted to meet the dynamical ranges of the two detectors respectively.

Figure 4.19 shows example pulses collected with the APD detector and Table 4.6 lists pulse height, calculated light sheet height, pulse duration and signal-to-noise ratio (SNR) for the different optical setups and utilized detectors. Pulse height and pulse duration are determined by averaging over large sample sizes. With the flow rate of $(1000 \pm 30)\,\mathrm{cm}^3/\mathrm{min}$ and nozzle diameter of $(570 \pm 10)\,\mu\mathrm{m}$ the particle speed is easily calculated, which allows to estimate the light sheet height from the pulse duration during operation.

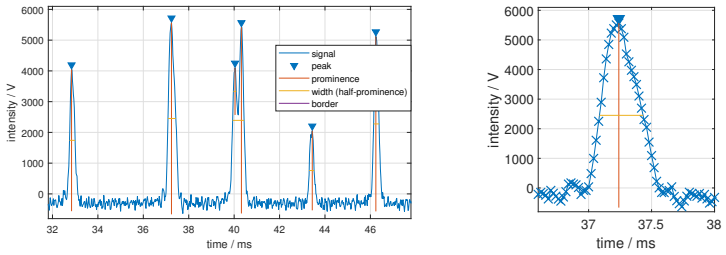

(a) Example of the pulse height distribution of the raw signal

(b) Magnification of a representative pulse

Figure 4.19.: Inspection of the pulses, data was sampled with 50 MHz.

Based on the APD measurement, we obtain a light sheet height of $(20 \pm 3)\,\mu\mathrm{m}$ which is in agreement with the knife edge measurement of $(22.2 \pm 0.2)\,\mu\mathrm{m}$ (including the entrance window, see Sec. 4.3). Compared to the old OPC the pulse duration and, correspondingly the light sheet height, could be reduced by ∼45 %. We attribute this performance increase to the laser collimation quality of the new laser source. The ∼20 % longer pulse duration obtained with the PD, compared to the APD, might be caused by transfer function of the amplifier after the PD. The pulse height and the SNR were both significantly increased with the new setup, which we ascribe to the microscopy-like approach in combination with the optimized blocking

strategy of the main beam. For example, with the PD the SNR is increased by a factor of three.

	new setup, APD	new setup, PD	old setup, APD	old setup, PD
pulse duration	(300 ± 20) µs	(370 ± 35) µs*	(560 ± 35) µs	-
light sheet height	(20 ± 3) µm	(24 ± 3) µm	(36 ± 5) µm	-
pulse height	(1050 ± 150) mV**	(4500 ± 800) a.u.**	(390 ± 100) mV	< 1600 a.u.
SNR	50	23	19	8

Table 4.6.: Comparison of old setup (2f) and new setup (microscope-like) with two different detectors. The pulse duration is measured at $1/e^2$-level; APD. . . . . avalanche photo diode; reg. PD. . . regular photo diode (CPC sensor board by AVL); *limited by the amplifier transfer function; **adjusted to meet the dynamical range of the detector

OPC linearity

The operation of the OPC was verified and tested for linearity by measurements on a butanol based condensation nuclei magnifier (CNM) at ambient temperatures ($T_{optics} \approx 40°C$) first. Figure 4.20 shows the flow scheme for determination of the HT-OPCs linearity and maximum count rate. NaCL particles generated with an atomizer were lead through an TSI 3082 differential mobility analyzer (DMA). Subsequently, the flow was split and fed to the butanol based CNM with the HT-OPC for test as well as a TSI 3775 CPC as reference.

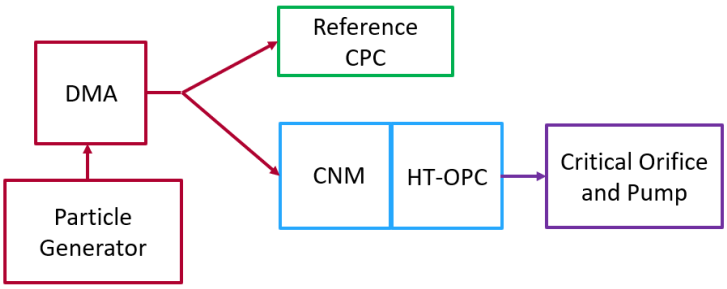

Figure 4.20.: Flow scheme for the testing of the HT OPC

The measurement was performed with mono-disperse NaCl particles of 50 nm mobility diameter over a concentration range 0 #/cm^3 to 5.5×10^4 #/cm^3, the results are shown in figure 4.21. The counting of the device is in good agreement until a concentration of 3×10^4 #/cm^3, which marks the maximum count rate. Above this concentration coincidence effects have to be considered and the measured values of the untreated HT OPC setup naturally deviate from the TSI CPC with its coincidence correction.

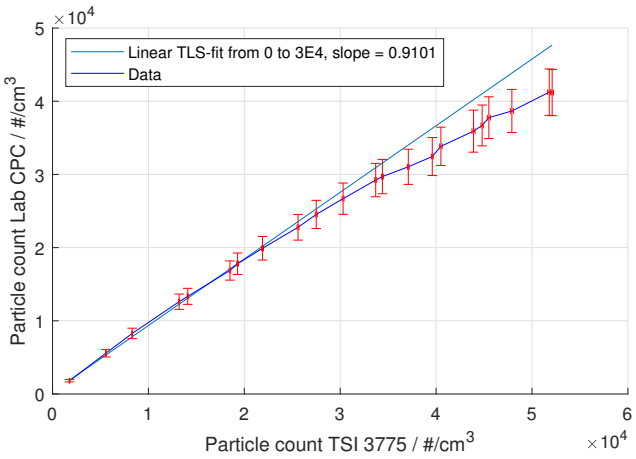

Figure 4.21.: Linearity of the HT OPC against the TSI 3775. Results of the linearity measurement with monodisperse NaCl particles at 50 nm in a range between 0 #/cm³ to 5.5 × 10^4 #/cm³.

Acknowledgement

This work was performed within the Competence Centre ASSIC - Austrian Smart Systems Research Center, co-funded by the Austrian Federal Ministries of Transport, Innovation and Technology (bmvit) and Science, Research and Economy (bmwfw) and the Federal Provinces of Carinthia and Styria within the COMET Programme.

This work was supported by AVL List GmbH.

4.4. Static Light Scattering on Aerosols

Scattering technique is a very broad term, describing various measurements for diverse applications. As already mentioned in section 2.2.3 also particle measurement by light scattering is possible. Within this thesis, the topic was treated as a supportive measurement technique for the HTCPC development. A setup for static light scattering (SLS) was used for the condensed droplet characterization within a CPC

SLS describes the measurement of the angle resolved intensity of scattered light. In an ideal approach the the scattered light is detected by an spherical array of photo detectors with a punctual target (or scattering center) in its

center. By inspection of the intensity distribution, conclusions about the target are possible, if the size of the target and the wavelength of the light is about equal. Only under this condition the scattering happens in the so called *Mie* regime, as already mentioned in section 2.2.3.

The Mie theory was derived by *Gustav Mie* in the beginning of the 20^{th} century, as a solution of the Maxwell equations for the scattering function of spherical particles [Mie, 1908]. Basing on these findings, scattering as a measurement technique was developed and is now widely used for various applications [Axmann, 2014; Ogendal, 2013]. Light scattering can also be used for the examination of fractal particulates [Sorensen, 2001].

The realization of a setup for the inspection of the droplets at the end of the condenser of a CPC, a simple approach was chosen. Since it can be assumed that the droplets are nearly equal in size, the measurement does not have to be done at one droplet for all angles. Rather the scattered light of many droplets is integrated for a better signal. The setup was as follows: the scattering target was the aerosol stream after the nozzle of the condenser of a CPC. For the scattering a focused laser beam was used and the scattered light was detected by a photo diode, movable on a swinging arm with the target in its rotational center.

The setup was developed, characterized and improved by four bachelor and master thesis, accompanied by the author of this thesis. The feasibility of the realization was done within the master thesis of Martin Cresnoverh [Cresnoverh, 2015]. An automated and dedicated setup for SLS on aerosols was realized in the bachelor thesis of Anton Buchberger [Buchberger, 2015] and characterized in the bachelor thesis of Klaus Irgang [Irgang, 2016]. Further improvements and characterizations were done in the bachelor thesis of Patrick Swaschnig [Swaschnig, 2017]. Within the master thesis of Michael Kügler, the optical setup was optimized and adapted for the HTCPC. Then measurements were done with the HTCPC, to check the predicted droplet size.

The setup will here be described only briefly in its final stage, since it was already described detailed elsewhere [Buchberger, 2015; Cresnoverh, 2015; Irgang, 2016; Kügler, 2018; Swaschnig, 2017]. See figure 4.22 for the scheme and a picture of the setup. The following main components were used: a laser with 532 nm wavelength (Thorlabs CPS532), three lenses: biconvex f = 35 mm (Thorlabs LB1811-A), plano-convex f = 200 mm (horlabs LA1708-A),

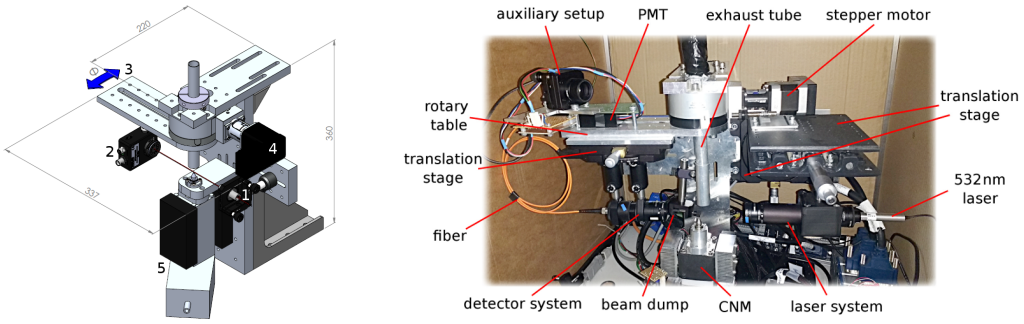

(a) Scheme of the original SLS (1) laser module, (2) detector, (3) swinging arm, (4) stepper motor, (5) CNM

(b) Final stage of the SLS

Figure 4.22.: The setup for SLS as original scheme and the final stage.

plano-convex f = 50 mm (horlabs LA1131-A), three neutral density flters: OD = 0:1 (Thorlabs NE01A), OD = 0:2 (Thorlabs NE02A), OD = 0:3 (Thorlabs NE03A), an optical fiber (Brugg FG5), a photo multiplier tube (Hamamatsu H13320-04), a rotary table (MM engineering MDT36012) and a stepper motor (Gunda electronics SM17H1.3OC).

As described in section 4.2, the SLS was used for inspection of the droplet size at the HTCPC, to verify the results of the preliminary simulations on the condensation behavior of the working fluid at the high temperatures. The ratio of the estimated droplet size of some µm and the wavelength of the laser cause scattering in the Mie-regime, as already briefly explained above and in section 2.2.3. Thus the intensity distribution over the scattering angle is characteristic for the size and shape of the target. Since the droplets can be seen as spheres, a comparatively easy modeling and thus analysis of the droplet size is possible.

4.5. Summary and Outlook

This chapter is dedicated to the main topic of this thesis, a HTCPC for automotive exhaust. It consists of two journal papers, comprising the development from a concept to a working prototype, which was used for measurements on automotive exhaust at a chassis dynamometer. Within the first paper the proof of concept and the feasibility for exhaust measurement is described. A dedicated high-temperature working fluid was identified and a high-temperature optics module was designed and built. The device was then characterized, revealing reliable linearity and a size dependent counting efficiency which would comply with the current legislative PNC specifications (see section 1.2.3). The long term stability was proven with tests at a chassis dynamometer, sampling automotive exhaust for almost 4 h and thus the first compendious research question, "*Is it possible to measure particulate emissions directly without a influencing preconditioning?*", can be answered clearly with *yes*. Evaluation of the data showed good correlation with the reference devices, a constant difference in the absolute PN was measured. Thus the second compendious research question, "*Will the direct measurement and the measurement using preconditioning match?*", cannot be answered simply with *yes* or *no*, since both applies. After the verification of the first design, improvements to facilitate measurements on automotive exhaust were approached. These activities are topic of the second paper and comprise a redesign of the device, a study on wick materials to improve the long term stability and improvements on the optics module. The improved HTCPC design includes an inherent dilution concept, enabling direct sampling of raw exhaust and a steady operation. As a supporting activity to the HTCPC development a setup for static light scattering was built to examine the droplet size.

Our activities around the HTCPC are basing on the work of Nick Collings and Kanchit Rongchai from 2013, what is considered as state-of-the art, since no further work regarding high temperature CPCs is known to the author. Thus, the work presented in this chapter can be considered as scientific contribution.

Although the development of a HTCPC device itself is scientific effort, the more important impact may be caused by its usage for measurements. A direct PN measurement at raw exhaust would give e.g. the possibility to

characterize a sampling system on raw exhaust for the first time. Until now the characterization is done with model aerosols under laboratory conditions. Also, a reliable PN measurement of solid particles at very small sizes would be a important support to the research on the nature of ultrafine particles. Also the second compendious research question of this thesis, "*Will the direct measurement and the measurement using preconditioning match?*", should be addressed detailed with further work. The pure sensor performance should be evaluated with different references and various aerosols, but also various applications and different of preconditioning systems should be examined. The real potential of a high temperature measurement would appear, if it can establish a method which is insensitive to variations caused by exhaust preconditioning.

5. Complementary Approach - LII

Within the thesis different techniques for the measurement of particulates were studied to address the research questions stated in section 1.3. Beside the HTCPC, also a setup for a Laser Induced Incandescence (LII) system was realized within the scope of this thesis. It was chosen because of its high potential for an in-situ application, a very fast measurement and the possibility of a highly robust setup.

First a summary of the LII theory is be given, to explain the complex LII process. Then, a proceedings paper [Kupper, Pulko, et al., 2019] is integrated which comprises most of the done experiments, followed by the description of subsequent activities and a survey about LII system calibration.

5.1. LII Theory

LII refers to a measuring technique in which by extremely short and high energetic, but defined laser pulses, particles are heated to the emission of black-body radiation. The incandescence of the particles, more precisely the decay of the incandescence, is optically detected and by suitable analysis the size and number of particles can be assessed.

It is challenging because the incandescence of the particles lasts only a few 100 ns and the intensity of the emitted radiation covers a big range from the maximum temperature down to the cold particle. Furthermore, the detectable intensity scales with the amount of substance that is irradiated. For efficient excitation, shorter pulses are advantageous, since an energy dissipation already occurs during the energy deposition, therefore pulses of a few ns are usually used in order to deposit the necessary energy of a few mJ. This results in an irradiated power in the MW range, which can be provided at a very high frequency because of the short irradiation time.

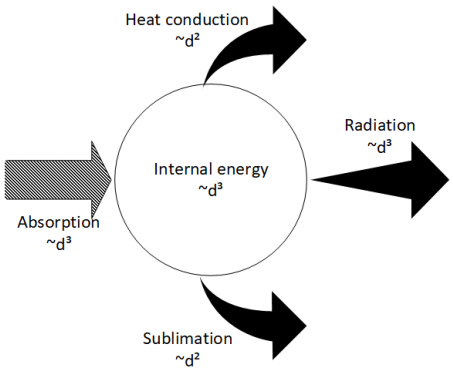

Figure 5.1.: Symbolization of the energy transport mechanisms considered in the described LII model and the corresponding dependency to the particle diameter d [Bladh, Johnsson, and Bengtsson, 2008].

The process is studied since several decades and can be described as follows. A LII signal is the result of a complex interplay of four processes which, under the assumption of spherical particles, can be related to the diameter particles diameter d: absorption ($\sim\ d^3$), radiation ($\sim\ d^3$), thermal conduction ($\sim\ d^2$), and sublimation ($\sim\ d^2$) - see figure 5.1. These processes do not occur coincidentally, so sublimation of particle mass occurs, if at all, only during and shortly after the beam absorption, therefore the overall influence is quite low. Later, the dominant process is the heat conduction, that is the "cooling" of the particle. Via the temperature directly related to that is the radiation, what is the detected physical quantity. In sum, this results in a nonlinear dependence of the LII signal to the particle size [Bladh, Johnsson, and Bengtsson, 2008]. Analysis thus is challenging, a possible way is comparison of the signal with a model. From the LII signal the mean size of the irradiated particles can be determined [Mewes and Seitzman, 1997] and if the measurement of the LII signal was done at two wavelengths, further a determination of PN is possible. Finally from the particle size and PN the volume fraction or the mass fraction can be assessed [Snelling, Smallwood, and Gülder, 2000].

According to Bladh, Johnsson, and Bengtsson, 2008 the detectable LII signal S_{LII}, so the radiation at a certain wavelength λ, can be written as:

$$S_{LII} \propto \pi D^2 N_p \int_0^{\inf} R(\lambda) \frac{4\pi DE(m)}{\lambda} \cdot \frac{2\pi hc^2}{\lambda^5} \cdot \left(\frac{1}{e^{hc/\lambda\ k_B T - 1}} - \frac{1}{e^{hc/\lambda\ k_B T_B - 1}}\right) d\lambda \tag{5.1}$$

With D the particle diameter, N_P the particle number, R the spectral characteristic of the system, E the absorption function, h Planck constant, λ the wavelength, c the speed of light, k_B Boltzmann constant, T the particles temperature and T_g the gas temperature. Equation 5.1 is explicitly depending on the particle number and size, thus one property of the particle has to be known to determine the other by the equation. Mewes and Seitzman, 1997 pointed out that for instance by formation of the so called "wavelength ratio" a LII signal analysis is still possible. For that the LII signal has to be measured simultaneously at two wavelengths and the ratio calculated. By the formation of the ratio of eq. 5.1 at two wavelengths:

$$Ratio_\lambda = \frac{S_{LII,\,\lambda 1}}{S_{LII,\,\lambda 2}} \tag{5.2}$$

N_P, the particle number, cancels since it is outside the integral. Thus the mean particle size can be determined in this way and insertion into 5.1 given then the particle number. From that the volume fraction can be calculated and therewith also the mass fraction, if a particle density can be assumed. The described approach considers spherical particles, for fractal particles, like present in automotive exhaust, another model can be applied e.g. considering primary particles [Vander Wal, Ticich, and Brock Stephens, 1999].

Different models for LII signal have been developed over the years, with different advantages and disadvantages for different kinds of particulates and LII setups [Michelsen et al., 2007]. The above described approach is a possible way for a comparatively easy realizable and possible online signal analysis for a LII setup as presented in the next chapter.

5.2. First Steps towards a Super-Compact In-Situ Laser-Induced-Incandescence Sensor System

Section 5.2 was published as *M. Kupper, J. Pulko, M. Kraft, and A. Bergmann, "First Steps towards a Super-Compact In-Situ Laser-Induced-Incandescence Sensor System, Proceedings 2, 1017 (2019)"* in the proceedings journal to the Eurosensors 2018 Conference, Graz, Austria, September 9–12, 2018 [Kupper, Pulko, et al., 2019].

Abstract

To realize an actual in-situ Laser-Induced Incandescence (LII) sensor system for measurements in an exhaust pipe of a combustion engine, suitable components for such an application were chosen, integrated in a first prototype and tested. Key components for the proposed LII system are a super-compact high-power DPSS laser (CTR HiPoLas©) as excitation source, fast KETEK silicon photomultipliers (SiPM) as detectors and a specially designed optical measurement setup. Using a defined aerosol from a soot generator (Jing 5201 miniCAST), signals were collected at different laser energies and soot concentrations. By comparing the recorded behaviour with the literature, the incandescence effect could be reliably identified as the true source of the signal. Further long-term tests at an AVL engine testbed were performed.

Introduction

Laser-Induced Incandescence (LII) is a promising and widely known technology in science for studying soot in flames and aerosols and particles of other materials [Vander Wal, Ticich, and West, 1999]. Its capability to measure different aerosol parameters simultaneously with high accuracies, and it ability to meet legally mandated limits, makes it of high interest for measuring soot concentrations in automotive exhausts [Wainner and Seitzman, 1999]. Given by the fast nature of the LII process, single measurements are very short (few 100 ns). Thus, transient events, like fast changes in engine load and the thereby occurring short and high soot emissions, can be resolved with high accuracy. The limits to this are set by the repetition rate of the laser and the dynamics of the detectors and electronics used. LII is stimulated by a short, some ns long, laser pulse with an energy density of about $3\,\mathrm{mJ\,mm^{-2}}$ to $4\,\mathrm{mJ\,mm^{-2}}$. While laser systems capable of producing this kind of pulses with a high frequency are nowadays commercially available, such laser systems are usually big, bulky devices that have to be operated under controlled conditions and maintained with care. CTR developed a super-compact laser measuring just a few cm that is capable of producing pulses suitable for LII excitation. Furthermore, having initially been developed as a laser spark plug, and tested recently for use as a laser ignition system (LIS) for the main and upper stage engines of ESA's Ariane

6 launch vehicle, this device is very robust and easy in operation [Peach, 2015].

Stimulated particle incandescence lasts for a few 100 ns and requires very sensitive and fast detectors for light detection. The usual choice are photo multiplier tubes (PMTs), which are suitably sensitive and fast, but hard to integrate into an in-situ field setup. However, recent developments made silicon photo multipliers (SiPMs) available at very low costs, which are highly robust against vibrations and show even better dynamic range. Around these major components, an optical setup within a measurement cell was designed and optimized for collection of LII signals. This setup was then used for extensive investigations into the capability of performing neat LII, with a view to the realization of a highly compact in-situ LII system applicable directly at an automotive exhaust pipe.

While appearing very simple – shoot a high-power laser on particles and detect their glowing – LII measurements are based on several interlinked, complex and fast processes. In general, four thermal transport processes must be considered [Bladh, Johnsson, and Bengtsson, 2008; Snelling, Smallwood, and Gülder, 2000]: absorption, radiation, sublimation and convection. The particles absorb the incoming laser pulse according to their material properties, are heated and emit blackbody radiation. This radiation release of thermal energy is the contribution we measure as "LII signal". The main transport process of heat is convection, sublimation occurs mostly during the illumination with the laser pulse and shortly after [Michelsen et al., 2007]. So, the measured decay in the LII signal mainly depends on a combination of radiation and convection, whereby convection is the dominant process [Bladh, Johnsson, and Bengtsson, 2008]. For analysis of these signals, these processes have to be modelled well and consider the dependencies on particle size and material [Bladh, Johnsson, and Bengtsson, 2008; Michelsen et al., 2007; Snelling, Smallwood, and Gülder, 2000; Vander Wal, Ticich, and Brock Stephens, 1999; Vander Wal, Ticich, and West, 1999; Wainner and Seitzman, 1999]. The realization of any LII sensor system thus requires careful preparation and data analysis. Yet, since the behaviour of the LII signal in dependency of laser fluence, particle size and mass concentration is unique, it is possible to reliably differentiate the LII signal from e.g. light scattering of the laser excitation and thus survey the quality of the LII experiment.

Materials and Methods

Experimental setup

The main components of the setup are i) a super-compact high-power diode pumped solid state (DPSS) laser, ii) fast and compact SiPMs, and iii) as specially designed measurement cell. The laser source (CTR HiPoLas®, CTR AG, A) is a radially diode-pumped, monolithic solid-state Nd:YAG laser, which emits pulses at 1064 nm at an adjustable repetition rate with a spot size of about 8 mm^2. Originally developed for use as a laser spark plug, it is very robust and compact – the laser head of the latest generation (gen. 5) only measures 50 x 50 x 30 mm. Auxiliary equipment, including a water cooler and the laser driver electronics in a control box with an interlock, can be flexibly connected and thus deployed away from the harsh conditions of e.g. an automotive engine, or its exhaust line. For the experiments presented here, a HiPoLas generation (gen.) 3 was used, experiments using a latest generation 5 laser head are ongoing and results will be presented at the 2018 Eurosensors conference. The gen. 3 HiPoLas is capable of a continuous repetition rate up to 3 Hz with 6 ns / 20 mJ pulses. The gen. 5 laser was adjusted to LII specifications and emits 20 mJ pulses with a continuous repetition rate up to 5 Hz.

SiPMs, very sensitive solid-state photodetectors, were selected for various reasons. Firstly, SiPMs are available at low prices, compared to photo multiplying tubes (PMT), similarly sensitive and significantly more robust. In particular, the threshold for radiation damage for SiPMs is high, the temperature influence is comparably low, and they are completely insensitive to vibrations. A SiPM detector is an array of hundreds to thousands of micro avalanche photodiodes (APD) operated in Geiger-mode [Mewes and Seitzman, 1997]. Each APD is capable of single photon detection, but needs to recover after an event. The "recovery-time" of the SiPMs used here was 15 ns, which provides good dynamics for the detection of LII signals. For this study, "custom array" sensor modules consisting of 4 SiPMs with 3 x 3 mm SiPM arrays each (KETEK PM 3315, 15 µm micro-cell size; KETEK GmbH, D) were used. The signals were read out without pre-amplification. For data collection in this proof-of-concept setup, a PICO PicoScope 6000 USB oscilloscope was used that provides a continuous sampling rate of up to 1 GHz.

Experimental methods

The main topic of the measurements was to assure that the initiated and detected process is indeed neat LII. As mentioned in the introduction, LII signals are the result of the complex interplay of different processes, which create a unique signal behaviour. To validate this, in a first step the detectors were carefully shielded from the laser beam, using a combination of optical bandpass and band filters, a closed housing, and pieces of a laser safety curtain in such a way, that no signal is detected without a specimen inside the measurement cell. Next, the measurement cell was challenged with defined aerosol particles from a miniCAST 5201 (Jing Ltd., CH) and the laser fluence varied using a variable beam splitter, whereby the second beam was measured with a power meter. Since the total laser power is constant, the measurement of one beam defines also the power of the second. The measured dependency of the detected signal to the laser fluence was then compared to literature, to check if the slope follows the characteristic LII behaviour [Wainner and Seitzman, 1999]. Following the initial proof-of-principle phase, the setup was expanded i) to comprise four SiPMs, operated at different gains to cover a wider dynamic range and ii) a sampling system for automotive exhaust gases, supplied by AVL (AVL GmbH, A), and encased in a black box to warrant class 1 laser safety. This setup was then installed to an AVL engine testbed for long-term measurements on actual exhausts. At the engine testbed, the LII was continuously operated with optimal settings at 1 Hz, as defined from the feasibility stage, for 10 hours straight. An AVL MicroSoot Sensor (MSS) was used as reference device throughout the measurements.

Results and Discussion

A detailed examination of the signal behaviour, are shown in Fig. 5.2(a), proved i) that the incandescence signals are clearly distinguishable from scattered laser light and ii) show the typical characteristics of neat LII signals. Rising laser fluence heats the particles at the interaction volume to higher temperatures, causing the dominant heat transport process to change since they scale differently with particle size and temperature [Bladh, Johnsson, and Bengtsson, 2008; Mewes and Seitzman, 1997; Wainner and Seitzman, 1999]. This effect is non-linear, while scattered light would scale linearly with particle size and laser fluence [Ogendal, 2013]. The actual measured signals follow this LII behaviour [Wainner and Seitzman, 1999 very well.

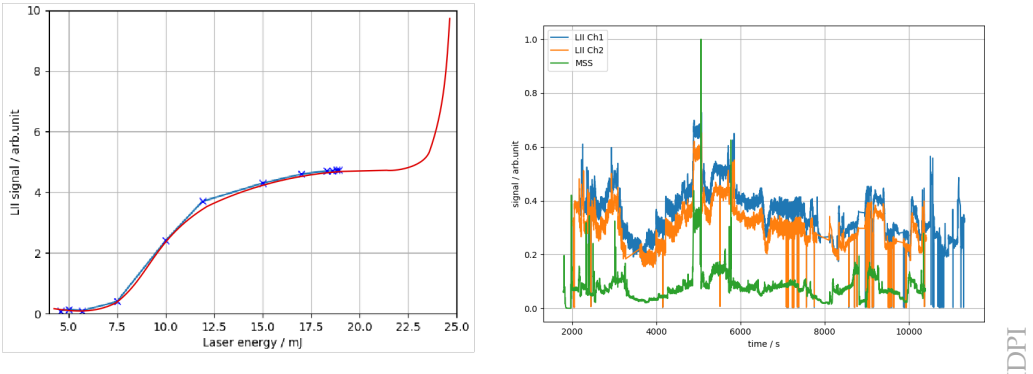

(a) (b)

Figure 5.2.: Measurement data collected with our LII system (a) a qualitative comparison of the LII signal at different laser energies with results from [Wainner and Seitzman, 1999]; (b) raw data from the measurements on the engine testbed, with an AVL MSS as reference, showing an excellent qualitative correlation.

So, since the data in Fig. 1a is in good compliance with the theoretical behaviour, one can be quite sure that the measured signals originate from LII. The pulse energies of the gen. 3 laser we used are not fully sufficient for a stabile LII system, since the plateau regime is not reached. But the fundamental feasibility of realising an in-situ LII probe was thereby proven. This opens a vision to replace the previously used extractive cells and large-scale laser sources by compact, field-operable components, creating an approach for a true in-situ particle sensor. In Fig 5.2(b) the LII data is qualitatively compared against the PM measurements obtained from the AVL MSS (MSS data was scaled down, so the transient behaviour can be compared directly). While quantitatively there is no linear dependency, nor a correlation that could be easily established, they follow the same event changes in soot concentration. In general, it can be said that the LII signal follows the MSS very well, and all load changes were accurately captured.

Conclusion

A LII system was realized using components suitable for an in-situ probe. Measurements with defined soot from a MiniCAST soot generator and subsequent comparison of the signal behaviour with LII literature and theory proved the gained signals to be LII in nature. Further long-term measurement at an engine testbed on exhaust gases proved the basic feasibility of an in-situ probe. Still, due to the challenging analysis of LII signals, realising an actual sensor capable of providing quantitative data that is

back-traceable to standard methods will require further R&D efforts into signal processing, as well as into deeper systems integration. The results presented here were gained from experiments using a generation 3 HiPoLas and shall be considered as preliminary. Experiments using a generation 5 HiPoLas which was adjusted for LII are ongoing, results will be presented at the 2018 Eurosensors conference.

5.3. Subsequent LII Experiments

As the used gen. 3 HiPoLas did not provide high enough pulse energies for a stable LII measurement, the signal behavior measurement was repeated with a gen. 5 HiPoLas. The setup was same as described in section 5.2, *Materials and Methods*, *Experimental Setup*, except the gen. 3 laser was replaced with the gen. 5 laser. See figure 5.3 for the components.

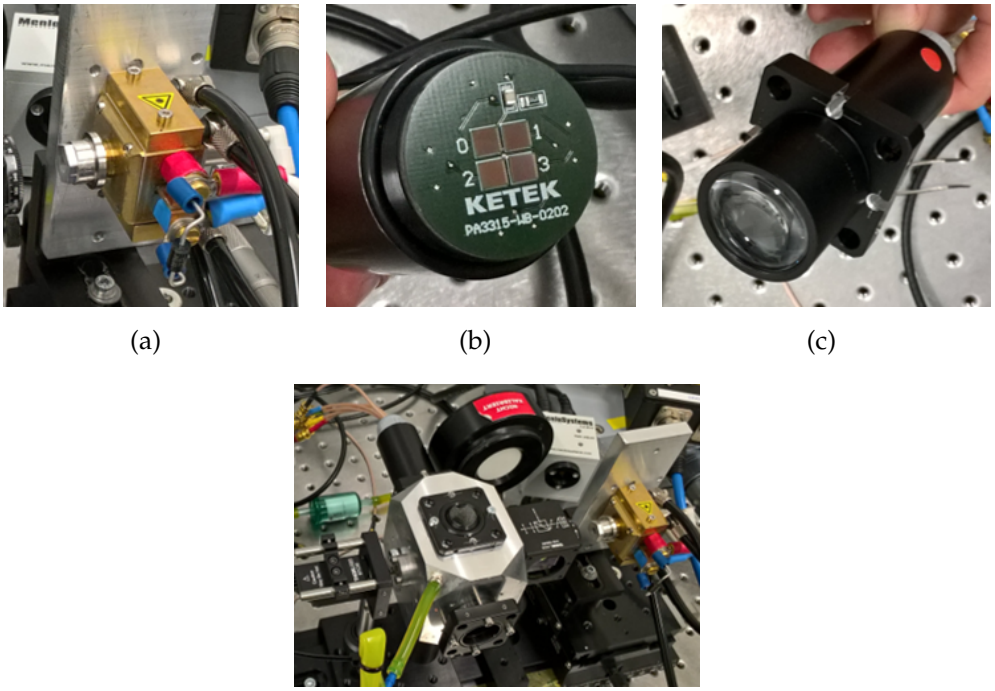

(a) (b) (c)

(d)

Figure 5.3.: Components of the LII measurement setup. a) HiPoLas gen. 5, b) SiPM, c) assebeled detector unit, d) measurement cell.

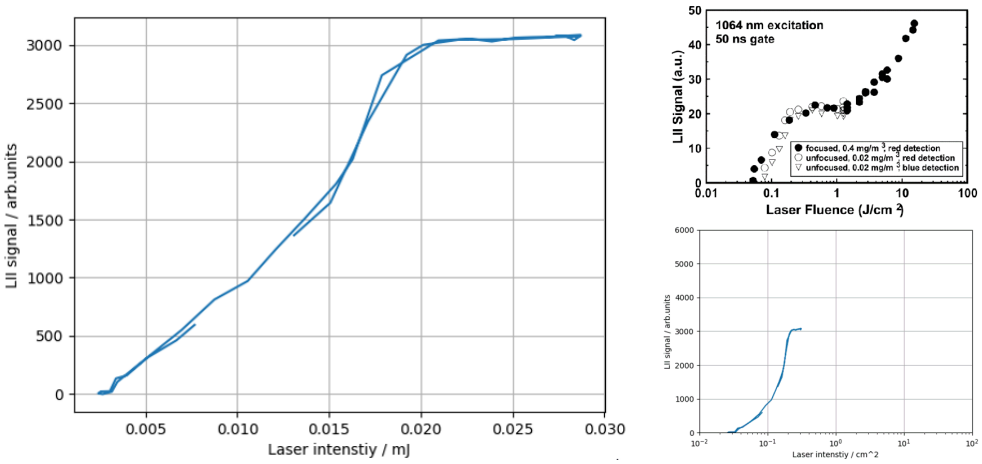

(a) (b)

Figure 5.4.: Results of the LII measurement using the gen. 5 HiPoLas. a) mean raw data of four SiPMs from one detector unit, b) the data scaled for comparison with [Wainner and Seitzman, 1999].

To check the signal quality of the LII, the test was repeated as described in 5.2, *Materials and Methods*, *Experimental Methods*. Since the robustness of the system is not influenced by the change of the laser head, the test at the engine testbed was not repeated.

As shown in figure 5.4, the pulse energy of the gen. 5 HiPoLas is sufficient for stable LII operation. In figure 5.4(a) the raw data in linear presentation shows that the plateau regime is very distinct, since it stretches over an energy rango of almost 10 mJ. In direct comparison to the values from Wainner and Seitzman, 1999, both signals follow the same behavior (figure 5.4(b)). Thus, the feasibility of the realization of a compact LII system, using the described components is proven.

5.4. Calibration of a LII System for PM Measurement

The quality of a measurement system is depending on the quality of the signal generation. Beginning with the sensor effect, its detection, the electronic

signal generation ends with the signal processing. Nevertheless, the utility of such a system is coming from its calibration.

For a LII setup, which should be used as an in-situ measurement system on engine exhaust, the calibration is an unsolved issue. Ideally this topic is addressed during the development of the LII measurement system and the data analysis algorithm. In this section a strategy for the development of a reliable calibration procedure is proposed.

The aerosols used for these activities are critical and specific influences on the LII signal caused e.g. by the particulates morphology should be sufficiently known. Thus, different model aerosols should be used at different stages of the calibration process. An appropriate model aerosol is characterized by the knowledge of its properties and the possibility of a defined variation of them. Further, the characteristic properties like PN, PM and particle size have to be determinable by reference methods (aerosol instrumentation is described in section 2.2). Different model aerosols have to be used for the study of variation of different properties (particle generators are described in section 2.4).

Before calibrating a LII system, the signal quality and the processing have to be assured. Beginning with an ideal model aerosol with spherical particles to generate an ideal LII signal, the data analysis strategy explained in section 5.1 should be realized. As a generator a tube furnace may be reasonable [Scheibel and Porstendörfer, 1983]. Also appropriate data processing electronics have to be available, capable for a comparison of the measured signal with model data in real time. The model has to be chosen basing on experimental evaluation since different models consider different effects [Michelsen et al., 2007].Thus, the development of the algorithm for the signal analysis should ideally be done during this phase, since it has to be adopted to the used model.

After a stable realization in the laboratory under these ideal conditions was successful, the transfer towards fractal particles should be headed. Therefor again an appropriate model aerosol is needed. First experiments should not be done with soot particles, rather simple fractal particles from a pure substance should be used. Such particles might be generated again with a tube furnace without a sintering stage [Scheibel and Porstendörfer, 1983] or a spark particle generator with metal electrodes. Again an appropriate model for data analysis, considering fractal particles has to be implemented into the

algorithm (e.g. according to Vander Wal, Ticich, and Brock Stephens, 1999). These activities primarily head for signal linearity for fractal particles.

Finally, when also a stable adaptation to fractal particles succeeded, measurements on soot from a CAST (section 2.4.1) should be done with an appropriate reference system for PM, PN and particle size. From this stage on also influences from the combustion have to be considered which exceed the scope of a LII model, like moisture or volatile compounds. Thus, the signal analysis algorithm should not be adjusted with this kind of model aerosol. Rather now calibration measurements should be performed, to establish a reference of the LII to a PM measurement. Tests should also be done at automotive exhaust, using the same reference equipment as in the lab at the best, to benchmark the quality of calibration. Also, the assignment of the mass value to the volume value of the LII signal should be done by calibration at automotive exhaust.

5.5. Summary and Outlook

LII is presented as a complementary PM measurement technique for harsh environments, since the HTCPC described in chapter 4 represents a PN measurement technique. First the theoretical background is described, followed by a proceedings paper which treats the realization of a LII setup, its characterization and first measurements. It comprises a setup, realized with components suitable for a compact in-situ probe, the verification of LII measurement by comparison of the signal behavior with peer reviewed literature and measurements at an engine testbed with a AVL MSS as an established PM measurement device as a reference. Furthermore, additional experiments to the paper are presented, where a more appropriate laser was used. Finally, an approach for the calibration of a LII system for automotive exhaust is presented.

LII is widely known as a measurement technique for particle measurement and also commercial devices are available for measurement of PM in automotive exhaust, but until now the correlation of these LII measurements to established PM measurement could not be proven. Also, big advantages of LII were not utilized, namely the possibility for very fast measurements and the possibility of a very robust setup for in-situ measurements. The

authors contribution in this regard is the proof of principle for a compact and robust setup, a very fast measurement , which is only limited by the laser repetition rate, and a proposal for a system calibration which would establish a reliable correlation to established PM measurement devices.

Since the presented work comprises a proof of principle and the proposal for a calibration, the next step could be the realization of an in-situ probe with the verified components and the execution of the calibration. A fast, in- situ PM measurement would e.g. allow the examination of engine load for very dynamic driving, thus the optimization of the combustion and lowering of emissions. Also the possibility to resolve single piston strokes within the exhaust concentration would allow an extension of combustion optimization.

6. Conclusion

To address the research questions stated in section 1.3, a High-Temperature Condensation Particle Counter (HTCPC) and a setup for Laser Induced Incandescence (LII) have been realized. The decision for these two techniques is basing on a review of state-of-the-art technology for automotive exhaust measurement, summarized in chapter 2.

The development of the HTCPC was accompanied by a study of the physical fundamentals of CPC operation. After a review of Classical Nucleation Theory (CNT), the awareness of the importance of material and particle influences had risen. Most of the available CPCs operate with the same working fluids at comparable temperatures, thus their characteristic behavior is also comparable. For the introduction of a CPC at unusual, or rather extreme, operation conditions and further with an unknown working fluid, a good understanding for the processes behind its operation had to be provided. Thus, in section 3.2.1 a study of the dependencies of CPC counting efficiency is presented. Experiments were performed with particles from different materials, using n-Butanol and n-Decane as working fluids. n-Decane was chosen because of its chemical affinity to n-Eicosane, our dedicated high-temperature working fluid. Since the found behavior cannot be described by CNT, capillary condensation was studied and used for an approach for the description of condensation on fractal particles. To facilitate these considerations with experiments, an attempt for Small Angle X-Ray Scattering (SAXS) on aerosols was made.

Starting with a concept, basing on the work of Nick Collings and Kanchit Rongchai from 2013, a working prototype of a HTCPC was developed. Beginning with an extensive literature review, where possible candidates for high-temperature working fluids have been identified. n-Eicosane, an aliphatic hydrocarbon, turned out to be our best candidate. A setup for an HTCPC was then realized to proof the principle of operation, a first characterization and to test for long-term stability on engine exhaust. These

results are provided within the publication in section 4.2, where we present the working fluid, the flow design of the device and a high-temperature optics module. We show the linearity of the device up to 30 000 #/cm^3 and a counting efficiency in compliance with the current legislative constraints for Particle Number Counters (PNC). Also measurements at an chassis dynamometer were done, revealing long-term stability and a first comparison to reference devices. In section 4.3 we present improvements on the verified concept which should optimize the device in regards of applicability. A study on wick materials improves the long-term persistence of the working-fluid, with a mixed-flow design a inherent dilution concept is introduced, which would allow direct sampling of raw exhaust. Improvements on the high-temperature optics module were made to ensure reliable and robust operation. A setup for Static Light Scattering (SLS) was built to support the development of the HTCPC and characterize the droplet size, it is presented in section 4.4

As a complementary method to the HTCPC, LII was evaluated for robust particle mass (PM) measurements. An experimental setup was realized to proof the feasibility of an compact in-situ system. Its realization, characterization and measurements at an engine testbed are presented in section 5.2. Furthermore, in section 5.4 a calibration procedure is proposed, considering the characteristics of the LII signal generation and detection, by what a correlation to established PM measurements would be possible.

Bibliography

Abdul-Khalek, Imad S. and David B. Kittelson (2010). "Real Time Measurement of Volatile and Solid Exhaust Particles Using a Catalytic Stripper." In: *SAE Technical Paper Series* 1.412. DOI: 10.4271/950236 (cit. on p. 40).

Agarwal, J. K. and G. J. Sem (1980). "Continuous flow, single-particle-counting condensation nucleus counter." In: *Journal of Aerosol Science* 11.4, pp. 343–357. ISSN: 00218502. DOI: 10.1016/0021-8502(80)90042-7 (cit. on p. 71).

Ahn, Kang-Ho and Benjamin Y H Liu (1990a). "Particle activation and droplet growth processes in condensation nucleus counter-I. Theoretical background." In: *Journal of Aerosol Science* 21.2, pp. 249–261. DOI: 10.1016/0021-8502(90)90008-L (cit. on p. 53).

Ahn, Kang-Ho and Benjamin Y.H. Liu (1990b). "Particle activation and droplet growth processes in condensation nucleus counter—II. Experimental study." In: *Journal of Aerosol Science* 21.2, pp. 263–275. DOI: 10.1016/0021-8502(90)90009-M. URL: https://www.sciencedirect.com/science/article/pii/002185029090009M (cit. on p. 53).

Ahner, T. Torsten, Sergey Sokolov, Ralph Kraehnert, Jörg Polte, Friedmar Delissen, Franziska Emmerling, and Andreas F. Thünemann (2010). "Mechanism of gold nanoparticle formation in the classical citrate synthesis method derived from coupled in situ XANES and SAXS evaluation." In: *Journal of the American Chemical Society* 132.4, pp. 1296–1301. DOI: 10.1021/ja906506j (cit. on p. 60).

Antti, Lauri Johannes (2006). "Theoretical and computational approaches on heterogeneous nucleation." Academic dissertation. University of Helsinki, p. 56. URL: https://helda.helsinki.fi/handle/10138/23320 (cit. on p. 51).

AVL List GmbH (2019). *APCplus AVL Particle Counter*. URL: https://www.avl.com/de/-/apcplus-avl-particle-counter (visited on 04/19/2019) (cit. on p. 41).

Axmann, Harald (2014). "Verfahren zur Bestimmung der Partikelkonzentration in Abgasen von Verbrennungsmotoren Dissertation Eidesstattliche Erklärung Affidavit." PhD Thesis. Graz Universtiy of Technology (cit. on pp. 28, 105).

Bainschab, Markus, Alexander Bergmann, P Karjalainen, Jorma Keskinen, Jon Andersson, B. Giechaskiel, Christoph Haisch, O Piacenza, Athanasios Mamakos, Aandreas Klug, Leonidas Ntziachristos, and Zissis Samaras (2017). "Extending Particle Number Limits to below 23 nm: First Results of the H2020 DownToTen Project." In: *2017 ETH-Conference on Combustion Generated Nanoparticles* 49.6, pp. 3644–3652. DOI: 10.1021/es505109u (cit. on pp. 3, 53, 76).

Baltzopoulou, P, A.D. Melas, D. Deloglou, N.D. Vlachos, E. Papaioannou, J.F. de la Mora, and A.G. Konstandopoulos (2018). "High-temperature solid particle emission measurements in the sub-23nm m mobility size range with the Advanced Half-Mini DMA." In: *Aerosol Technology 2018 (AT 2018)*; 724136, p. 724136. DOI: 10.5281/zenodo.1298554 (cit. on pp. 3, 53).

Barmpounis, K., A. Ranjithkumar, A. Schmidt-Ott, M. Attoui, and G. Biskos (2018). "Enhancing the detection efficiency of condensation particle counters for sub-2 nm particles." In: *Journal of Aerosol Science* 117.October 2017, pp. 44–53. DOI: 10.1016/j.jaerosci.2017.12.005. URL: https://doi.org/10.1016/j.jaerosci.2017.12.005 (cit. on pp. 66, 86).

Baron, Paul A. and Klaus Willeke (2001). *Aerosol Measruement*. 2nd. Wiley-Interscience, p. 1063. ISBN: 0471356360 (cit. on pp. 5, 26, 27, 35, 36, 51, 58, 59, 81).

Bauer, P. S., H. Amenitsch, B. Baumgartner, G. Köberl, C. Rentenberger, and P. M. Winkler (2019). "In-situ aerosol nanoparticle characterization by small angle X-ray scattering at ultra-low volume fraction." In: *Nature Communications* 10.1. ISSN: 20411723. DOI: 10.1038/s41467-019-09066-4 (cit. on pp. 52, 61).

Bell, Alexander Graham (1880). In: *American Journal of Science* 20, p. 305 (cit. on p. 32).

Berry, J. D., M. J. Neeson, R. R. Dagastine, D. Y. C. Chan, and R. F. Tabor (2015). "Measurement of surface and interfacial tension using pendant drop tensiometry." In: *Journal of Colloid and Interface Science* 454, pp. 226–237. DOI: 10.1016/j.jcis.2015.05.012 (cit. on pp. 70, 78).

Binnig, J., J. Meyer, and G. Kasper (2007). "Calibration of an optical particle counter to provide PM2.5 mass for well-defined particle materials." In:

Journal of Aerosol Science 38.3, pp. 325–332. DOI: 10.1016/j.jaerosci.2006.12.001 (cit. on p. 30).

Bladh, H., J. Johnsson, and P. E. Bengtsson (2008). "On the dependence of the laser-induced incandescence (LII) signal on soot volume fraction for variations in particle size." In: *Applied Physics B: Lasers and Optics* 90.1, pp. 109–125. DOI: 10.1007/s00340-007-2826-0 (cit. on pp. 3, 110, 113, 115).

Bond, T. C., S. J. Doherty, D. W. Fahey, P. M. Forster, T. Berntsen, B. J. Deangelo, M. G. Flanner, S. Ghan, B. Kärcher, D. Koch, S. Kinne, Y. Kondo, P. K. Quinn, M. C. Sarofim, M. G. Schultz, M. Schulz, C. Venkataraman, H. Zhang, S. Zhang, N. Bellouin, S. K. Guttikunda, P. K. Hopke, M. Z. Jacobson, J. W. Kaiser, Z. Klimont, U. Lohmann, J. P. Schwarz, D. Shindell, T. Storelvmo, S. G. Warren, and C. S. Zender (2013). "Bounding the role of black carbon in the climate system: A scientific assessment." In: *Journal of Geophysical Research Atmospheres* 118.11, pp. 5380–5552. DOI: 10.1002/jgrd.50171. arXiv: arXiv:1011.1669v3 (cit. on pp. 1, 8, 15–17, 19).

Boretti, Alberto (2017). "The Future of the Internal Combustion Engine After "Diesel-Gate"." In: *SAE Technical Paper Series* 1. DOI: 10.4271/2017-28-1933 (cit. on p. 2).

Broekhoff, J C P and J H Boer (1967). "Studies on pore systems in catalysts: IX. Calculation of pore distributions from the adsorption branch of nitrogen sorption isotherms in the case of open cylindrical pores A. Fundamental equations." In: *Journal of Catalysis* 9.1, pp. 8–14. DOI: 10.1016/0021-9517(67)90174-1 (cit. on pp. 59, 159).

Brook, Robert D., Sanjay Rajagopala, C. Arden Pope, Jeffrey R. Brook, Aruni Bhatnagar, Ana V. Diez-Roux, Fernando Holguin, Yuling Hong, Russel V: Luepker, Murray A. Mittleman, Annette Peters, David Siscovick, Sidney Smith, Laurie Whitsel, and Joel D. Kaufman (2010). "Particulate Matter Air Pollution and Cardiovascular Disease." In: *Circulation* 121.21, pp. 2331–2378. DOI: 10.1161/cir.0b013e3181dbece1 (cit. on pp. 6, 15).

Brunnhofer, Georg, Alexander Bergmann, Andreas Klug, and Martin Kraft (2019). "Design and Validation of a Holographic Particle Counter." In: *Sensors* 19.22, p. 4899. DOI: 10.3390/s19224899. URL: https://www.mdpi.com/1424-8220/19/22/4899 (cit. on p. 29).

Buchberger, Anton (2015). "Statische Lichtstreuung an Aerosolen." PhD thesis (cit. on p. 105).

Burtscher, H., U. Baltensperger, N. Bukowiecki, P. Cohn, C. Hüglin, M. Mohr, U. Matter, S. Nyeki, V. Schmatloch, N. Streit, and E. Weingartner (2001). "Separation of volatile and non-volatile aerosol fractions by thermodesorption: Instrumental development and applications." In: *Journal of Aerosol Science* 32.4, pp. 427–442. DOI: 10.1016/S0021-8502(00)00089-6 (cit. on p. 40).

Cohan, Leonard H. (1938). "Sorption Hysteresis and the Vapor Pressure of Concave Surfaces." In: *Journal of the American Chemical Society* 60.2, pp. 433–5. DOI: 10.1021/ja01269a058 (cit. on p. 58).

Cohen, Aaron J., Michael Brauer, Richard Burnett, H. Ross Anderson, Joseph Frostad, Kara Estep, Kalpana Balakrishnan, Bert Brunekreef, Lalit Dandona, Rakhi Dandona, Valery Feigin, Greg Freedman, Bryan Hubbell, Amelia Jobling, Haidong Kan, Luke Knibbs, Yang Liu, Randall Martin, Lidia Morawska, C. Arden Pope, Hwashin Shin, Kurt Straif, Gavin Shaddick, Matthew Thomas, Rita van Dingenen, Aaron van Donkelaar, Theo Vos, Christopher J.L. Murray, and Mohammad H. Forouzanfar (2017). "Estimates and 25-year trends of the global burden of disease attributable to ambient air pollution: an analysis of data from the Global Burden of Diseases Study 2015." In: *The Lancet* 389.10082, pp. 1907–1918. DOI: 10.1016/S0140-6736(17)30505-6 (cit. on pp. 1, 6).

Collings, Nick, Kanchit Rongchai, and J.P.R. Symonds (2014). "A condensation particle counter insensitive to volatile particles." In: *Journal of Aerosol Science* 73, pp. 27–38. ISSN: 00218502. DOI: 10.1016/j.jaerosci.2014.03.003. URL: http://www.sciencedirect.com/science/article/pii/S0021850214000433 (cit. on pp. 3, 66, 67).

Comite Européen de Normalisation (2009). *European Standard EN 1822-1:2009, "High efficiency air filters (EPA, HEPA and ULPA)"* (cit. on p. 25).

Cresnoverh, Martin (2015). "Realisation of a visual based condensation particle counter utilizing bright field technique." PhD thesis (cit. on p. 105).

Dastanpour, Ramin and Steven N. Rogak (2014). "Observations of a correlation between primary particle and aggregate size for soot particles." In: *Aerosol Science and Technology* 48.10, pp. 1043–1049. DOI: 10.1080/02786826.2014.955565 (cit. on pp. 15, 16).

Davis, Devra L, Michelle L Bell, and David Bates (2002). "Guest Editorials A Look Back at the London Smog of 1952 and the Half Century Since A Half Century Later :" in: *Environmental health perspectives* 110.12, pp. 734–735 (cit. on pp. 1, 15).

Declercq, Christophe, Christian Madsen, Georgios Grivas, Gudrun Weinmayr, Audrius Dėdelė, Gerard Hoek, Gioia Mosler, Éva Vaskövi, Klea Katsouyanni, Ming-Yi Tsai, Regina Gražulevičienė, Marieke Oldenwening, Rob Beelen, Frank de Vocht, Kees Meliefste, Giulia Cesaroni, Joachim Heinrich, Ole Raaschou-Nielsen, Bert Brunekreef, Kirsten Eriksen, Andrea Ranzi, Minas Iakovides, Marta Cirach, Barbara Hoffmann, Ulrich Quass, Orsolya Udvardy, Tom Bellander, Christophe Ampe, Kees de Hoogh, Mark Nieuwenhuijsen, Ursula Krämer, Michal Korek, Nicole Probst-Hensch, Audrey De Nazelle, Anna Mölter, Bernhard Anwander, Euripides Stephanou, Marloes Eeftens, Arto Pennanen, Josef Cyrys, Dorothee Sugiri, Alex Ineichen, Timo Lanki, Thomas Kuhlbusch, and Claudia Galassi (2012). "Spatial variation of PM2.5, PM10, PM2.5 absorbance and PMcoarse concentrations between and within 20 European study areas and the relationship with NO2 – Results of the ESCAPE project." In: *Atmospheric Environment* 62, pp. 303–317. DOI: 10.1016/j.atmosenv.2012.08.038 (cit. on pp. 1, 6).

Dekati Ltd. (2007). *Dekati® Thermodenuder — DEKATI*. URL: https://www.environmental-expert.com/products/dekati-thermodenuder-72345 (visited on 04/21/2019) (cit. on p. 40).

Dekati Ltd. (2019a). *Dekati Diluter*. URL: https://www.dekati.com/products/dekati-diluter/ (visited on 04/19/2019) (cit. on p. 39).

Dekati Ltd. (2019b). *Dekati eDiluter*. URL: https://www.dekati.com/products/ediluter/ (visited on 04/19/2019) (cit. on p. 39).

Derjaguin, B. (1940). "A theory of capillary condensation in the pores of sorbents and of other capillary phenomena taking into account the disjoining action of polymolecular liquid films." In: *Progress in Surface Science* 40.1-4, pp. 46–61. DOI: 10.1016/0079-6816(92)90032-D (cit. on p. 58).

Dillmann, A. and G. E A Meier (1989). "Homogeneous nucleation of supersaturated vapors." In: *Chemical Physics Letters* 160.1, pp. 71–74. DOI: 10.1016/0009-2614(89)87558-X (cit. on p. 49).

Eastwood, Peter (2008). *Particulate Emissions from Vehicles*. Wiley-Interscience, pp. 1–493. ISBN: 9780470724552. DOI: 10.1002/9780470986516 (cit. on pp. 2, 5, 7, 8, 11, 15–18, 33–39, 63).

Elliott, Martin A., Gerge J. Nebel, and Fred G. Rounds (1955). "The composition of exhaust gases from diesel, gasoline and propane powered motor coaches." In: *Journal of the Air Pollution Control Association* 5.2,

pp. 103–108. ISSN: 00022470. DOI: 10.1080/00966665.1955.10467686 (cit. on p. 7).

Erickson, Harold P. (2009). "Size and shape of protein molecules at the nanometer level determined by sedimentation, gel filtration, and electron microscopy." In: *Biological Procedures Online* 11.1, pp. 32–51. ISSN: 14809222. DOI: 10.1007/s12575-009-9008-x (cit. on p. 10).

European Commission (2008). "Comission regulation (EC) No 692/2008 of 18 July 2008." In: *Official Journal of the European Union*, p. 136 (cit. on p. 66).

European Environment Agency (2008). *Europes air today*. URL: https://www.eea.europa.eu/signals/signals-2013/articles/europes-air-today (visited on 03/07/2019) (cit. on p. 1).

European Environment Agency (2017). *Air Pollution*. URL: https://www.eea.europa.eu/themes/air/intro (visited on 03/07/2019) (cit. on p. 1).

Evans, R., U. Marini Bettolo Marconi, and P. Tarazona (1986). "Fluids in narrow pores: Adsorption, capillary condensation, and critical points." In: *The Journal of Chemical Physics* 84.4, p. 2376. DOI: 10.1063/1.450352. arXiv: arXiv:1011.1669v3. URL: http://scitation.aip.org/content/aip/journal/jcp/84/4/10.1063/1.450352 (cit. on p. 58).

Farrauto, Robert J, Lucas Dorazio, and Calvin H Bartholomew (2016). *Introduction to catalysis and industrial catalytic processes*. John Wiley & Sons (cit. on p. 99).

Feigin, L. A. and D. I. Svergun (1987). *Structure Analysis by Small-Angle X-Ray and Neutron Scattering*. Ed. by George W. Taylor. Boston, MA: Springer US. ISBN: 978-1-4757-6626-4. DOI: 10.1007/978-1-4757-6624-0. URL: http://link.springer.com/10.1007/978-1-4757-6624-0 (cit. on p. 60).

Fletcher, N. H. (1958). "Size Effect in Heterogeneous Nucleation." In: *Journal of Chemical Physics* 29.3, p. 572. DOI: 10.1063/1.1744540. arXiv: arXiv:1011.1669v3. URL: http://scitation.aip.org/content/aip/journal/jcp/29/3/10.1063/1.1744540 (cit. on p. 79).

Fontaras, Georgios, Theodoros Vlachos, Barouch Giechaskiel, Pierre Bonnel, Martin Weiss, Francesco Riccobono, Ricardo Suarez-Bertoa, and Pablo Mendoza-Villafuerte (2015). "Vehicle Emission Factors of Solid Nanoparticles in the Laboratory and on the Road Using Portable Emission Measurement Systems (PEMS)." In: *Frontiers in Environmental Science* 3.December, pp. 1–17. DOI: 10.3389/fenvs.2015.00082 (cit. on p. 2).

Fuchs, N A (1963). "On the stationary charge distribution on aerosol particles in a bipolar ionic atmosphere." In: *Geofisica Pura e Applicata* 56.1, pp. 185–193. DOI: 10.1007/BF01993343 (cit. on p. 35).

Gentner, Drew R., Gabriel Isaacman, David R. Worton, Arthur W. H. Chan, Timothy R. Dallmann, Laura Davis, Shang Liu, Douglas A. Day, Lynn M. Russell, Kevin R. Wilson, Robin Weber, Abhinav Guha, and Allen H. Harley, Robert (2012). "Elucidating secondary organic aerosol from diesel and gasoline vehicles through detailed characterization of organic carbon emissions." In: *Proceedings of the National Academy of Sciences* 109.45, pp. 18318–18323. DOI: 10.1073/pnas.1212272109 (cit. on p. 7).

Giechaskiel, Barouch (2019a). "Differences between tailpipe and dilution tunnel sub-23 nm nonvolatile (solid) particle number measurements." In: *Aerosol Science and Technology* 53.9, pp. 1012–1022. DOI: 10.1080/02786826.2019.1623378. URL: https://doi.org/10.1080/02786826.2019.1623378 (cit. on p. 19).

Giechaskiel, Barouch (2019b). "Effect of sampling conditions on the sub-23 nm nonvolatile particle emissions measurements of a moped." In: *Applied Sciences (Switzerland)* 9.15. DOI: 10.3390/app9153112 (cit. on p. 19).

Giechaskiel, Barouch, R Chirico, P. F. DeCarlo, M Clairotte, T Adam, Giorgio Martini, M. F. Heringa, R Richter, A. S.H. Prevot, Urs Baltensperger, and C Astorga (2010a). "Evaluation of the particle measurement programme (PMP) protocol to remove the vehicles' exhaust aerosol volatile phase." In: *Science of the Total Environment* 408.21, pp. 5106–5116. ISSN: 00489697. DOI: 10.1016/j.scitotenv.2010.07.010 (cit. on pp. 3, 20, 63).

Giechaskiel, Barouch, R Chirico, P. F. DeCarlo, M Clairotte, T Adam, Giorgio Martini, M. F. Heringa, R Richter, A. S.H. Prevot, Urs Baltensperger, and C Astorga (2010b). "Evaluation of the particle measurement programme (PMP) protocol to remove the vehicles' exhaust aerosol volatile phase." In: *Science of the Total Environment* 408.21, pp. 5106–5116. DOI: 10.1016/j.scitotenv.2010.07.010 (cit. on p. 41).

Giechaskiel, Barouch, Martin Cresnoverh, Herwig Jörgl, and Alexander Bergmann (2010a). "Calibration and accuracy of a particle number measurement system." In: *Measurement Science and Technology* 21.4. DOI: 10.1088/0957-0233/21/4/045102 (cit. on p. 41).

Giechaskiel, Barouch, Martin Cresnoverh, Herwig Jörgl, and Alexander Bergmann (2010b). "Calibration and accuracy of a particle number mea-

surement system." In: *Measurement Science and Technology* 21.4. DOI: 10.1088/0957-0233/21/4/045102 (cit. on p. 66).

Giechaskiel, Barouch., P. Dilara, E. Sandbach, and J. Andersson (2008). "Particle measurement programme (PMP) light-duty inter-laboratory exercise: comparison of different particle number measurement systems." In: *Measurement Science and Technology* 19.9, p. 095401. ISSN: 0957-0233. DOI: 10.1088/0957-0233/19/9/095401 (cit. on pp. 66, 86).

Giechaskiel, Barouch, Ameya Joshi, Leonidas Ntziachristos, and Panagiota Dilara (2019). "European regulatory framework and particulate matter emissions of gasoline light-duty vehicles: A review." In: *Catalysts* 9.7. DOI: 10.3390/catal9070586 (cit. on p. 19).

Giechaskiel, Barouch, Tero Lahde, Ricardo Suarez-Bertoa, Michael Clairotte, Theodoros Grigoratos, Alessandro Zardini, Adolfo Perujo, and Giorgio Martini (2018). "Particle number measurements in the European legislation and future JRC activities." In: *Combustion Engines* 174.3, pp. 3–16. DOI: 10.19206/CE-2018-301 (cit. on p. 19).

Giechaskiel, Barouch, Matti Maricq, Leonidas Ntziachristos, Christos Dardiotis, Xiaoliang Wang, Harald Axmann, Alexander Bergmann, and Wolfgang Schindler (2014). "Review of motor vehicle particulate emissions sampling and measurement: From smoke and filter mass to particle number." In: *Journal of Aerosol Science* 67, pp. 48–86. DOI: 10.1016/j.jaerosci.2013.09.003 (cit. on pp. 2, 15, 17, 18, 30, 37, 63, 86).

Giechaskiel, Barouch, J Vanhanen, M Väkevä, and Giorgio Martini (2017). "Investigation of vehicle exhaust sub-23 nm particle emissions." In: *Aerosol Science and Technology* 51.5, pp. 626–641. ISSN: 15217388. DOI: 10.1080/02786826.2017.1286291 (cit. on pp. 3, 6, 19, 53).

Giechaskiel, Barouch, X. Wang, D. Gilliland, and Y. Drossinos (2011). "The effect of particle chemical composition on the activation probability in n-butanol condensation particle counters." In: *Journal of Aerosol Science* 42.1, pp. 20–37. DOI: 10.1016/j.jaerosci.2010.10.006 (cit. on pp. 54, 78).

Glatter, Otto and Otto Kratky (1982). *Small angle x-ray scattering*. Academic Press Inc. ISBN: 0-12-286280-5. DOI: https://doi.org/10.1002/actp.1985.010360520 (cit. on p. 60).

Gleichweit, Michael (2019). "Optimization and Characterization of a High Temperature Optical Particle Counter for Automotive Applications." Master's Thesis. Graz University of Technology (cit. on pp. 64, 92, 95).

Gránásy, L (2000). "Comparison of modern theories of vapor condensation." In: *NUCLEATION AND ATMOSPHERIC AEROSOLS 2000: 15th Int.'l Conf.* 209.2000, pp. 209–212. ISSN: 0094243X. DOI: 10.1063/1.1361848. URL: http://scitation.aip.org/content/aip/proceeding/aipcp/10.1063/1.1361848 (cit. on p. 49).

Graz University of Technology (2012). *Curriculum for the Doctoral Programme in Technical Sciences*. URL: https://www.tugraz.at/fileadmin/public/Studierende%7B%5C_%7Dund%7B%5C_%7DBedienstete/Information/Doctoral%7B%5C_%7DSchools/Curriculum%7B%5C_%7DDoctoral%7B%5C_%7DProgramme%7B%5C_%7DTechnical%7B%5C_%7DSciences.pdf (cit. on p. 22).

GRIMM Aerosol (2019). *MODEL 7860 TUNGSTEN OXIDE GENERATOR*. URL: https://www.grimm-aerosol.com/products-en/nano-particle-measurement/aerosol-generators/7860-wox-generator/ (visited on 04/28/2019) (cit. on pp. 47, 56).

Grob, B., J. C. Wolf, B. Kiwull, and R. Niessner (2014). "Calibration system with an indirect photoelectric charger for legislated vehicle number emission measurement counters in the single counting mode." In: *Journal of Aerosol Science* 70, pp. 50–58. DOI: 10.1016/j.jaerosci.2014.01.001 (cit. on p. 47).

Hämeri, K., I. K. Koponen, P. P. Aalto, and M. Kulmala (2002). "The particle detection efficiency of the TSI-3007 condensation particle counter." In: *Journal of Aerosol Science* 33.10, pp. 1463–1469. DOI: 10.1016/S0021-8502(02)00090-3 (cit. on pp. 31, 66).

Haritash, A. K. and C. P. Kaushik (2009). "Biodegradation aspects of Polycyclic Aromatic Hydrocarbons (PAHs): A review." In: *Journal of Hazardous Materials* 169.1-3, pp. 1–15. DOI: 10.1016/j.jhazmat.2009.03.137 (cit. on p. 17).

Haynes, W. M. (2012). *CRC Handbook of Chemistry and Physics, 93rd Edition*. 100 Key Points. Taylor & Francis. ISBN: 9781439880494. URL: https://books.google.at/books?id=-BzP7Rkl7WkC (cit. on p. 69).

Heim, Michael, Benjamin J. Mullins, Heinz Umhauer, and Gerhard Kasper (2008). "Performance evaluation of three optical particle counters with an efficient "multimodal" calibration method." In: *Journal of Aerosol Science* 39.12, pp. 1019–1031. DOI: 10.1016/j.jaerosci.2008.07.006 (cit. on p. 29).

Hering, Susanne V. (2018). "From Particle Counting to Aerosol Collection: Just Add Water." In: *2018 IAC Abstract Book*, p. 1. URL: http://aaarabstracts.com/2018IAC/AbstractBook.pdf (cit. on p. 66).

Hering, Susanne V. and Mark R. Stolzenburg (2005). "A method for particle size amplification by water condensation in a laminar, thermally diffusive flow." In: *Aerosol Science and Technology* 39.5, pp. 428–436. DOI: 10.1080/027868290953416 (cit. on p. 86).

Hering, Susanne V., Mark R. Stolzenburg, Frederick R. Quant, Derek R. O'Berreit, and Patricia B. Keady (2005). "A laminar-flow, water-based condensation particle counter (WCPC)." In: *Aerosol Science and Technology* 39.7, pp. 659–672. DOI: 10.1080/02786820500182123 (cit. on pp. 32, 66, 86).

Hillemann, L., A. Zschoppe, R. Caldow, Gilmore J. Sem, and A. Wiedensohler (2014). "An ultrafine particle monitor for size-resolved number concentration measurements in atmospheric aerosols." In: *Journal of Aerosol Science* 68, pp. 14–24. DOI: 10.1016/j.jaerosci.2013.10.007. URL: http://dx.doi.org/10.1016/j.jaerosci.2013.10.007 (cit. on p. 86).

Hinds, W. C. and N. J. Kennedy (2000). "An ion generator for neutralizing concentrated aerosols." In: *Aerosol Science and Technology* 32.3, pp. 214–220. ISSN: 02786826. DOI: 10.1080/027868200303740 (cit. on pp. 8–11, 35, 36, 81).

Hooftman, Nils, Maarten Messagie, Joeri Van Mierlo, and Thierry Coosemans (2018). "A review of the European passenger car regulations – Real driving emissions vs local air quality." In: *Renewable and Sustainable Energy Reviews* 86.July 2017, pp. 1–21. DOI: 10.1016/j.rser.2018.01.012. URL: https://doi.org/10.1016/j.rser.2018.01.012 (cit. on pp. 2, 37).

Hueglin, Ch, L. Scherrer, and H. Burtscher (1997). "An accurate, continuously adjustable dilution system (1:10 to 1:104) for submicron aerosols." In: *Journal of Aerosol Science* 28.6, pp. 1049–1055. ISSN: 00218502. DOI: 10.1016/S0021-8502(96)00485-5. URL: http://linkinghub.elsevier.com/retrieve/pii/S0021850296004855 (cit. on p. 38).

Iida, K., M. R. Stolzenburg, and P. H. McMurry (2009). "Effect of working fluid on sub-2 nm particle detection with a laminar flow ultrafine condensation particle counter." In: *Aerosol Science and Technology* 43.1, pp. 81–96. ISSN: 15217388. DOI: 10.1080/02786820802488194 (cit. on p. 69).

infotherm.com (2015). URL: http://www.infotherm.com (cit. on p. 69).

Irgang, Klaus (2016). "Charakterisierung eines CNMs mittels eines Streulicht-Aufbaus." PhD thesis (cit. on p. 105).

Jacobson, Mark Z (2001). "Strong radiative heating due to mixing state of black carbon in atmospheric aerosol . mixing state of black carbon in atmospheric aerosols." In: 409.January 2001, pp. 695–697 (cit. on p. 17).

Jing, Lianpeng (1999). "Standard Combustion Aerosol Generator (SCAG) for Calibration Purposes." In: *3rd ETH Workshop "Nanoparticle Measurement", ETH Hönggerberg Zürich* (cit. on p. 43).

Johnson, Timothy (2016). "Vehicular Emissions in Review." In: *SAE International Journal of Engines* 9.2, pp. 1258–1275. ISSN: 19463936, 19463944. URL: http://www.jstor.org/stable/26284895 (cit. on p. 2).

Karjalainen, Panu (2014). "Vehicle Nanoparticle Emissions under Transient Driving Conditions." PhD Thesis. Tampere University of Technology (cit. on p. 15).

Karner, Alex A., Douglas S. Eisinger, and Deb A. Niemeier (2010). "Near-roadway air quality: Synthesizing the findings from real-world data." In: *Environmental Science and Technology* 44.14, pp. 5334–5344. DOI: 10.1021/es100008x (cit. on p. 19).

Kirk, R. E., D. F. Othmer, M. Grayson, and D. Eckroth (2007). "Kirk-Othmer Encyclopedia of Chemical Technology. Mass Transfer." In: *Kirk-Othmer Encyclopedia of Chemical Technology*, pp. 1–75. DOI: 10.1002/0471238961. URL: http://www.massey.ac.nz/%7B~%7Dychisti/MassTKirk.pdf (cit. on p. 69).

Koolen, Cedric D. and Gadi Rothenberg (2019). "Air Pollution in Europe." In: *ChemSusChem* 12.1, pp. 164–172. ISSN: 1864564X. DOI: 10.1002/cssc.201802292 (cit. on p. 1).

Kozáková, Jana, Pavel Mikuška, Kamil Křůmal, Petra Pokorná, Jan Hovorka, Pavel Moravec, Lucie Ondráčková, Jaroslav Schwarz, Jakub Ondráček, and Petr Vodička (2018). "The influence of local emissions and regional air pollution transport on a European air pollution hot spot." In: *Environmental Science and Pollution Research* 26.2, pp. 1675–1692. ISSN: 0944-1344. DOI: 10.1007/s11356-018-3670-y (cit. on p. 2).

Kraft, Martin, Tristan Reinisch, and Alexander Bergmann (2016). "Non-Reactive Working Fluids for Reliably Sensing Nanoparticles in Automotive Exhaust Gases." In: *Procedia Engineering* 168, pp. 51–54. ISSN: 18777058. DOI: 10.1016/j.proeng.2016.11.143 (cit. on p. 54).

Kreidenweis, S. M., L. M. McLnnes, and F. J. Brechtel (1998). "Observations of aerosol volatility and elemental composition at macquarie island

during the first aerosol characterization experiment (ACE 1)." In: *Journal of Geophysical Research: Atmospheres* 103.D13, pp. 16511–16524. ISSN: 21698996. DOI: 10.1029/98JD00800 (cit. on p. 40).

Kuang, Chongai, Modi D Chen, Peter H. McMurry, and Jian Wang (2012). "Modification of Laminar Flow Ultrafine Condensation Particle Counters for the Enhanced Detection of 1 nm Condensation Nuclei." In: *Aerosol Science And Technology* 46.3, pp. 309–315. DOI: 10.1080/02786826.2011.626815 (cit. on pp. 30, 31, 53, 66, 86).

Kügler, Michael (2018). "Particle Detection and Experimental Evaluation of Different Material Combinations for Saturators of Particle Counting Devices." Master's Thesis. Graz University of Technology (cit. on pp. 64, 75, 81, 99, 105).

Kupper, Martin, Martin Kraft, Adam Boies, and Alexander Bergmann (2019). "High-Temperature Condensation Particle Counter Using a Systematically Selected Dedicated Working Fluid For Automotive Applications." In: *Aerosol Science and Technology*. DOI: 10.1080/02786826.2019.1702920 (cit. on p. 65).

Kupper, Martin, Jožef Pulko, Martin Kraft, and Alexander Bergmann (2019). "First Steps towards a Super-Compact In-Situ Laser-Induced-Incandescence Sensor System." In: *Proceedings* 2.13, p. 1017. ISSN: 2504-3900. DOI: 10.3390/proceedings2131017. URL: https://www.mdpi.com/2504-3900/2/13/1017 (cit. on pp. 34, 109, 111).

Landesanstalt für Umwelt Messungen und Naturschutz (2014). "PEMS-Messungen an drei Euro 6-Diesel-Pkw auf Streckenführungen in Stuttgart und München sowie auf Außerortsstrecken." In: (cit. on p. 2).

Leach, Felix, Andrew Lewis, Sam Akehurst, James Turner, and David Richardson (2019). "Sub-23 nm Particulate Emissions from a Highly Boosted GDI Engine." In: *SAE Technical Papers* 2019-September.September. DOI: 10.4271/2019-24-0153 (cit. on pp. 2, 19).

Lee, Sangdon, Myoseon Jang, and Richard M. Kamens (2004). "SOA formation from the photooxidation of α-pinene in the presence of freshly emitted diesel soot exhaust." In: *Atmospheric Environment* 38.16, pp. 2597–2605. DOI: 10.1016/j.atmosenv.2003.12.041 (cit. on p. 19).

Magnusson, Lars Erik, John A. Koropchak, Michael P. Anislmov, Valeriy M. Poznjakpvskly, and Juan Fernandez de la Mora (2003). "Correlations for Vapor Nucleating Critical Embryo Parameters." In: *Journal of Physical and Chemical Reference Data* 32.4, pp. 1387–1410. DOI: 10.1063/1.1555590 (cit. on pp. 54, 68, 78).

Maierhofer, Paul, Georg Röhrer, Markus Bainschab, and Alexander Bergmann (2019). "On the Inherent Variability of Particulate Matter Concentrations on Small Scales and the Consequences for Miniaturized Particle Sensors." In: *Aerosol and Air Quality Research*, pp. 1–10. DOI: 10.4209/aaqr.2019.01.0048 (cit. on p. 29).

Mäkelä, Jyrki M., Pasi Aalto, Boris Z. Gorbunov, and Pekka Korhonen (1992). "Size distributions from aerosol spark generator." In: *Journal of Aerosol Science* 23.SUPPL. 1, pp. 233–236. DOI: 10.1016/0021-8502(92)90392-9 (cit. on p. 44).

Marjamäki, Marko, Jorma Keskinen, Da Ren Chen, and David Y.H. Pui (2000). "Performance evaluation of the electrical low-pressure impactor (ELPI)." In: *Journal of Aerosol Science* 31.2, pp. 249–261. DOI: 10.1016/S0021-8502(99)00052-X (cit. on pp. 36, 42).

Marple, Virgil A., Benjamin Y.H. Liu, and Kenneth T. Whitby (1974). "Fluid mechanics of the laminar flow aerosol impactor." In: *Journal of Aerosol Science* 5.1. DOI: 10.1016/0021-8502(74)90002-0 (cit. on p. 42).

Marrero, T. R. and E. A. Mason (1972). *Binary Diffusion Coefficients.Pdf* (cit. on p. 69).

McGraw, Robert, Jian Wang, and Chongai Kuang (2012). "Kinetics of Heterogeneous Nucleation in Supersaturated Vapor: Fundamental Limits to Neutral Particle Detection Revisited." In: *Aerosol Science and Technology* 46.9, pp. 1053–1064. ISSN: 0278-6826. DOI: 10.1080/02786826.2012.687844. URL: http://www.tandfonline.com/doi/abs/10.1080/02786826.2012.687844 (cit. on pp. 49, 52).

McMurry, Peter H. (2000). "A Review of Atmospheric Aerosol Measurements." In: *Atmospheric Environment* 34.12-14, pp. 1959–1999 (cit. on pp. 30, 66, 86).

Mewes, B. and J.M. Seitzman (1997). "Soot volume fraction and particle size measurements with laser-induced incandescence." In: *Applied optics* 36.3, pp. 709–17. ISSN: 0003-6935. DOI: 10.1364/AO.36.000709. URL: http://www.ncbi.nlm.nih.gov/pubmed/18250729 (cit. on pp. 110, 111, 114, 115).

Michelsen, H. A., F. Liu, B. F. Kock, H. Bladh, A. Boiarciuc, M. Charwath, T. Dreier, R. Hadef, M. Hofmann, J. Reimann, S. Will, P. E. Bengtsson, H. Bockhorn, F. Foucher, K. P. Geigle, C. Mounaïm-Rousselle, C. Schulz, R. Stirn, B. Tribalet, and R. Suntz (2007). "Modeling laser-induced incandescence of soot: A summary and comparison of LII models." In:

Applied Physics B: Lasers and Optics 87.3, pp. 503–521. ISSN: 09462171. DOI: 10.1007/s00340-007-2619-5 (cit. on pp. 111, 113, 119).

Mie, Gustav (1908). "Beiträge zur Optik trüber Medien, speziell kolloidaler Metallösungen." In: *Annalen der Physik* 330.3, pp. 377–445. DOI: 10.1002/andp.19083300302. URL: http://doi.wiley.com/10.1002/andp.19083300302 (cit. on p. 105).

Mikkanen, Pirita, Mikko Moisio, Jorma Keskinen, Jyrki Ristimäki, and Marko Marjamäki (2010). "Sampling Method for Particle Measurements of Vehicle Exhaust." In: *SAE Technical Paper Series* 1.724. DOI: 10.4271/2001-01-0219 (cit. on p. 38).

Moore, Richard H., Luke D. Ziemba, Dabrina Dutcher, Andreas J. Beyersdorf, Kevin Chan, Suzanne Crumeyrolle, Timothy M. Raymond, Kenneth L. Thornhill, Edward L. Winstead, and Bruce E. Anderson (2014). "Mapping the operation of the miniature combustion aerosol standard (Mini-CAST) soot generator." In: *Aerosol Science and Technology* 48.5, pp. 467–479. DOI: 10.1080/02786826.2014.890694 (cit. on p. 44).

Nakamura, Kazuki, Christos Dardiotis, Athanasios Mamakos, and Waldemar Rodriguez (2019). "Instrumentation Challenges for Measuring Sub-23 nm Particle Number Emissions from Transportation Sources." In: *International Journal of Automotive Engineering* 10.2, pp. 205–212. ISSN: 2185-0984 (cit. on p. 19).

Nishida, Robert Takeo (2018). "Measuring Aerosol Nanoparticles by Ultraviolet Photoionisation." PhD thesis. University of Cambridge (cit. on p. 35).

Ntziachristos, L., G. Mellios, D. Tsokolis, M. Keller, S. Hausberger, N. E. Ligterink, and P. Dilara (2014). "In-use vs. type-approval fuel consumption of current passenger cars in Europe." In: *Energy Policy* 67.2014, pp. 403–411. ISSN: 03014215. DOI: 10.1016/j.enpol.2013.12.013 (cit. on p. 2).

Ntziachristos, Leonidas, Barouch Giechaskiel, Panayotis Pistikopoulos, Zissis Samaras, Urs Mathis, Martin Mohr, Roberto Casati, Volker Scheer, and Rainer Vogt (2004). "Performance Evaluation of a Novel Sampling Particle Characterization." In: *Engineering* 2004.724 (cit. on p. 39).

Official Journal of the European Union EN (2015). "Regulation No 83 of the Economic Commission for Europe of the United Nations (UNECE) — Uniform provisions concerning the approval of vehicles with regard to the emission of pollutants according to engine fuel requirements [2015/1038]." In: *Official Journal of the European Union*, pp. 44–47 (cit. on pp. 2, 3, 13, 14, 16, 26, 27, 37, 40, 41, 86).

Ogendal, L. (2013). *Light Scattering Demystified Theory and Practice*. July, p. 129. URL: http://igm.fys.ku.dk/%7B~%7Dlho/personal/lho/lightscattering%7B%5C_%7Dtheory%7B%5C_%7Dand%7B%5C_%7Dpractice.pdf (cit. on pp. 29, 105, 115).

Ohlwein, Simone, Ron Kappeler, Meltem Kutlar Joss, Nino Künzli, and Barbara Hoffmann (2019). "Health effects of ultrafine particles: a systematic literature review update of epidemiological evidence." In: *International Journal of Public Health* 7.Hei 2013. ISSN: 1661-8556. DOI: 10.1007/s00038-019-01202-7. URL: http://link.springer.com/10.1007/s00038-019-01202-7 (cit. on pp. 3, 6).

Öktem, Berk, Michael P. Tolocka, Bin Zhao, Hai Wang, and Murray V. Johnston (2005). "Chemical species associated with the early stage of soot growth in a laminar premixed ethylene-oxygen-argon flame." In: *Combustion and Flame* 142.4, pp. 364–373. DOI: 10.1016/j.combustflame.2005.03.016 (cit. on pp. 17, 19).

Orthaber, Doris, Alexander Bergmann, and Otto Glatter (2000). "SAXS experiments on absolute scale with Kratky systems using water as a secondary standard." In: *Journal of Applied Crystallography* 33.2, pp. 218–225. DOI: 10.1107/S0021889899015216 (cit. on p. 60).

Papazian, Harold A. (1971). "Correlation of Surface Tension between Various Liquids." In: *Journal of the American Chemical Society* 93.22, pp. 5634–5636. ISSN: 15205851. DOI: 10.1021/acs.est.7b01959 (cit. on p. 69).

Peach, Matthew (2015). *Austrian researchers to adapt laser ignition for rockets*. URL: http://optics.org/news/6/11/12 (visited on 06/18/2018) (cit. on p. 113).

Peineke, C., M. B. Attoui, and A. Schmidt-Ott (2006). "Using a glowing wire generator for production of charged, uniformly sized nanoparticles at high concentrations." In: *Journal of Aerosol Science* 37.12, pp. 1651–1661. DOI: 10.1016/j.jaerosci.2006.06.006 (cit. on p. 47).

Penner, Joyce E. and T. Novakov (1996). "Carbonaceous particles in the atmosphere: A historical perspective to the Fifth International Conference on Carbonaceous Particles in the Atmosphere." In: *Journal of Geophysical Research: Atmospheres* 101.D14, pp. 19373–19378. DOI: https://doi.org/10.1029/96JD01175. URL: https://agupubs.onlinelibrary.wiley.com/doi/abs/10.1029/96JD01175 (cit. on pp. 8, 15, 16).

Pérez, Noemí, Jorge Pey, Michael Cusack, Cristina Reche, Xavier Querol, Andres Alastuey, and Mar Viana (2010). "Variability of particle number, black carbon, and PM10, PM 2.5, and PM1 Levels and Speciation: Influ-

ence of road traffic emissions on urban air quality." In: *Aerosol Science and Technology* 44.7, pp. 487–499. DOI: 10.1080/02786821003758286 (cit. on p. 1).

Pey, Jorge, Rita Van Dingenen, Jean Philippe Putaud, Andrés Alastuey, Xavier Querol, and Sergio Rodríguez (2009). "Source apportionment of urban fine and ultra-fine particle number concentration in a Western Mediterranean city." In: *Atmospheric Environment* 43.29, pp. 4407–4415. ISSN: 13522310. DOI: 10.1016/j.atmosenv.2009.05.024 (cit. on p. 2).

Philip, J R (1977). "Unitary Approach to Capillary Condensation and Adsorption." In: *Journal of Chemical Physics* 66.11, pp. 5069–5075. DOI: Doi10.1063/1.433814 (cit. on pp. 59, 79).

Poling, B. E., J. M. Prausnitz, and J. P. O'Connel (2001). *The Properties of Gases and Liquids*. 5th ed. The McGraw-Hill Companies, p. 803. DOI: 10.1036/0070116822 (cit. on pp. 69, 77, 78).

Pratsinis, Sotiris E. and Kyo Seon Kim (1989). "Particle coagulation, diffusion and thermophoresis in laminar tube flows." In: *Journal of Aerosol Science* 20.1, pp. 101–111. ISSN: 00218502. DOI: 10.1016/0021-8502(89)90034-7 (cit. on p. 10).

Raaschou-Nielsen, Ole, Zorana J. Andersen, Rob Beelen, Evangelia Samoli, Massimo Stafoggia, Gudrun Weinmayr, Barbara Hoffmann, Paul Fischer, Mark J. Nieuwenhuijsen, Bert Brunekreef, Wei W. Xun, Klea Katsouyanni, Konstantina Dimakopoulou, Johan Sommar, Bertil Forsberg, Lars Modig, Anna Oudin, Bente Oftedal, Per E. Schwarze, Per Nafstad, Ulf De Faire, Nancy L. Pedersen, Claes Göran Östenson, Laura Fratiglioni, Johanna Penell, Michal Korek, Göran Pershagen, Kirsten T. Eriksen, Mette Sørensen, Anne Tjønneland, Thomas Ellermann, Marloes Eeftens, Petra H. Peeters, Kees Meliefste, Meng Wang, Bas Bueno-de-Mesquita, Timothy J. Key, Kees de Hoogh, Hans Concin, Gabriele Nagel, Alice Vilier, Sara Grioni, Vittorio Krogh, Ming Yi Tsai, Fulvio Ricceri, Carlotta Sacerdote, Claudia Galassi, Enrica Migliore, Andrea Ranzi, Giulia Cesaroni, Chiara Badaloni, Francesco Forastiere, Ibon Tamayo, Pilar Amiano, Miren Dorronsoro, Antonia Trichopoulou, Christina Bamia, Paolo Vineis, and Gerard Hoek (2013). "Air pollution and lung cancer incidence in 17 European cohorts: Prospective analyses from the European Study of Cohorts for Air Pollution Effects (ESCAPE)." In: *The Lancet Oncology* 14.9, pp. 813–822. DOI: 10.1016/S1470-2045(13)70279-1 (cit. on p. 6).

Raza, Mohsin, Longfei Chen, Felix Leach, and Shiting Ding (2018). "A Review of particulate number (PN) emissions from gasoline direct injection (gdi) engines and their control techniques." In: *Energies* 11.6. ISSN: 19961073. DOI: 10.3390/en11061417 (cit. on pp. 2, 19).

Rubino, L., P. Bonnel, M. Carriero, and A. Krasenbrink (2010). "Portable Emission Measurement System (PEMS) For Heavy Duty Diesel Vehicle PM Measurement: The European PM PEMS Program." In: *SAE International Journal of Engines* 2.2, pp. 660–673. ISSN: 1946-3944. DOI: 10.4271/2009-24-0149 (cit. on p. 33).

Sauvain, Jean Jacques, T. Vu Duc, and M. Guillemin (2003). "Exposure to carcinogenic polycyclic aromatic compounds and health risk assessment for diesel-exhaust exposed workers." In: *International Archives of Occupational and Environmental Health* 76.6, pp. 443–455. DOI: 10.1007/s00420-003-0439-4 (cit. on pp. 7, 15, 17).

Scheibel, H. G. and J. Porstendörfer (1983). "Generation of monodisperse Ag- and NaCl-aerosols with particle diameters between 2 and 300 nm." In: *Journal of Aerosol Science* 14.2, pp. 113–126. DOI: 10.1016/0021-8502(83)90035-6 (cit. on pp. 47, 119).

Schindler, Wolfgang, Christoph Haisch, Harald A. Beck, Reinhard Niessner, Eberhard Jacob, and Dieter Rothe (2010). "A Photoacoustic Sensor System for Time Resolved Quantification of Diesel Soot Emissions." In: *SAE Technical Paper Series* 1.724. DOI: 10.4271/2004-01-0968 (cit. on p. 33).

Schulz, C., B. F. Kock, M. Hofmann, H. Michelsen, S. Will, B. Bougie, R. Suntz, and G. Smallwood (2006). "Laser-induced incandescence: Recent trends and current questions." In: *Applied Physics B: Lasers and Optics* 83.3, pp. 333–354. DOI: 10.1007/s00340-006-2260-8 (cit. on p. 35).

Seinfeld, John H. and Spyros N. Pandis (2006). *Atmospheric Chemistry and Physics: From Air Pollution to Climate Change*. 2nd. Wiley-Interscience, p. 1152. ISBN: 9780471720188 (cit. on pp. 4, 49).

Seipenbusch, M., A. Binder, and G. Kasper (2008). "Temporal evolution of nanoparticle aerosols in workplace exposure." In: *Annals of Occupational Hygiene* 52.8, pp. 707–716. DOI: 10.1093/annhyg/men067 (cit. on pp. 30, 66, 86).

Sem, Gilmore J. (2002). "Design and performance characteristics of three continuous-flow condensation particle counters: A summary." In: *Atmospheric Research* 62.3-4, pp. 267–294. DOI: 10.1016/S0169-8095(02)00014-5 (cit. on pp. 30, 53, 66).

Shiraiwa, Manabu, Kathrin Selzle, and Ulrich Pöschl (2012). "Hazardous components and health effects of atmospheric aerosol particles: Reactive oxygen species, soot, polycyclic aromatic compounds and allergenic proteins." In: *Free Radical Research* 46.8, pp. 927–939. ISSN: 10715762. DOI: 10.3109/10715762.2012.663084 (cit. on pp. 1, 19).

Siegmann, K. and H. C. Siegmann (2010). "Fast and Reliable "in situ" Evaluation of Particles and their Surfaces with Special Reference to Diesel Exhaust." In: *SAE Technical Paper Series* 1.724, p. 9. DOI: 10.4271/2000-01-1995. URL: https://www.sae.org/publications/technical-papers/content/2000-01-1995/ (cit. on pp. 35, 36).

Snelling, David R, Gregory J Smallwood, and Ömer L Gülder (2000). "Soot Volume Fraction Characterization Using the Laser-Induced Incandescence Detection Method." In: *Proceedings of the 10th International Symposium on Applications of Laser Techniques to Fluid Mechanics* figure 1, pp. 1–16 (cit. on pp. 110, 113).

Sorensen, Christopher M. (2001). "Light Scattering by Fractal Aggregates: A Review." In: *Aerosol Science and Technology* 35.2, pp. 648–687. DOI: 10.1080/02786820117868. URL: http://www.ingentaconnect.com/content/tandf/uast/2001/00000035/00000002/art00003%20http://www.tandfonline.com/doi/abs/10.1080/02786820117868 (cit. on pp. 29, 105).

Stolzenburg, Mark R. and Peter H. McMurry (1991). "An Ultrafine Aerosol Condensation Nucleus Counter." In: *Aerosol Science and Technology* 14.October 2014, pp. 48–65. DOI: 10.1080/02786829108959470 (cit. on pp. 30, 53, 66, 71, 86, 87).

Sutugin, A G and N A Fuchs (1970). "Formation of condensation aerosols under rapidly changing environmental conditions:: Theory and method of calculation." In: *Journal of Aerosol Science* 1.4, pp. 287–293. URL: http://www.sciencedirect.com/science/article/pii/0021850270900029 (cit. on p. 53).

Swanson, Jacob and David Kittelson (2010). "Evaluation of thermal denuder and catalytic stripper methods for solid particle measurements." In: *Journal of Aerosol Science* 41.12, pp. 1113–1122. ISSN: 00218502. DOI: 10.1016/j.jaerosci.2010.09.003 (cit. on pp. 40, 41, 63).

Swaschnig, Patrick (2017). "Characterization and optimization of a scattering light device." PhD thesis. Graz Universtiy of Technology (cit. on p. 105).

Thomas Mckinnon, J. and Jack B. Howard (1992). "The roles of pah and acetylene in soot nucleation and growth." In: *Symposium (International)*

on Combustion 24.1, pp. 965–971. DOI: 10.1016/S0082-0784(06)80114-1 (cit. on p. 17).

Tittarelli, A., A. Borgini, M. Bertoldi, E. De Saeger, A. Ruprecht, R. Stefanoni, G. Tagliabue, P. Contiero, and P. Crosignani (2008). "Estimation of particle mass concentration in ambient air using a particle counter." In: *Atmospheric Environment* 42.36, pp. 8543–8548. DOI: https://doi.org/10.1016/j.atmosenv.2008.07.056. URL: http://www.sciencedirect.com/science/article/pii/S135223100800695X (cit. on p. 30).

TSI Inc. (2002). *Model 3480 Electrospray aerosol generator -Instruction manual*. Tech. rep. October. URL: https://www.wmo-gaw-wcc-aerosol-physics.org/files/electrospray-3480.pdf (cit. on p. 47).

TSI Inc. (2019a). *Differential Mobility Analyzer 3081*. URL: https://www.tsi.com/products/particle-sizers/electrostatic-classifiers-and-dmas/differential-mobility-analyzer-3081/ (visited on 04/21/2019) (cit. on p. 42).

TSI Inc. (2019b). *ELECTROSPRAY AEROSOL GENERATOR 3482*. URL: https://www.tsi.com/electrospray-aerosol-generator-3482/ (visited on 04/28/2019) (cit. on p. 48).

TSI Inc. (2019c). *Electrostatic Classifier 3082*. URL: https://www.tsi.com/products/particle-sizers/electrostatic-classifiers-and-dmas/electrostatic-classifier-3082/ (visited on 04/21/2019) (cit. on p. 43).

TSI Inc. (2019d). *Scanning Mobility Particle Size Spectrometer 3938*. URL: https://www.tsi.com/products/particle-sizers/particle-size-spectrometers/scanning-mobility-particle-sizer-spectrometer-3938/ (visited on 04/21/2019) (cit. on p. 43).

United Nations (1958). *UN Regulation No. 24 - Rev.2*. DOI: 10.1093/iclqaj/24.3.577. URL: https://www.unece.org/?id=39142 (cit. on p. 27).

United Nations (2014). "GTR 15 - Global Registry Worldwide harmonized Light vehicles Test Procedure." In: *Global Registry* 15. URL: http://www.unece.org/fileadmin/DAM/trans/main/wp29/wp29r-1998agr-rules/ECE-TRANS-180a15e.pdf (cit. on pp. 14, 53, 66, 67, 82).

Vander Wal, R. L. (2009). "Laser-induced incandescence: Excitation and detection conditions, material transformations and calibration." In: *Applied Physics B: Lasers and Optics* 96.4, pp. 601–611. DOI: 10.1007/s00340-009-3521-0 (cit. on p. 3).

Vander Wal, R. L. and K. J. Weiland (1994). "Laser-induced incandescence: Development and characterization towards a measurement of soot-

volume fraction." In: *Applied Physics B Laser and Optics* 59.4, pp. 445–452. ISSN: 09462171. DOI: 10.1007/BF01081067 (cit. on p. 33).

Vander Wal, Randall L., Thomas M. Ticich, and A. Brock Stephens (1999). "Can soot primary particle size be determined using laser-induced incandescence?" In: *Combustion and Flame* 116.1-2, pp. 291–296. ISSN: 00102180. DOI: 10.1016/S0010-2180(98)00040-6. URL: http://www.sciencedirect.com/science/article/pii/S0010218098000406 (cit. on pp. 111, 113, 120).

Vander Wal, Randall L., Thomas M. Ticich, and Joseph R. West (1999). "Laser-induced incandescence applied to metal nanostructures." In: *Applied Optics* 38.27, p. 5867. ISSN: 0003-6935. DOI: 10.1364/AO.38.005867. URL: https://www.osapublishing.org/abstract.cfm?URI=ao-38-27-5867 (cit. on pp. 112, 113).

VDI-Gesellschaft (2005). *VDI-Wärmeatlas*. VDI-Wärmeatlas. Springer Berlin Heidelberg. ISBN: 9783540255031. URL: https://books.google.at/books?id=FyJBFadu8c0C (cit. on pp. 69, 77–79, 153).

Vesala, Timo, Markku Kulmala, Richard Rudolf, Aron Vrtala, and Paul E. Wagner (1997). "Models for condensational growth and evaporation of binary aerosol particles." In: *Journal of Aerosol Science* 28.4, pp. 565–598. DOI: 10.1016/S0021-8502(96)00461-2 (cit. on p. 49).

Volkswagen Ag (2012). "Motor Vehicle Exhaust Emissions : Composition, Emission, Standards, etc." In: *Self Study Program VW Audi* 1, pp. 2–22 (cit. on p. 7).

Wainner, R and J Seitzman (1999). "Soot diagnostics using laser-induced incandescence in flames and exhaust flows." In: *37th Aerospace Sciences Meeting and Exhibit*. DOI: doi:10.2514/6.1999-640 (cit. on pp. 34, 35, 112, 113, 115, 116, 118).

Wang, Xiaoliang, Robert Caldow, Gilmore J. Sem, Naoya Hama, and Hiromu Sakurai (2010). "Evaluation of a condensation particle counter for vehicle emission measurement: Experimental procedure and effects of calibration aerosol material." In: *Journal of Aerosol Science* 41.3, pp. 306–318. DOI: 10.1016/j.jaerosci.2010.01.001 (cit. on pp. 30, 66).

webbook.nist.gov (2015). URL: https://webbook.nist.gov (cit. on p. 69).

Wehner, B., H. Siebert, M. Hermann, F. Ditas, and A. Wiedensohler (2011). "Characterisation of a new Fast CPC and its application for atmospheric particle measurements." In: *Atmospheric Measurement Techniques* 4.5, pp. 823–833. ISSN: 18671381. DOI: 10.5194/amt-4-823-2011 (cit. on pp. 30, 66, 86).

Wei, Qiang, David B. Kittelson, and Winthrop F. Watts (2001). "Single-Stage Dilution Tunnel Performance." In: *SAE Transactions, Section 4: JOURNAL OF FUELS AND LUBRICANTS* 110, pp. 247–258. URL: https://www.jstor.org/stable/44742637 (cit. on pp. 11, 37).

Wiedensohler, A., E. Lütkemeier, M. Feldpausch, and C. Helsper (1986). "Investigation of the bipolar charge distribution at various gas conditions." In: *Journal of Aerosol Science* 17.3, pp. 413–416. DOI: 10.1016/0021-8502(86)90118-7 (cit. on p. 35).

Wiedensohler, A., D. Orsini, D. S. Covert, D. Coffmann, W. Cantrell, M. Havlicek, F. J. Brechtel, L. M. Russell, R. J. Weber, J. Gras, J. G. Hudson, and M. Litchy (1997). "Intercomparison study of the size-dependent counting efficiency of 26 condensation particle counters." In: *Aerosol Science and Technology* 27.2, pp. 224–242. DOI: 10.1080/02786829708965469 (cit. on pp. 52, 53).

Winkler, Paul M., Gerhard Steiner, Aron Vrtala, Hanna Vehkamäki, Madis Noppel, Kari E.J. Lehtinen, Georg P. Reischl, Paul E. Wagner, and Markku Kulmala (2008). "Heterogeneous nucleation experiments bridging the scale from molecular ion clusters to nanoparticles." In: *Science* 319.5868, pp. 1374–1377. ISSN: 00368075. DOI: 10.1126/science.1149034 (cit. on p. 52).

Winkler, Paul M., Aron Vrtala, Gerhard Steiner, Daniela Wimmer, Hanna Vehkamki, Kari E.J. Lehtinen, Georg P. Reischl, Markku Kulmala, and Paul E. Wagner (2012). "Quantitative characterization of critical nanoclusters nucleated on large single molecules." In: *Physical Review Letters* 108.8, pp. 1–5. ISSN: 00319007. DOI: 10.1103/PhysRevLett.108.085701 (cit. on p. 52).

Winkler, Paul M., Aron Vrtala, and Paul E. Wagner (2008). "Condensation particle counting below 2 nm seed particle diameter and the transition from heterogeneous to homogeneous nucleation." In: *Atmospheric Research* 90.2-4, pp. 125–131. DOI: 10.1016/j.atmosres.2008.01.001 (cit. on p. 49).

Yon, Jérôme, François Xavier Ouf, Damien Hebert, James Brian Mitchell, Nadine Teuscher, Jean Luc Le Garrec, Alexandre Bescond, Werner Baumann, Djoudi Ourdani, Thomas Bizien, and Javier Perez (2018). "Investigation of soot oxidation by coupling LII, SAXS and scattering measurements." In: *Combustion and Flame* 190, pp. 441–453. ISSN: 15562921. DOI: 10.1016/j.combustflame.2017.12.014. URL: https://doi.org/10.1016/j.combustflame.2017.12.014 (cit. on p. 61).

Yu, Fangqun (2005). "Modified Kelvin-Thomson equation considering ion-dipole interaction: Comparison with observed ion-clustering enthalpies and entropies." In: *Journal of Chemical Physics* 122.8. DOI: 10.1063/1.1845395 (cit. on p. 49).

Zhang, Zhen, Stephan Stadlbauer, Richard Viskup, Alexander Bergmann, Tristan Reinisch, and Luigi del Re (2014). "Fast Measurement of Soot by In-Situ LII on a Production Engine." In: *Proceedings of the ASME 2014 Internal Combustion Engine Division Fall Technical Conference* (cit. on p. 3).

Zhang, Zhiqun and Benjamin Y.H. Liu (1991). "Performance of TSI 3760 condensation nuclei counter at reduced pressures and flow rates." In: *Aerosol Science and Technology* 15.4, pp. 228–238. ISSN: 15217388. DOI: 10.1080/02786829108959530 (cit. on pp. 30, 66, 86).

Zheng, Zhongqing, Kent C. Johnson, Zhihua Liu, Thomas D. Durbin, Shaohua Hu, Tao Huai, David B. Kittelson, and Heejung S. Jung (2011). "Investigation of solid particle number measurement: Existence and nature of sub-23nm particles under PMP methodology." In: *Journal of Aerosol Science* 42.12, pp. 883–897. DOI: 10.1016/j.jaerosci.2011.08.003 (cit. on pp. 40, 41, 63).

Zhuang, Ye, Yong Jin Kim, Tai Gyu Lee, and Pratim Biswas (2000). "Experimental and theoretical studies of ultra-fine particle behavior in electrostatic precipitators." In: *Journal of Electrostatics* 48.3-4, pp. 245–260. ISSN: 03043886. DOI: 10.1016/S0304-3886(99)00072-8 (cit. on p. 11).

Zizak, G. (2000). "Laser Induced Incandescence (LII) of soot." In: *Combustion* Lii, pp. 18–22 (cit. on pp. 3, 34).

A. Data From Counting Efficiency Measurements in Section 3.2.2

A.1. AVL CPC n-Butanol and TSI 3790

Mean values of 5 measurements.

	10	23	30	40	90
Spark Soot	0	0,85878053	0,95618191	1,02032421	1
NaCl	0	0,04003892	0,39929548	0,84710292	1
WOx	0	0,8358347	0,90533895	0,93844697	1
ZnO	0,85199817	1,01931142	1,02224331	1,02314927	1
CAST	#DIV/0!	0,78049155	0,9288106	0,9664923	1

Table A.1.: Data from the AVL CPC, using n-Butanol as working fluid.

	10	23	30	40	90
Spark Soot	0	0,89654103	0,97551221	0,97114883	1
NaCl	0	0,12695261	0,54278146	0,84297831	1
WOx	0	0,85367647	0,88240132	0,95894608	1
ZnO	0,71521717	1,04464037	1,04618015	1,04622737	1
CAST	#DIV/0!	0,80922131	0,89934621	0,93198087	1

Table A.2.: Data from the TSI 3790.

A.2. AVL CPC n-Decane and TSI 3790

Mean values of 5 measurements.

	10	23	30	40	90
Spark Soot	0	0,95	1,00383197	1,01336441	1
NaCl	0	0,83429539	0,93903418	0,96881062	1
WOx	0	0,91424603	0,96088793	0,9837619	1
ZnO	0	0,91029412	0,95197964	0,98717188	1
CAST	0	0,92418478	0,94045714	0,95917874	1

Table A.3.: Data from the AVL CPC, using n-Decane as working fluid.

	10	23	30	40	90
Spark Soot	0	0,87269231	0,97115385	0,96677913	1
NaCl	0	0,08485711	0,45896806	0,79189189	1
WOx	0	0,81746032	0,92222222	0,9982684	1
ZnO	0,70390171	1,01668697	1,00313693	1,01078846	1
CAST	0	0,71160204	0,88647742	0,98017359	1

Table A.4.: Data from the TSI 3790, using n-Decane as working fluid.

B. Figures of the Counting Efficiencies Sorted by Material

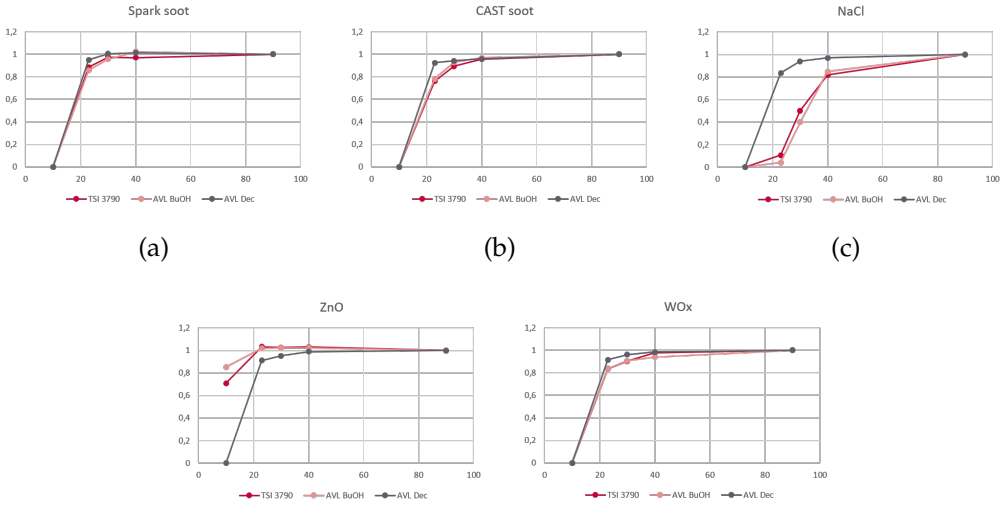

(a) (b) (c)

(d) (e)

Figure B.1.: Measured counting efficiencies, sorted by the particulate material.

C. Appendix to HTCPC Paper I - Principle

C.1. Inspection of the graphite surface

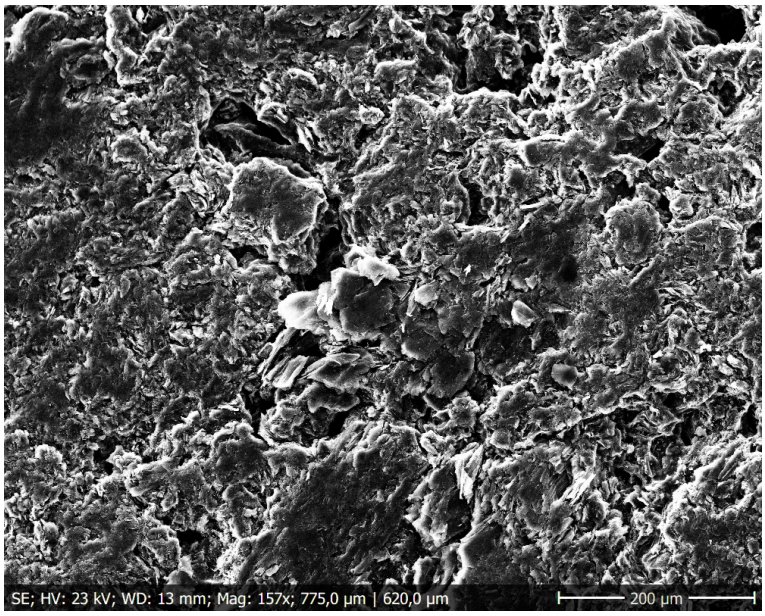

Figure C.1.: SEM picture of the graphite surface before the measurement of the contact angle of the working fluid.

C.2. Selection criteria for the working fluid selection

	T_m [°C]	T_b [°C]	T_f [°C]	T_i [°C]	η [mPa]	ϵ [-]	cs [mL h^{-1}]	d_K [nm]
Good	<-10	>350	>300	>350	>100	<20	0.5 - 5	
Moderate	<20	>290	>250	>250	>10	<40	0.1 - 15	<35
Bad	>20	<290	<250	<250	<10	>40		>35

Table C.1.: Selection criteria applied for the preselection of the working fluid candidates. T_m melting point, T_b boiling point, T_f flash point, T_i ignition point, η vapor pressure at 25 °C, ϵ polarity, **cs** estimated consumption, d_K Kelvin diameter at 125 % saturation

C.3. Parameters of the CFD simulation

Fluid	Gas	Wick
Density $\rho_{Fl}(T)$	Specific heat capacity $c_{p,gas}(T)$	Specific heat capacity $c_{p,wick}(T)$
Surface tension $\sigma_{Fl}(T)$	Vapor pressure η_{gas}	Viscosity $WLF_{wick}(T)$
Enthalpy of vaporation$H_{evap}(T)$	Viscosity $WLF_{gas}(T)$	Density $\rho_{wick}(T)$
	Diffusion coefficient $D(T)$	

Table C.2.: Material parameters in the simulation were thermal dependency was considered. It was distinguished between the gas phase and liquid phase of the working fluid and the wick.

General	
Molar mass / [g mol^{-1}]	282,56
Vapor pressure / [Pa]	$5.6482^{-05} \cdot T^4$–$0.095515 \cdot T^3 + 60.833 \cdot T^2 - 17286 \cdot T + 1.8482^{06}$
Enthalpy of evaporation / [J kg^{-1}]	$-433.58 \cdot T + 474675$
Gas	
Specific heat [J kg^{-1} K]	$4.84088 \cdot T + 199.1$
Viscosity [Pa s]	$1.4147^{-08} \cdot T - 1.1713^{-06}$
Thermal conductivity [W mK^{-1}]	$7.588^{-08} \cdot T^2 - 8^{-06} \cdot T + 1.52^{-03}$
Binary diffusion coefficient in air / [m^2 s^{-1}]	$2.0857^{-11} \cdot T^2 + 5.4627^{-09} \cdot T - 6.7575^{-07}$
Liquid	
Density / [g cm^{-3}]	$-5.7032^{-07} \cdot T^2 - 1.7642^{-04} \cdot T + 0.88$
Surface tension / [mN m^{-1}]	$5.6210^{-05} \cdot T^2 - 0.12501 \cdot T + 61.09$
Kelvin diameter / [nm]	$\frac{55189.62 - 81.804511 \cdot T}{-0.00590663 \cdot T^2 + 8.35098 \cdot T \cdot \ln S}$

Table C.3.: Polynomial fits of the material parameters of the working fluid used for the CFD simulation. T... temperature / [K], S... saturation ratio / [−].

C.4. Results of the surface tension measurements

Temperature / [°C]	80	100	120	140	160	180	200	220
Density / [g cm^{-3}]	0,748	0,735	0,723	0,710	0,697	0,683	0,669	0,654
Measured surface tension / [mN m^{-1}]	28,0	26,2	24,4	22,4	21,7	20,0	17,5	15,7

Table C.4.: The measured surface tension of n-Eicosane from the pendent droplet experiment and the associated density values from literature (VDI-Gesellschaft, 2005) and temperatures. The uncertainty of the measured surface tension is $\pm 2.1\,\mathrm{mN\,m^{-1}}$

C.5. Substances considered as possible high temperature working fluids

Table C.5.: Table of the considered substances for possible high temperature working fluids. Bold values mark knock-out criteria.

	M	Tm [°C]	TS [°C]	FP [°C]	IT [°C]	$\sigma_{25\,°C}$ [mN m^{-1}]	$\sigma_{200\,°C}$ [mN m^{-1}]	$\eta_{25\,°C}$ [mPa s]	$\eta_{200\,°C}$ [mPa s]	ϵ_r [-]	μ [-]	$p_{v,25\,°C}$ [Pa]	$p_{v,200\,°C}$ [Pa]	$\rho_{25\,°C}$ [g cm^{-3}]	$\rho_{200\,°C}$ [g cm^{-3}]	$CS_{200\,°C}$ [mL h^{-1}]	d_K [nm]
Carboxylic acids																	
Decanoic acid	172.26	31.4	268.7	**110**			15.22		0.125		1.15	0.038	11570	0.893	0.763	**34**	14.16
Tetradecanoic acid	228.38	54.16	326	**114**			17.1		0.23			7.00E-05	2000	0.882	0.7588	8	21.21
Palmitic acid	256.424	62.49	351	206			18		2	2.417		1.30E-07	1083	0.882	0.759	5	25.06
Oleic acid	282.46	13.4	360	**189**		30.4	23	34.1	2.5	2.336	1.18	1.90E-06	460	0.895	0.768	2	34.87
Alcohols																	
Glycerine	92.095	18.1	290	**199**	370	63.5	44.5	934	1.6	**46.53**	2.56	0.025	5739	1.257	1.112	6	15.19
Ethers																	
Ditolylether	198.26	-54	283	**135**	545	37.2	22	5.89	0.46			0.22	11000	1.053	0.89	**32**	20.20
Dibenzylether	198.26	1.8	260	**135**		26.8	14	3.5	0.252	3.821		2	24000	1.065	0.939	**68**	12.18
Glycols & Glycol ethers																	
Triethylene	150.173	-9.4	288.6	**177**	371	45.2	29	34.4	1	**23.69**		0.2	8000	1.1195	0.98	**16**	18.31
Tetraethyleneglycol	194.226	-4.1	328	**200**		44	25.5			15.7		0.01	1550	1.1203	0.99	4	20.62
Diethyleneglycoldibutylether	218.332	-60.2	254.6	**118**	310	27	13.5	2.12	0.25			5	25580	0.882	0.75	**97**	16.20
Aliphatische HC																	
Tetradecane	198.388	5.82	253.4	**112**	**200**	26.2	11.8	2.13	0.29	2.0343	0	1.9	25340	0.757	0.6302	**101**	15.31
Pentadecane	212.42	9.9	270.5			26.7	12.5	2.81	0.32	2.0391	0	0.6	15620	0.762	0.6385	**66**	17.14
Hexadecane	226.45	18.2	286.7	**136**	**202**	27.2	12.9	3.03	0.35	2.046	0	0.2	9766	0.767	0.6462	**44**	18.63
Heptadecane	240.47	21.97	302.5			27.5	13.4	3.38	0.38	2.0578	0	0.06	5987	0.77	0.6535	**29**	20.32
Octadecane	254.5	28.2	316.3		227	28	13.9		0.41	2.064	0	0.03	3824	0.774	0.6594	**19**	22.11
Nonadecane	268.53	31.5	330.1		230	28.3	14.2		0.46	2.0706	0	0.006	2347	0.778	0.6644	12	23.65
Eicosane	282.56	36.4	343.9		232	28.7	14.5		0.5	2.081	0	0.001	1532	0.7886	0.6689	8	25.24
Aromatic HC																	
Biphenyl	154.21	69.1	255	**113**	540		22.5		0.37	2.53		3.5	25540	1.04	0.8909	**58**	16.05
1-Ethylnaphthaline	156.23	-14.5	258.2		480	37.9	21	3.37	0.56			3.3	23877	1.0082	0.8775	**56**	15.41
2-Ethylnaphthaline	156.23	-7.3	258.3			36.7	19.9	2.6	0.42			4.1	24607	0.987	0.8631	**59**	14.84
Diphenylmethane	168.23	25.2	264.6	**130**	485	38.3	21.2	2.8	0.38	2.54		1.9	19945	0.998	0.8636	**51**	17.02
Triphenylmethane	244.34	**92.1**	359.4	**100**			25.6		0.84	2.46		0.009	1244	1.014	0.9395	5	27.44
Octadecylbenzene	330.59	35	400				20.6		0.94			2.80E-05	230	0.85	0.75	1	**37.43**
Dibenzylttoluene	272.3835	-34	390	210	450	42.6	22	49				1.62E-03	570	1.04	0.903	2	27.35
Amines																	
Diethanolamine	105.136	27.9	271.2	**172**	662	47.2	29	390	0.3	**25.75**	2.8	0.02	10580	1.0937	0.962	16	13.06
Triethanolamine	149.188	20.5	335.4	**179**	325	47.5	30	609	0.73	**29.36**	3.6	5.00E-03	1090	1.1242	1.01	2	18.26
Diphenylamine	169.23	**53**	305.1	**153**	634		25.1		0.5	3.73		0.2	6880	1.158	0.944	15	18.54
Ketones																	
Benzophenone	182.22	48.2	305.9				26		0.4	12.62		0.17	6150	1.111	0.97	15	20.13
Esters																	
Dimethylphthalate	194.184	5.5	283.7	**146**	490	41.8	24	14.36	0.25	8.66		0.5	11100	1.1905	1.025	**28**	18.74
Diethylphthalate	222.237	-40.5	295	**161**	457	36	21.8	10.5	0.3	7.86		0.1	7000	1.12	0.962	**21**	20.76
Tributylphosphate	266.313	-79	289	**146**		11		3.9		8.34	3.07		1.00E+04	0.9727	0.82	**42**	
Methylpalmitate	270.451	29.6	417							3.124				0.8247			

Dibutylphthalate	278.344	-35	340	**157**	402				16.63			6.58	2.82				1.0465			
Dibutylsebacate	314.461	-9.2	356	**178**	365							4.54	2.48				0.9405			
Tri-o-Kresylphosphate	368.363	11	410	225	385							6.7	2.87	0.0002			1.1955			
Bis(2-ethylhexyl)phthalate	390.557	-55	384	218								5.3	2.84	0.00005			0.981			
Dioctylphthalate	390.557	25	415									5.22								
Dioctylsebacate	426.673	18	**218**	210			30.9			23		4.01					0.9074			
Didecylphthalate	446.663	2.5	463														0.9639			
Others																				
Gallium	69.723	29.7646	2229			715	700	1.34	0.93				2.45	6.00E-36	2.00E-19	6.095	5.975			**33.67**
2-Pyrrolidone	85.105	25.92	250.5	**129**		41	20	13.4	0.5		**28.18**	3.5	4	25000	1.12	0.995		**29**		7.05
Phosphoric acid	97.995	42.4	407																	
Sulfuric acid	98.08	10.31	337			51.7		26.7			**101**				1.8305					
Sulfolane	120.171	27.6	287.3	**177**							**43.26**	4.8	10		1.2723					
3-methylsulpholane	134.197	1	277			50.9					**29.4**				1.188					
Mercury	200.59	-38.829	356.619			485.48	415	1.526	1.11	1.00074			2.613	2307	13.5336	13.112		1		26.17
Polydimethylsiloxane																				

D. Appendix to HTCPC Paper II - Instrumentation

D.1. Thermal distribution of the counting optics module during heat-up

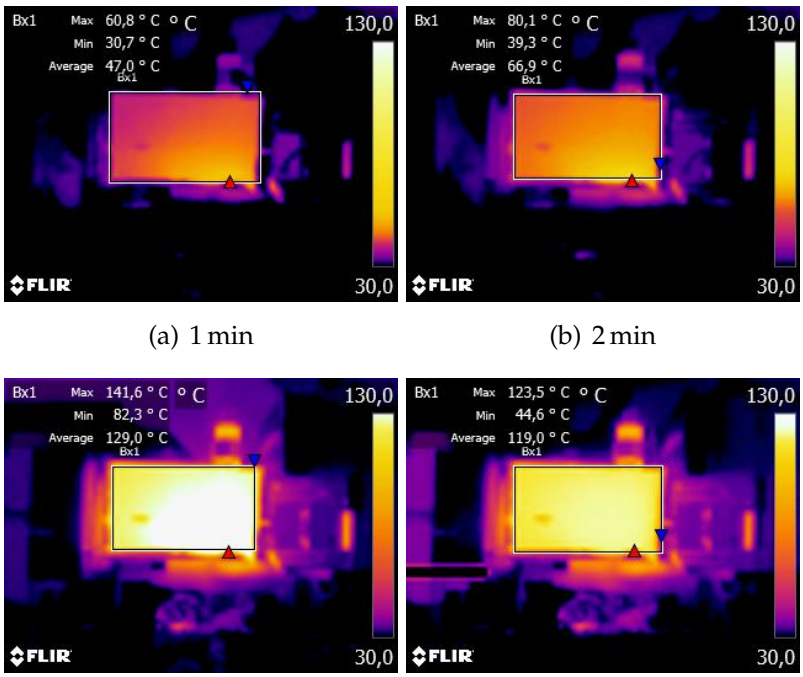

(a) 1 min (b) 2 min

(c) 6 min (d) 12 min

Figure D.1.: Thermal distribution during heat-up of the OPC. The rectangle marks the scattering chamber outline. Deviation in temperature measurement is ±2°C.

E. Capillary Condensation Model

Beginning with equation 9 from [Broekhoff and Boer, 1967]:

$$\frac{d}{2} - t_a = \frac{\gamma\ V_m}{RT\ ln(\frac{p_0}{p_D})} + \int_{t_a}^{d/2} \frac{F(t)}{RT\ ln(\frac{p_0}{p_D})} \tag{E.1}$$

With t_a the thickness of the adsorbed layer, μ the thermodynamic potential, $F(t)$ a function of the layer thickness t, p_D the evaporation pressure, V_m the mol volume and γ the surface tension.

The following assumptions for $F(t)$ from [Broekhoff and Boer, 1967] shall be valid for the solution of equation 9 from [Broekhoff and Boer, 1967]. Because $t > 1$ and the neglected terms are $<< 1$. Thus $\frac{F(t)}{2.303 \cdot RT} = \frac{c}{t^2}$ generalizes with $c = \{^{13.99 \text{ for t } <10\,\text{Å}}_{16.11 \text{ for t } >6\,\text{Å}}$ to :

$$\frac{F(t)}{2.303 \cdot RT} = \frac{13.99}{t^2} - 0.034 \qquad \Rightarrow \quad \frac{F(t)}{2.303 \cdot RT} = \frac{13.99}{t^2} \tag{E.2}$$

$$\frac{F(t)}{2.303 \cdot RT} = \frac{16.11}{t^2} - 0.1682\ e^{-0.1137 \cdot t} \qquad \Rightarrow \quad \frac{F(t)}{2.303 \cdot RT} = \frac{16.11}{t^2} \tag{E.3}$$

With this integration of equation E.1 gives:

$$\frac{d}{2} - t_a = \frac{\gamma\ V_m}{RT\ ln(\frac{p_0}{p_D})} - \frac{2.303 \cdot c}{ln(\frac{p_0}{p_D})} \Bigg|_{t_a}^{\frac{d}{2}} \quad \text{with} \quad c = \{^{13.99 \text{ for t } <10\,\text{Å}}_{16.11 \text{ for t } >6\,\text{Å}} \tag{E.4}$$

With $\frac{d}{2} - t_a \hat{=} d_K$, this model can be transferred into the classic Kelvin equation.

For the plot of figure 3.5, the limits were inserted into equation E.4 and then the equation solved for t. Then t was calculated in a loop over values for S and d.

Doctoral Viva / Rigorosum

Date and Time: January, 28th 2020 at 9:00

Location: Room HF01088D, Institute of Microwave and Photonic Engineering, Inffeldgasse 12, 8010 Graz

Charirman: A.o. Univ.-Prof. Werner Renhart

First Examiner: Univ.-Prof. Alexander Bergmann

External Examiner: Assoc. Univ.-Prof. Topi Rönkkö (University of Tampere)